Modelling of Embankment Construction on Soft Clay in the Mk II Mini-Drum Centrifuge

by
H.R.Barker[a], N.Sartain[b],
A.N.Schofield[c] and K.Soga[d]

CUED / D - SOILS / TR 303 (1997)

[a] PhD Research Student, Geotechnical Group, Department of Engineering, University of Cambridge
[b] MEng Student, Department of Engineering, University of Cambridge
[c] Professor, Geotechnical Group, Department of Engineering, University of Cambridge
[d] Lecturer, Geotechnical Group, Department of Engineering, University of Cambridge

SUMMARY

This report is prepared for presentation at the University of Western Australia Workshop on Geotechnical Centrifuge Modelling on 10- 12 June 1997.

One module of the teaching of final year MEng students in Cambridge University Engineering Department concerned a sand embankment, constructed on a layer of soft clay, in a mini-drum centrifuge. The students were taught the principles of physical and numerical modelling with reference to this problem. The students were required to submit three reports on their coursework: one such set of reports is appended.

The use of the mini-drum centrifuge is also the topic of the forthcoming PhD thesis of the first author.

Key Words: *geotechnical centrifuge, physical and numerical modelling, teaching, embankments, soft ground.*

CONTENTS

PART B - MEng MODULE TESTS

PART C - FURTHER DEVELOPMENT

1. INTRODUCTION

This report deals with system development and novel patented techniques for use of the Cambridge University Engineering Department (CUED) Mk II mini-drum geotechnical centrifuge' for the modelling of reinforced and unreinforced embankment construction. Tests will be reported that have been undertaken as part of:

- CUED MEng research projects;
- CUED MEng teaching module A3 - 'Geotechnical Modelling';
- PhD research by the first author.

1. I Reinforced embankments on soft clay

Geotechnical engineering teaching of third and fourth year undergraduates at CUED involves discussion of challenges that construction on soft soil poses for designers of embankments. Measures undertaken can include sand drains, soil excavation and replacement or the use of geotextile reinforcement. These reinforcing layers can be placed either under or within the embankment, hoping to improve stability and reduce deformations under construction and working loads.

Conventional and finite element analyses of the various possible modes of failure have been undertaken previously, by e.g. Sharma *et al* (1994) and Sharma (1994) who also undertook physical tests to validate his analyses. Modelling of prototype embankments at full scale is difficult due to the large costs involved. Embankments constructed at full scale have been monitored, Fowler (198 1) and Olivera (1982), although this does not usually allow for a study of the effect of the various parameters on the embankment.

Small scale modelling is inaccurate unless it accurately replicates stresses within the embankment and foundation. Centrifuge modelling can be used to overcome this problem.

1.2 Centrifuge modelling of reinforced embankment construction

The advantages and principles of small scale modelling of prototype soil structures by making use of the increased self-weight in a centrifuge have been stated by many authors, e.g. Schofield (1980). The International Society for Soil Mechanics and Foundation Engineering (ISSMFE) set up a technical committee, TC2, in 1982 and the publications of that committee' form a principle resource of information about the technique. A textbook has recently been published by Taylor (1995).

Various researchers, e.g. Terashi & Kitazume (1988), Liu *et al* (1991), have conducted beam centrifuge tests on reinforced embankments. Exact modelling of prototype structures and events was not achieved due to the inability in some cases to pour the embankment in-flight, and by not using an accurately scaled-down geotextile reinforcement. More accurate model prototype embankments were made at CUED by Bolton & Sharma (1994). Embankments were poured in-flight at 40g on reinforced and unreinforced soft clay foundations. A reduced modulus geotextile, described in detail by Springman *et al* (1992), was produced in order to model accurately the strains produced in a commercially available geotextile reinforcement.

---

[1] Patents pending on behalf of the University of Cambridge and Andrew N. Schofield & Associates Ltd.
[2] Notably Centrifuge '84, '88, '91 and '94, Balkema, Rotterdam.

1.3 Mini-drum centrifuge modelling

The recently developed Mk II mini-drum geotechnical centrifuge at CUED differs from the beam centrifuge in that it carries a 0.74m diameter rotating ring channel with a soil layer of depth 60mm. This gives an available circumferential length of [π x (0.74 - 0.06) =] 2.13m. With this length, there is the possibility of conducting a number of tests sequentially on identical soil specimens which enables parametric studies to be conducted quickly and cheaply in order to better understand basic principles behind various processes; it also provides the possibility of the tests described below.

1.4 Format of report

The report is in three main parts:

Part A: Description of the Mk II mini-drum system and the principles behind its use for modelling prototype structures. A new technique for preparing layers of clay in the mini-drum is described and some of the issues raised by such a technique are discussed.

Part B: The MEng Geotechnical Modelling A3 Module as taught at CUED in 1995/6, which considered the construction of reinforced and unreinforced embankments on soft clay. Experimental procedures and results from the centrifuge tests are detailed, together with a brief summary of the finite element package used by the students in their complementary analytical work.

Part C: Further developments in the methods for modelling embankment construction in the mini-drum centrifuge. Modifications and improvements to the original method and the development of a completely new method are covered.

Appendix A contains calculations of the effect of the mini-drum centrifuge's reduced dimensions on the accurate modelling of prototype stresses. Appendix B contains the three MEng A3 Module coursework reports of Nicholas Sartain, a 4th year student from Girton College.

PART A

2 MK II MINI-DRUM GEOTECHNICAL CENTRIFUGE

2. I Drum centrifuge development

A 2m diameter drum centrifuge was designed by Mr Philip Turner for Andrew N. Schofield & Associates Ltd (ANS&A). The details were kept confidential to the University of Cambridge and to ANS&A and were publicly disclosed in 1991 at the TC2 conference in Boulder, Colorado[3] . Provisional patents were taken out prior to this conference. The cost of design and development of the 2m diameter drum centrifuge was met in part by CUED and in part by ANS&A. It was used in a series of experiments, culminating in work on foundation fixity of offshore mobile jack-up platforms. A series of contracts were funded by Esso Exploration and Production UK (EEPUK) Ltd and reported in the theses of Tsukamoto (1994), Sasakura (1996) and Hsu (1997). A series of ANS&A reports by Dean and others were made to EEPUK Ltd relating to the contracts.

When it became clear that a smaller mini-drum centrifuge would be particularly useful in teaching and research in CUED and elsewhere, ANS&A had a series of designs prepared by Mr Keith Wilkinson, who undertook the manufacture of two machines for ANS&A.

2.2 Previous mini-drum experimentation

The original Cambridge mini-drum geotechnical centrifuge, the ANS&A Mk I, was used initially during 1993 in Cambridge. However, Professor Osamu Kusakabe, who had been an associate of ANS&A closely involved in drum centrifuge development, wanted to have a machine for his use and in late 1993 the original mini-drum was transfered to Hiroshima University and Professor Kusakabe at cost. The experiments that were carried out on it in Cambridge are documented by Evans *et al* (1993), Evans (1994), Bolton & Chin (1994) and Chin (1996); experiments in Hiroshima were published by Kusakabe, Gurung and others.

A successor, the Mk II mini-drum centrifuge, was then manufactured by ANS&A. It has been in operation since May 1995 and used for a variety of tests which have been reported by Barbosa *et al* (1995), McKinley *et al* (1996) and McBride (1996).

2.3 Mk II mini-drum description

Figure 1 shows the elevation of the Mk II mini-drum centrifuge, with the drive shaft horizontal. It is a feature of both the Mk I and Mk II mini-drums, covered by the patent application, that soil and water can be loaded into the channel with the axis horizontal. It is then possible to rotate the drum through 90” about the pivot until the drive shaft is vertical, without stopping the spuming drum. In the Mk II, this rotation is performed by an Enerpac hydraulic system[4] . Testing of models is carried out with the axis vertical to eliminate the flg variation in centripetal acceleration which is experienced by the model when the axis is horizontal.

[3] Sekiguchi and Philips (199 1).
[4] Type: BRD 1610 cylinders

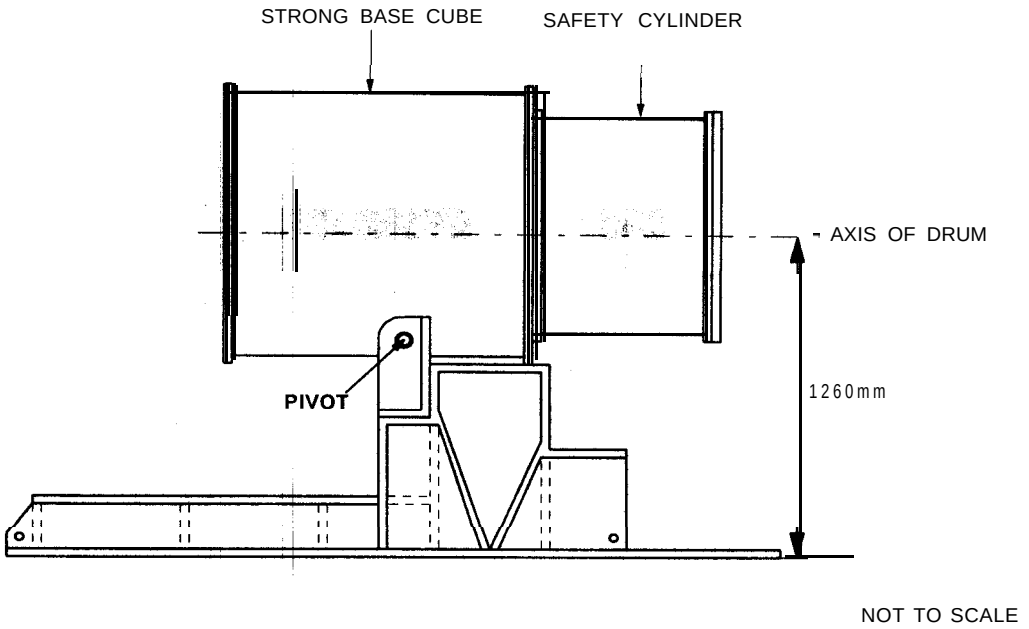

Figure 1 - Elevation of the Mk II Mini-drum Centrifuge with Axis Horizontal

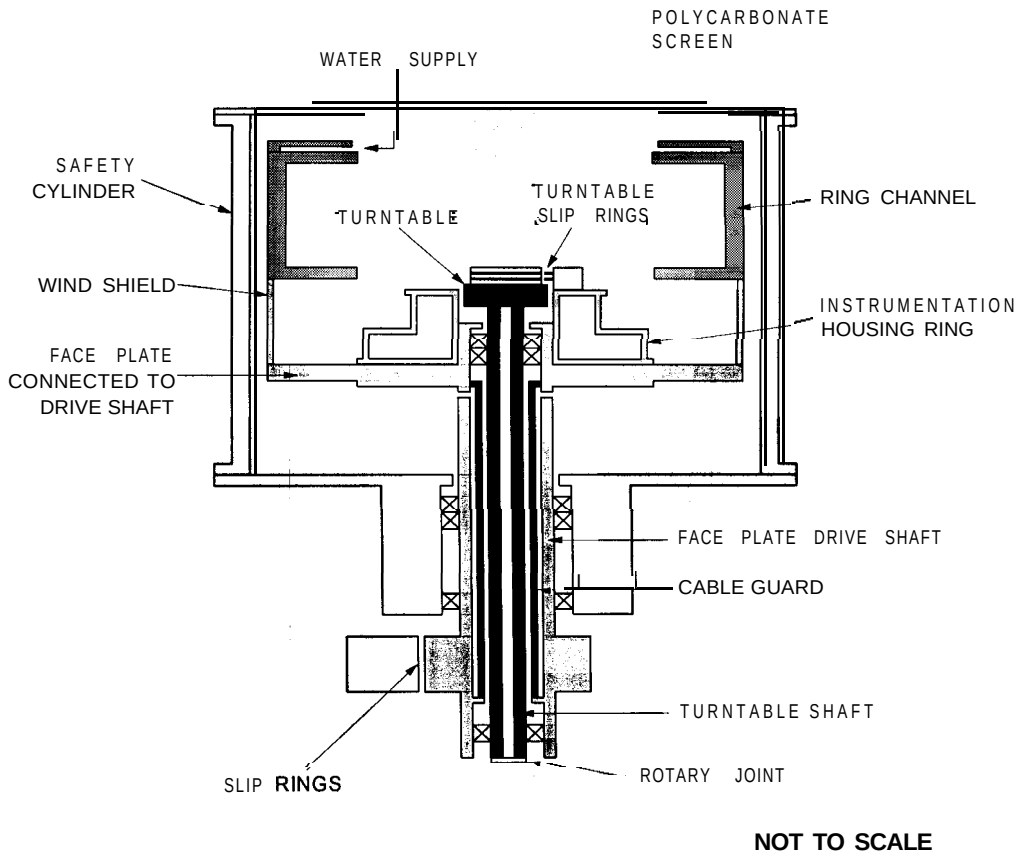

Figure 2 - Section through Mk II Mini-Drum Centrifuge with Axis Vertical

Figure 2 shows a section through the main rotating components of the centrifuge and their housing. The face plate serves to support and drive both the ring channel and the instrumentation housing ("doughnut") ring. The face plate is permanently secured to a shaft which is rotated (via a drive belt) by a Parker Digiplan ZX640 motor'. The maximum spindle speed of the motor limits the face plate to a maximum of 1067rpm. This corresponds to 471g at a radius of 370mm (the base of the channel). There are twin shafts with a central turntable shaft which is driven concentrically to the face plate. Its velocity and/or orientation relative to the face plate can be varied. Velocities of $V_{FP} \pm 100$rpm can be achieved.

The centrifuge and any models therein are viewed in flight with a hand-held stroboscope[6]. This can be set to trigger at either the main face plate speed or the turntable speed, should this be different.

2.4 Dimensions

The ring channel of the Mk II mini-drum has a width of 180mm and a depth of 120mm. The inner and outer radii of the channel are 250mm and 370mm respectively. These radial dimensions are an order of magnitude smaller than those in a typical beam centrifuge . The effect of this reduction on the accurate modelling of prototype stresses is examined in detail in Appendix A.

2.5 Slip-rings

There are 20 electrical slip rings connecting the face plate shaft with the external environment; the number of electrical slip-rings is limited by the friction between the brushes and the shaft. Slip-rings l-10 are used to supply power and control to the variable level standpipe and power to the turntable slip rings; 1 l-20 are allocated for the operation of the data acquisition system in the doughnut ring.

There is a rotary joint at the base of the central shaft through which high-pressure air at 100psi is supplied to the rotating environment.

2.6 Turntable slip-rings

Any actuator mounted on the central turntable which has to rotate relative to the face plate receives power via the additional turntable slip-rings, as shown in figure 2. A variable voltage, ± 15V, is supplied via two of the main slip-rings to a pair of spring-mounted brushes fixed on top of the doughnut ring. The turntable slip-rings comprise two circular copper discs between insulating plates.

---

[5] 4.40kW, rated speed 1600rpm, rated current (line) 14.1 A (rms.)

[6] Turbostrobe 333 Digital stroboscope (capable of O-360" phase shift and frequencies from 60-18500Hz)

2.7 Water supply and drainage

Water is supplied to the channel as shown in figures 2 & 3. Water supplied in this way will go into the base of the model through two diametrically opposite supply holes. Water can be added directly to the surface of any model in the channel but this can cause scouring problems. In cases where identical water supply (and drainage) conditions around the entire periphery of the channel are required, a high permeability base layer is used.

Drainage from the channel is also through two diametrically opposite drainage holes in the channel wall. Water flows from these holes into a circular drainage tube which in turn is connected to a standpipe. Two Druck PDCR81 350 kPa pore pressure transducers are installed in the drainage tube to enable the water pressure in the drainage layer at the base of the model to be monitored.

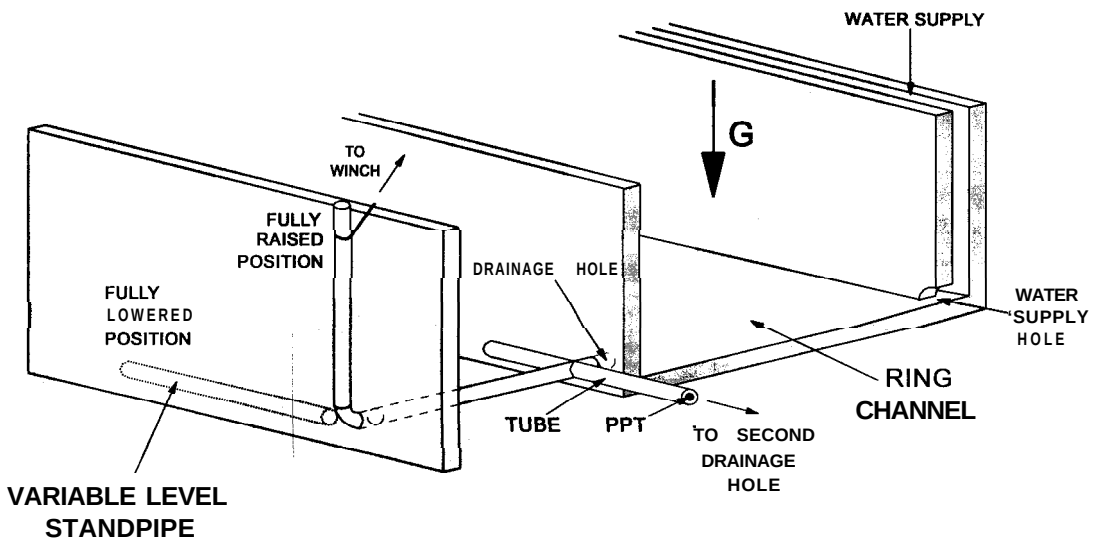

Figure 3 - Schematic Isometric View of Channel Drainage and Variable Level Standpipe

2.8 Variable level standpipe

The inclination of the standpipe can be controlled by an air motor so as to change the maximum level of water in the channel. The general arrangement is shown in figure 3.

High-pressure air is supplied at 100psi via a rotary joint slip-ring at the base of the turntable shaft to two three-port solenoid valves, which are connected to the air motor[7]. The choice of solenoid valve engaged and hence the direction of rotation of the motor is controlled by the external operator.

The standpipe winch motor, rated at 2300rpm, is connected via a planetary gearhead to a capstan, forming a winch capable of 7.5 rpm and completely raising or lowering the standpipe in 25 seconds. Limit switches are set at the extremities of travel.

A rotary potentiometer[8] is connected to the capstan. The output from this is transmitted via the slip-rings and is monitored using a digital voltmeter (DVM). The maximum water level in the channel can be controlled to ±1mm in this way.

[7] Type: Atlas Copco LZB 11A,-AR
[8] Type: Spectrol 10 turn MOD534

2.9 Data acquisition

The data acquisition system is located in the instrumentation housing ring, shown in figure 2. Around the periphery of this housing there are 16 ports for amphenol bayonet lock connectors. The power supplied to these ports is controlled by means of switches inside the housing. It is possible to supply ±5V, or OV and ±5V

A schematic diagram of the data acquisition set-up is shown below (figure 4). The multiplexer unit within the doughnut ring is controlled by means of an S-bit binary signal from the data acquisition terminal. This signal carries information setting the gain for each of the 16 channels via the Programmable Gain Amplifier (PGA) card and controlling the multiplexer's frequency of cycling through the channels. The multiplexer is only capable of cycling through the channels sequentially, which can impose limitations on the data acquisition capabilities - Barker (1996) gives further details.

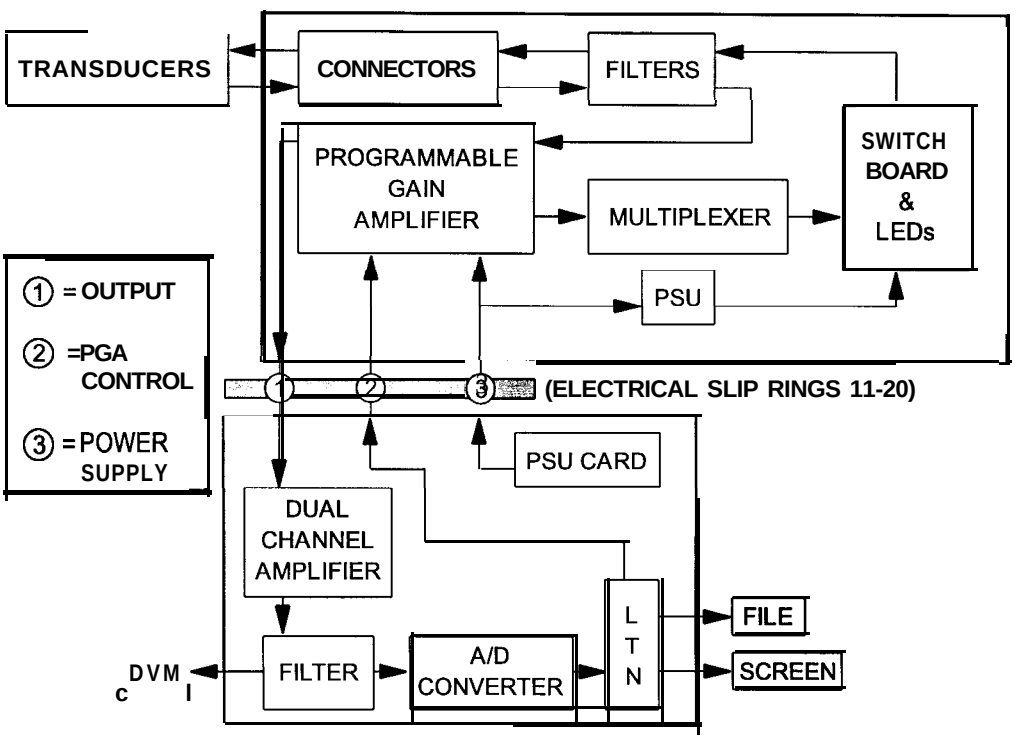

Figure 4 - Schematic Diagram of the Mini-Drum Data Acquisition System

Output data passes through a dual channel amplifier (with a gain of unity), is filtered and is then converted by an Analogue to Digital (A/D) card. This digital signal is processed by the data acquisition software Labtech© Notebook' (LTN).

[9] Initially LTN 7.30 on a PC-610 Industrial Computer, then from March 1997, LTN 8.0 for Windows on a Dell Optiplex PC.

3 PREPARATION OF CLAY SAMPLES

3. I Introduction

Clay for tests in the Mk II mini-drum centrifuge is prepared by consolidation from slurry in-flight. This section describes a new technique developed by the authors, different from that used by Evans (1994). The following section addresses some of the issues raised by such consolidation from slurry at high g-levels.

3.2 Previous technique

The previous technique for introducing clay slurry to the channel was developed by Evans (1994) on the similar Mk I mini-drum centrifuge.

The pre-consolidation procedure took place with the mini-drum axis in the horizontal position. A fixed paddle (178mm wide) was positioned such that its tip could be raised or lowered within the rotating channel.

The base drainage layer consisted of sand: 10mm depth of coarse 14/25 Leighton Buzzard sand overlain by 5mm of finer 100/170 Leighton Buzzard sand. This was poured into the channel in-flight. Following saturation of the sand layer, clay slurry was poured onto the paddle and thence down into the channel. The height of the paddle blade was continually adjusted so as to be just above the surface of the clay slurry at all times.

Once clay pouring was complete, the paddle was removed and the mini-drum was rotated until its axis was vertical. Consolidation proceeded in this orientation.

3.3 Need for improvement

3.3.1 Channel obstruction

The use of a paddle to pour clay slurry into the channel in a controlled manner requires that the channel is completely free from obstruction prior to pouring. The need to accurately position instrumentation within the clay (both during consolidation and for subsequent tests) led to the development of perspex instrumentation mounts fixed to the base of the channel and the need for a different method of clay preparation.

3.3.2 Base drainage layer

The use of a sand base drainage layer also imposes limitations on the technique. If the sand particles are too large, or the clay particles too fine, the clay will filter through the drainage layer and be lost. The filter bed theory espoused by the US Army Waterways Experiment Station in the 1940s quoted a factor of 5 between the d_{15} drainage layer size and the d_{85} clay particle size before any loss of fines will take place. Taylor (1948) cites experimental evidence showing that the ratio may in fact be as high as 10 before significant problems arise. Potter (1996) quotes the d_{15}/d_{85} ratio for 100/170 sand and E-grade kaolin as 6.3, which is acceptable using the Taylor criterion. For speswhite kaolin, the ratio is 3 1.6 and a significant loss of clay into the drainage layer would be expected. An alternative method of base drainage is therefore preferred when speswhite kaolin is to be used in the mini-drum centrifuge.

[10] The technique was first reported briefly by McKinley *et al* (1996). Contaminant migration test BAP2 was conducted on a clay specimen prepared by the first author using the new technique for the first time.

3.4 New technique

3.4. I Introduction

The new technique developed to pour clay slurry has been used since February 1996 on ten tests'[1] in the mini-drum centrifuge. Both E-grade and speswhite kaolin have been successfully poured. Two changes have been made:

- the sand base drain is replaced by a geotextile layer;
- a spreader is used to pour the clay with the axis of the mini-drum vertical.

The latter change eliminates the need for tilting the mini-drum in-flight and will result in future mini-drums being safer and more robust.

3.4.2 Preparation

Prior to clay pouring, a 6mm geotextile[12] base drainage layer is fixed around the channel. This allows drainage both through and in the plane of the geotextile, creating identical drainage conditions around the entire periphery. Holes are cut where necessary to allow instrumentation mounts to be fixed to the channel base. The bases of these mounts are made from 6mm thick perspex so that their tops lay flush with the geotextile. A layer of filter paper is placed on top of the geotextile and instrumentation mount bases, to reduce any loss of the finer clay particles into the geotextile. Transducers are fixed as appropriate and connected securely to the doughnut ring.

3.4.3 Spreader

With the mini-drum axis vertical, the clay spreader is fastened to the central turntable. The spreader consists of two horizontal PVC pipes (3 lmm 0) connected to the base of a vertical PVC pipe (73mm 0). The two horizontal pipes extend 217 mm from the central pipe, bringing their nozzles 3mm beyond the inner channel radius (250mm). The pipe soffits are 9mm above the channel. See figure 5.

3.4.4 Clay Pouring

With the face plate and turntable running at 155rpm and with the standpipe fully raised, the base drain is saturated with water. The turntable is taken to V_{FP}+3rpm and clay slurry[13] is poured continuously into the rotating spreader via a stationary funnel (see figure 5) until the desired quantity has been added. Weighing by difference is used to determine the mass of slurry added.

---

[11] Test designations: BAP2 (McKinley et *al* 1996), MCB1 (McBride 1996), HRB04a, HRB04b, HB01, HB02, HB03, HB04, HBA36 (Barker 1997) and 2 tests for the MEng Module A3 ***'Geotechnical Modelling'***

[12] Filtram, supplied by ICI Fibres Ltd. It consists of a 100% polyethylene 'Netlon' structured core between two sheets of Terram 1000, a non-woven filter membrane.

[13] In tests to date, E-grade kaolin slurry has been poured at 100% moisture content, speswhite kaolin at 120%. The slurry is mixed for 24 hours below a vacuum prior to pouring, to achieve as near to 100% saturation as possible.

The funnel is then rinsed with water to ensure that all of the calculated mass of slurry has indeed been transferred to the channel. This results in several millimetres of water overlying the slurry at the start of consolidation, which is desired ▪ see Section 4.4.2.

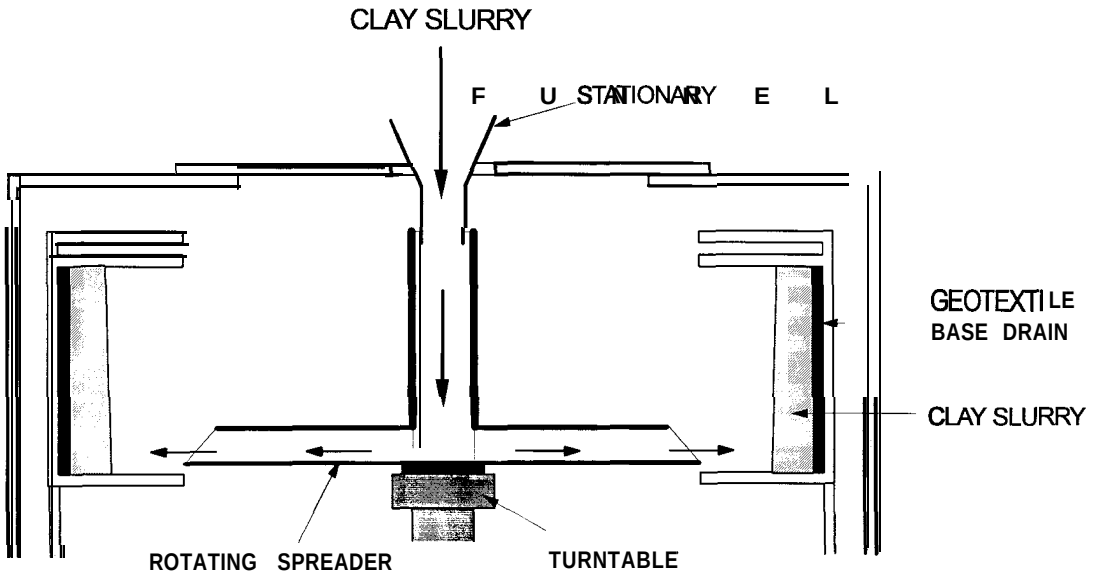

Figure 5 ▪ Clay Pouring Technique

4. CONSOLIDATION

4. I Introduction

Once the slurry pour was completed, the in-flight consolidation procedure commenced. Procedures varied according to the desired final state and stress history of the clay layer for each individual test.

Evans (1994) found that consolidating from slurry at high g-levels could initiate pockmark formation on the surface of the clay. He found that this could be inhibited by the presence of a downwards hydraulic gradient due to seepage during consolidation, but did not fully investigate the reasons for it.

It is inappropriate to use the standard Terzaghi expression

$$\frac{\partial U}{\partial t} = C_v \frac{\partial^2 U}{\partial t^2}, \qquad (1)$$

to predict excess pore pressure dissipation during consolidation, as there are large strains and changing permeabilities involved in the consolidation from slurry. Instead, the Gibson *et al* (1967) general governing equation for self-weight consolidation from slurry will be used along with the Lee & Sills (1981) solution. This solution equation (4) will be quoted directly for a full discussion of its derivation and adaptation for use in a centrifuge environment, the reader is referred to Barker (1997).

4.2 Pockmarking

Pockmarks are formed on the surface of the clay due to piping within the sample. They arise when clay is consolidated under increased self-weight and they are especially significant when consolidating from slurry in the mini-drum centrifuge. Evans (1994) conducted a series of tests in the Mistral benchtop centrifuge to investigate their formation, plus three tests in the Mk I mini-drum centrifuge. His key findings were:

- pockmarking is not due to air escaping from the sample;
- samples undergoing re-consolidation do not experience pockmarking;
- pockmarking only occurs after a short period of consolidation has elapsed;
- externally applied hydraulic gradients/seepage flows during consolidation can promote/inhibit pockmark formation.

4.3 Hydraulic gradients

4.3. I Introduction

The hydraulic gradient within a pore fluid is defined as

$$i = -\frac{1}{\gamma_w}\frac{\partial u}{\partial z}. \qquad (2)$$

Piping in sand has been observed by many researchers to occur at a critical hydraulic gradient - one at which the water pressure at a certain depth is equal to the weight of solid particles above that depth. This critical hydraulic gradient is given by

$$i_{crit} = \frac{G_s - 1}{1+e} \qquad \left(= \frac{\gamma - \gamma_w}{\gamma_w}\right) \qquad (3)$$

Evans (1994) proposed that piping occurs in a clay sample if i approaches i_{crit}.

4.3.2 Pore pressures & hydraulic gradients during consolidation

When the slurry is initially poured into the channel at N g, the pore water pressure distribution is as shown in figure 6a* . If the pour is completed instantaneously, there is initially zero effective stress throughout the slurry, although this is never achievable in practice. The idealised excess pore pressure profile is shown in figure 6b as the straight line for T=O.

The initial hydraulic gradient throughout the slurry is i_{crit} by definition - the entire weight of the slurry is being supported by water pressure. As (two-way) consolidation progresses, the excess pore pressure will dissipate as shown, according to the equation

$$U_{(z,t)} = 2Ng(\rho_s - \rho_w)z_0 \sum_n \frac{\sin n\pi y}{n\pi} \exp(-n^2\pi^2 T), \qquad (4)$$

where n=l, 2, 3 . . . . . [after Evans (1994)]

$$\text{and} \quad T = \frac{C_F t}{z_0^2}. \qquad (5)$$

. The overall depth of clay will change with time. Figures 6a, b & c are plotted for normalised height, z/z_0 (=y), where z_0 is the current height of the clay surface.

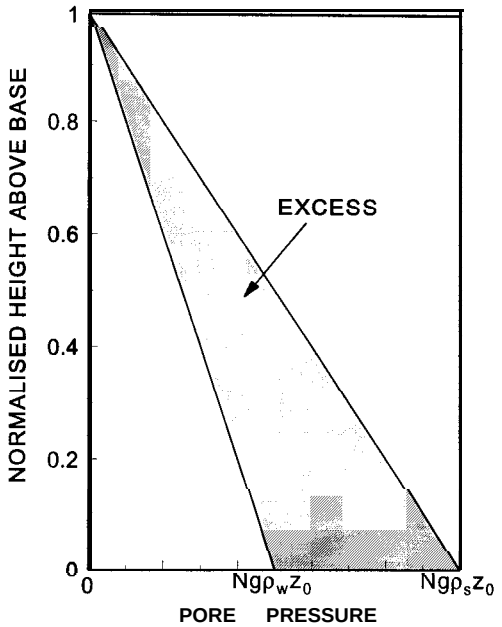

Figure 6a - Initial Pore Pressure Distribution

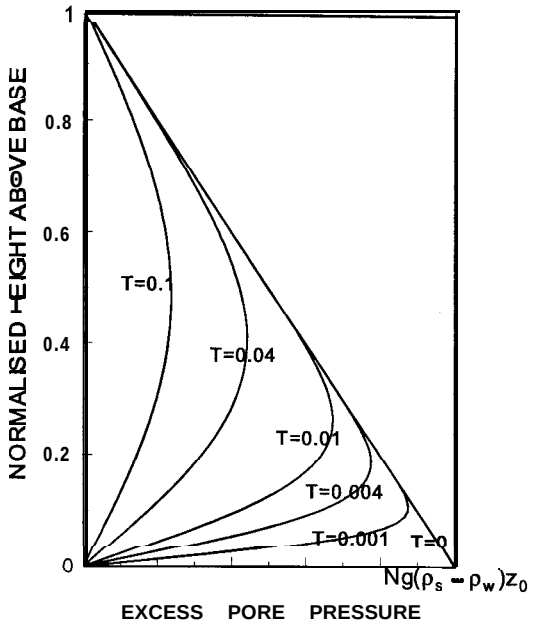

Figure 6b - Excess Pore Pressure Dissipation

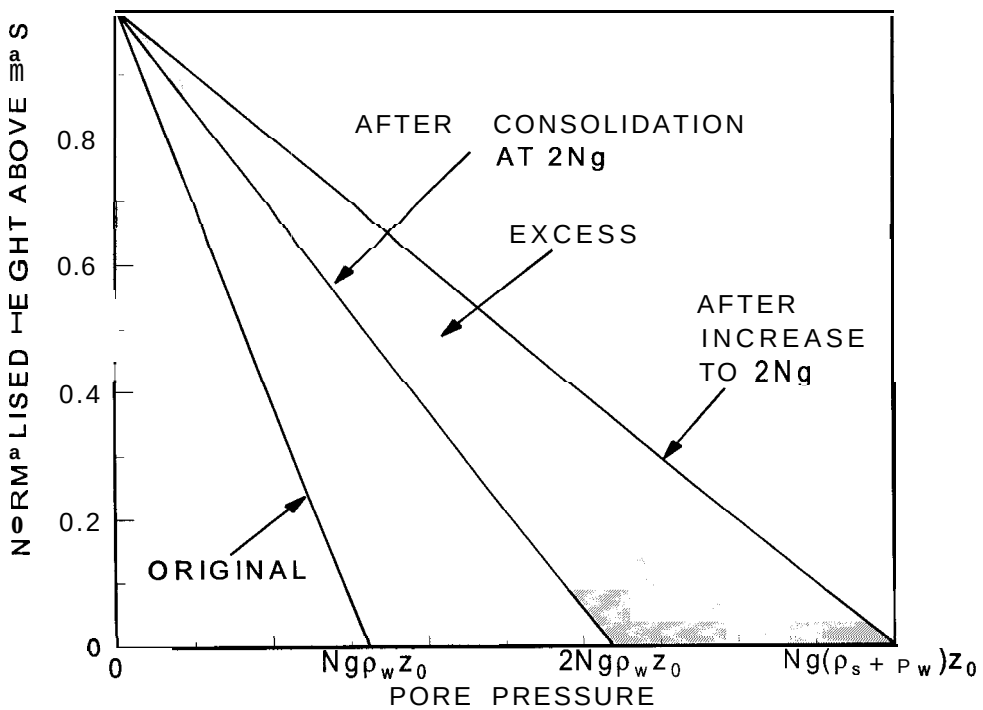

Figure 6c - Pore Pressure Distribution, Ng to 2Ng

Once consolidation is complete at N g, the g-level can be increased further to a value of e.g. 2N g. This produces pore water pressure and excess pore water pressure profiles as shown in figure 6c. The excess pore pressures generated and their dissipation with time are as for the initial N g consolidation (figure 6b). The hydraulic gradient profile and its variation, however, is not the same for this second g-level stage. There is now an effective stress of $(\rho-\rho_w)Ngz$ at any depth at the start of consolidation and the pore water pressure only supports the self-weight increase of the solid particles due to the increased g-level. The hydraulic gradient no longer starts with an initial value of i_{crit} throughout the clay. It can be seen from figures 6c that for any g-level rise, from g_{orig} to g_{new}, the maximum positive value of i possible is given by

$$i_{max} = i_{crit}\frac{g_{new} - g_{orig}}{g_{new}}, \qquad (6)$$

4.4 Applied hydraulic gradients

4.4. I Introduction

It is possible to control the water pressure in the base drain during consolidation by altering the level of the variable standpipe. Hydraulic gradients can be applied across the whole model in either direction using this method.

In his three tests on the mini-drum, Evans (1994) found that the application of an upwards hydraulic gradient (raising the water level in the outer water supply ring) promoted pockmarking, while applying a downwards hydraulic gradient appeared to inhibit pockmark formation. He stated simply that

> *'It seems that vector addition of the actually applied hydraulic gradient and that due to consolidation will yield the actual value of hydraulic gradient at a point and therefore determine whether piping will occur. '*

4.4.2 Application and maintenance of applied hydraulic gradients

In a simple example of an applied hydraulic gradient, with the standpipe completely lowered to give zero water pressure in the base drain and the surface just wetted, the post-consolidation steady-state condition has zero water pressure and a downward hydraulic gradient of 1 throughout the model as shown in figure 7. In order to maintain this condition, water must be added to the surface at the same rate at which it is lost into the base drain. Direct addition (e.g. via the still rotating spreader) is the only option available, but it can lead to scouring as the water impacts on the clay surface.

To reduce this problem, a layer of water is maintained above the surface of the clay, with the standpipe raised to an appropriate height if a downwards hydraulic gradient of 1 is still desired.

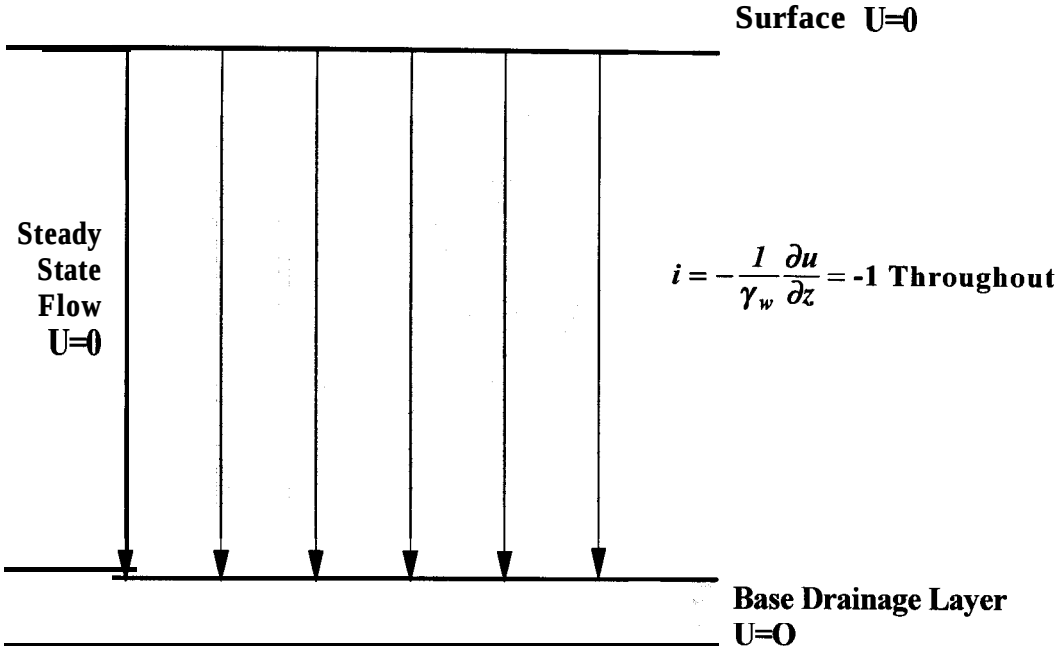

Figure 7 - Steady State Condition, Standpipe Fully Lowered

4.4.3 *Effect of applied hydraulic gradients*

During normal consolidation under self-weight, the vertical effective stress at a particular depth z is given by the buoyant weight of solid particles above that point:

$$\sigma_v' = \int_0^z \frac{Ng(\rho_s - \rho_w)}{1+e}\, dz \qquad (7)$$

If there is an applied hydraulic gradient, there will also be a drag force acting on the soil particles due to the seepage flow[14]. This leads to a change in the effective stress at any depth

$$\sigma_v' = \int_0^z \left[\frac{Ng(\rho_s - \rho_w)}{1+e} + \rho_w iNg \right] dz, \qquad (8)$$

and consequently a changed void ratio distribution. A detailed analysis of these changes is beyond the scope of this report and the reader is referred to Evans (1994) and Barker (1997).

[14] Model tests on sand conducted by e.g. Zelikson (1969), (1978), Yan & Byrne (1989) used a downwards hydraulic gradient in order to increase the self-weight of the soil particles and hence allow reduced-scale modelling

4.5 Consolidation procedure used

Equation (6) suggests that it is the early stages of consolidation which are most vital when determining whether or not pockmark formation will occur. Applied downwards hydraulic gradients have been shown to inhibit pockmark formation. There is also evidence[15 16] to suggest that the magnitude of g-level increments in the early stages of consolidation can influence pockmark formation. Taking these factors into account, the procedure used is therefore as follows:

- to consolidate initially in the presence of an applied downwards hydraulic gradient, pouring the slurry at a low g-level and making several small g-level increments;
- substantial dissipation (85%) of excess pore pressures is allowed for on each successive consolidation increment before increasing the g-level further;
- immediately following the deposition of the clay slurry, the speed is increased to 150g and then returned again to its initial value. This surge technique has the effect of quickly smoothing out any irregularities in the surface profile of the slurry. Not enough time is allowed for the formation of pockmarks to begin.

The pore pressure response from a typical PPT within a clay sample (E-grade kaolin) during this consolidation procedure is shown in figure 8.

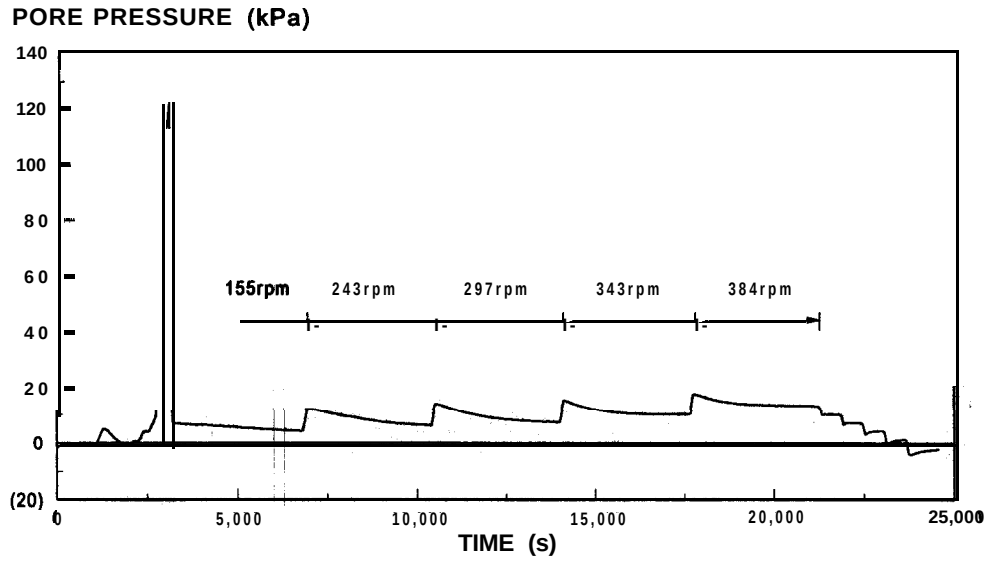

Figure 8 - Test HB01, Day 1. Response of PPT situated 27mm above channel base

[15] Evans (1994)

[16] Tests HRB01 & HRB02 were the first two tests carried out on the Mk II mini-drum centrifuge. In both tests, the original Evans technique was used with the standpipe completely lowered during consolidation - an applied downwards hydraulic gradient of 1. In test HRB 1, the initial consolidation took place at 259rpm. In test HRB2, the initial consolidation was at 155rpm (28g & 10g respectively at the base of the ring channel). Every other aspect of the tests were identical. Severe pockmarking was observed on the surface of test HRB 1. None was observed in test HRB2.

The prediction of the times required for each of the consolidation increments is discussed in the following section.

4.6 Consolidation times

4.6. I Introduction

This section deals with the calculation of times to full consolidation for the clay slurry, using the approach of Lee & Sills (198 1) and Evans (1994). Their approximations and idealisation of the situation will be discussed. The general solution is modified for consideration of second and subsequent g-level increment stages. Times will be calculated for varying degrees of consolidation.

4.6.2 Basic equation

The basic equation to be used is

$$U_{(z,t)} = 2Ng(\rho_s - \rho_w)z_0 \sum_n \frac{\sin n\pi y}{n\pi} \exp(-n^2\pi^2 T), \qquad (9)\ bis\ (4)$$

where n=l, 2, 3 . . . . . [After Evans (1994)]

This was derived using the assumptions that:

1) $C_F = -\frac{k}{\rho(1+e)}\frac{\partial\sigma'}{\partial e}$, varies much less than its component parts and can be assumed to have a constant value;

2) $k \propto$ (1+e)

Assumption (1) is commonly used; k is also frequently approximated by ae^b, Al-Tabbaa (1987), although this does not have the same effect in terms of simplifying the original, highly non-linear equation derived by Gibson *et al* (1967).

4.6.3 Initial conditions

Lee & Sills (198 1) investigated the effects on consolidation of instantaneous dumping of the entire mass of slurry, and of progressive dumping at various rates. Equation (9) is written assuming instantaneous dumping, which is clearly unachievable in practice. However the use of the surge technique (see Section 4.5 above), renders predictions for the first stage very approximate, and (4) suffices.

Of more interest is what happens on second and subsequent g-level increases, an aspect not considered by Lee & Sills (1981), who were working only in a lg environment, or Evans (1994). If full consolidation is assumed at N g prior to a further increase of M g, and the

original assumptions are maintained, the boundary conditions need to be altered but the basic equations to be solved remain unchanged;

Lee & Sills (198 1) (4) becomes $e(z,O) = e_i - \beta(z_0 - z)$, (10)

Lee & Sills (198 1) (8) becomes $e(0,t) = e_i - \gamma z_0$. (11)

Solving the basic equations with these boundary conditions leads to

$$U_{(z,t)} = 2(M+N)g(\rho_s - \rho_w)\frac{\gamma-\beta}{\gamma} z_0 \sum_n \frac{\sin n\pi y}{n\pi} \exp(-n^2\pi^2 T). \quad (12)$$

The initial assumptions lead to the expression

$$\frac{\gamma-\beta}{\gamma} = \frac{M}{M+N} \quad (13)$$

Equation (12) can thus be written

$$U_{(z,t)} = 2Mg(\rho_s - \rho_w)z_0 \sum_n \frac{\sin n\pi y}{n\pi} \exp(-n^2\pi^2 T). \quad (14)$$

Clearly, pore pressure dissipation during second and subsequent consolidation stages due to further increases in g-level can also be predicted using the basic equation (9) or (14).

4.6.4 Degree of consolidation

For T > 0.1, U_{max} occurs for y=0.5. Equation (9) then reduces to

$$U_{max} = 2Ng(\rho_s - \rho_w)z_0 \sum_m \frac{\sin(2m+1)\pi/2}{(2m+1)\pi} \exp(-\pi^2 (2m+1)^2 T), \quad (15)$$

where m=O, 1, 2, 3.....

The m = 0 term dominates[17] for T >0.1, giving

$$U_{max} = 2Ng(\rho_s - \rho_w)z_0 \frac{\exp(-\pi^2 T)}{\pi}, \quad (16)$$

and an excess pore pressure profile as shown in figure 9.

[17] m_1 term = 0.012% of m_0 term for T=0. 1

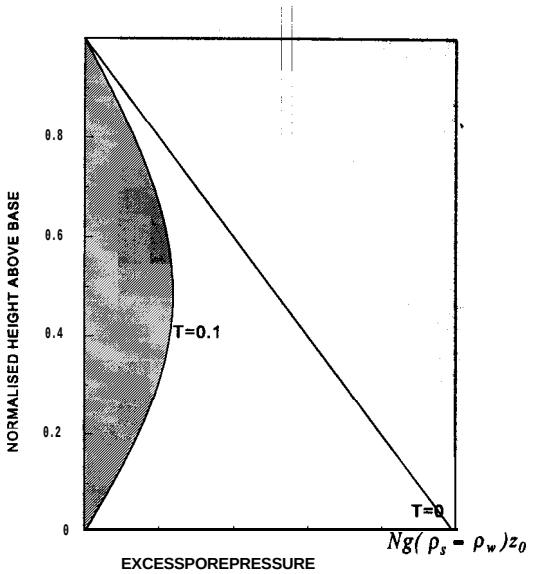

The area of the shaded region is given by

$$\int_0^1 2Ng(\rho_s - \rho_w)z_0 \frac{\sin \pi y}{\pi} exp(-\pi^2 T)\, dy$$

$$= 4Ng(\rho_s - \rho_w)z_0 \frac{exp(-\pi^2 T)}{\pi^2}$$

Figure 9 - Excess Pore Pressures, T=0. 1

The degree of consolidation completed is given by

$$R = \frac{\textit{Current Settlement}}{\textit{Final Settlement}} = 1 - \frac{8 exp(-\pi^2 T)}{\pi^2}. \qquad (17)$$

[cf. Lee & Sills (1981), eqns (22), (25)]

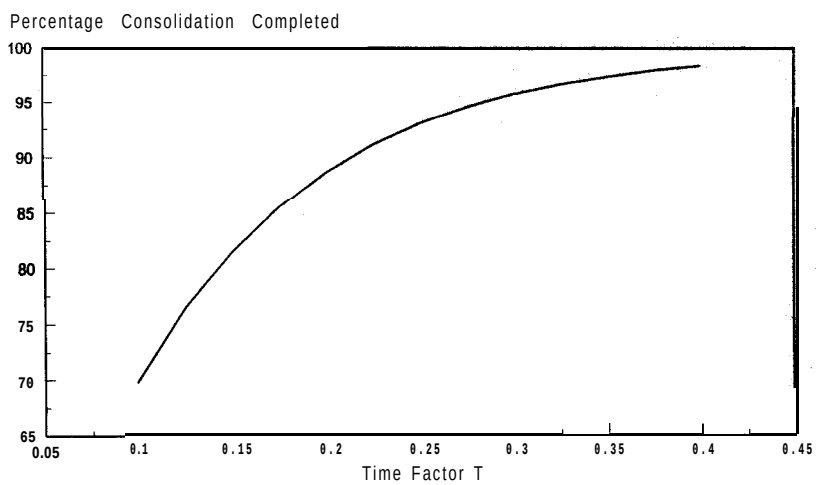

Figure 10 - Percentage Consolidation Completed

4.6.5 C_F for E-grade and speswhite kaolin

$$C_F = -\frac{k}{\rho(1+e)}\frac{\partial \sigma'}{\partial e}, \tag{18}$$

As stated previously, during consideration of finite strain consolidation, it is often assumed that the variation of C_F is much less than that of its components.

Summarising previous work, Elmes (1985) quoted values for speswhite kaolin as $0.5 mm^2 s^{-1}$ for normal consolidation and $1 mm^2 s^{-1}$ for isotropic rebound. There has been substantially less work carried out previously using E-grade kaolin. As such there is less certainty about its material parameters and widely varying figures have been previously quoted. Evans (1994) used a value of $0.1 mm^2 s^{-1}$ in his calculations. Elmes (1985) quoted $1 mm^2 s^{-1}$ for normal consolidation and $5 mm^2 s^{-1}$ for isotropic rebound.

PART B

INTRODUCTION

This part of the report describes two mini-drum centrifuge tests undertaken to examine the effect of reinforced and unreinforced embankment construction on soft clay foundations. The tests were conducted as part of the MEng Module A3 'Geotechnical Modelling' taught at CUED.

The two tests were conducted at 100g. In each test a 45mm high embankment was poured on a soft clay foundation layer (55mm deep) around the entire periphery of the mini-drum channel, modelling a 4.5m high prototype embankment. One segment of the foundation layer was reinforced. Construction times were varied between the two tests. The basic test geometry is shown in figure 11 below.

The speed and simplicity of the tests, coupled with the ease of operation of the mini-drum and the capability for the in-flight operations to be viewed directly by the students, made them ideal for demonstrating the principles and practical aspects of centrifuge modelling in addition to the specific effects of reinforcement and construction times.

In addition to their analysis of the two centrifuge tests, the MEng students were required to conduct complementary analysis using GEOFEAP, a finite element package. An introduction to this package and the work of the students is included in Section 9. The three typical coursework reports of a student, covering both aspects of the module, are included in this report as Appendix B.

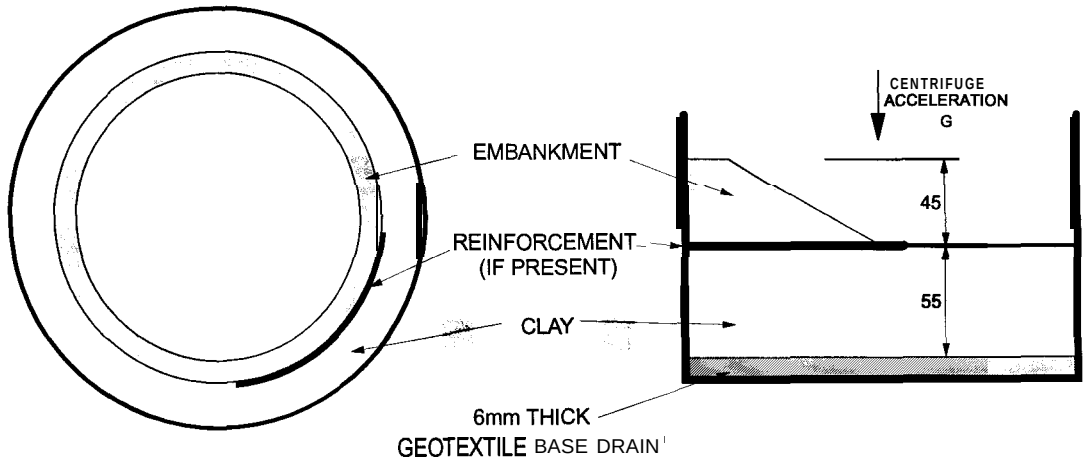

Figure 11 - Basic Test Geometry, MEng Tests

5 PRELIMINARIES

5.1 Materials

5.1. I Soft clay foundation

Speswhite kaolin was used for the soft clay foundation. It has been used for many remoulded soil tests at CUED and its material properties have been listed by Clegg (198 1). Speswhite was used in preference to the more permeable E-grade kaolin in order to allow more pore pressure generation and subsequent dissipation during embankment construction, for the purposes of demonstrating undrained clay behaviour.

5.1.2 Embankment

14/25 Leighton Buzzard sand was used for the embankment.

5. I. 3 Reinforcement

The reinforcement used was the same as that used in earlier beam centrifuge tests by Sharma (1994). It had been produced by Akzo Industrial Corporation BV, The Netherlands, specifically for his 40g tests, and attempted to reproduce the behaviour of a commercially available reinforcement at a scale of 1/40. Exact scaled reproduction proved impossible, but the reinforcement did display the required modulus 1/40 of that of the prototype.

The model reinforcement consisted of lmm strands, spaced at 3.4mm centres. The load-extension curve is shown in figure 12. Full details are given by Springman *et al* (1992).

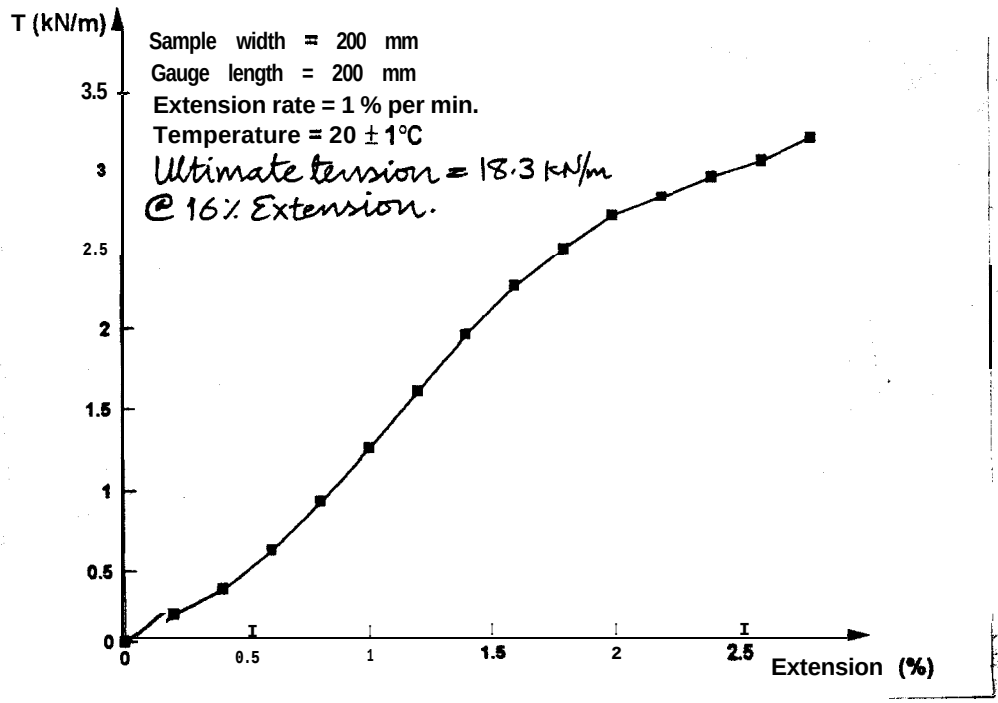

Figure 12 - Load-Extension Curve for Akzo Geotextile Reinforcement (After Sharma (1994))

Clearly, this reduced modulus reinforcement does not scale correctly for the 100g mini-drum tests, but this was not of concern as there was no attempt being made to model a specific type of reinforcement.

5.2 Instrumentation

5.2. I Pore pressure transducers

Druck PDCR81 350 kPa transducers were used throughout. They measure 11.3 mm in length and have a diameter of 6.35mm. They are capable of measuring pressures up to 350 kPa.

A silicon diaphragm is mounted at one end of the PPT. One side is exposed to the test environment; the other one is connected back via a tube to atmospheric pressure. Four strain gauges are mounted on the atmospheric side to form a wheatstone bridge arrangement. For a 5V power supply, the PPT will measure pressures of up to 350kPa to an accuracy of ±0.2kPa.

In order to ensure that the PPT measures pore water pressure and not total stress, a ceramic porous stone is placed over the diaphragm. These are de-aired by boiling in water for two hours, and are installed under water, to prevent any air from being trapped between the stone and diaphragm.

The PPTs were calibrated using a variable water pressure application unit, a digital pressuremeter and the mini-drum data acquisition system (see Section 2.9). The complete mini-drum system was used so as to ensure that there were no inconsistencies in supply voltage between calibration and testing.

The response of the PPTs was linear in the range considered.

5.3 Nominal acceleration

The centripetal acceleration experienced by the model varies with depth, as discussed in Appendix A. All g-levels quoted (and the corresponding rpm values) have been calculated for a radius of 3 1 Omm. This is mid-depth of the channel and the approximate level of the surface of the clay.

6 MODEL PREPARATION

6. I Clay preparation

The clay was introduced to the channel in-flight, as slurry at 120% moisture content, using the method of Section 3. Consolidation took place over two days. The clay was consolidated in stages up to 40g on the first day, with a downwards hydraulic gradient. The machine was then stopped and left overnight. The clay was fully consolidated at 100g (537rpm) on the second day, without the action of a hydraulic gradient. Consolidation times were calculated using the approach of Section 4. On each occasion, a clay layer was produced with a pockmark-free surface.

6.2 *Reinforcement*

105mm x 40mm strips of the Akzo reinforcement were anchored to the wall of the channel and placed over the clay surface, subtending a total arc of 73" circumferentially. The anchoring of the reinforcement for the half-embankment was required so that tension could develop in it. The anchoring system also had to allow for settlement of the centre of the embankment, i.e. the fastening point had to be capable of vertical movement. In order to achieve both of these criteria, the reinforcement was fixed to 35mm square steel plates lmm thick. These plates were placed against the wall and the reinforcement extended outwards from them. The back of the plates were lubricated with grease's to reduce friction between the plates and the wall, thus giving less resistance to vertical movement of the anchoring point. The grease also allows for a certain amount of tension to be developed.

There are two options available for the orientation of the plates with respect to the clay surface. These are shown in figure 13.

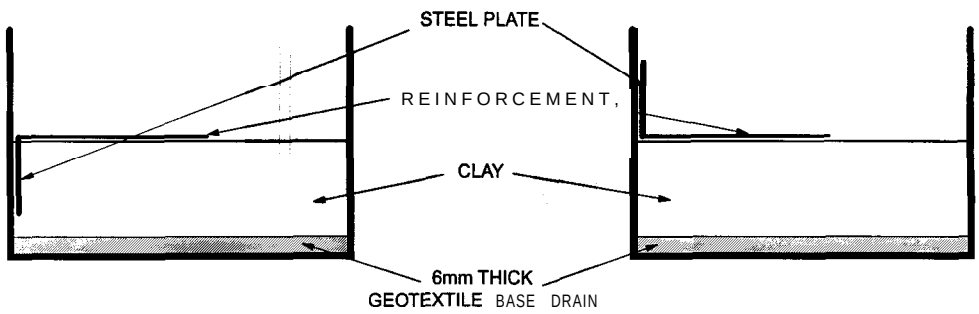

Figure 13 - Reinforcement Plate Orientation Options

Option A, in which the plates are installed between the clay and the channel wall, allows for more tension to be developed than Option B, in which the tensile capacity is provided solely by the adhesion between the wall and the plates given by the grease. However, Option A does not allow for such free vertical movement of the anchoring point as Option B.

Option A was used for the tests with the hopper as the nozzle would have collided with any plates mounted on the wall above the clay - the existing clearance between channel wall and hopper nozzle is less than the reinforcement plate thickness.

[18] **Duckhams** waterpump grease

4.3 Instrumentation

Eight PPTs were used to monitor the reinforced clay. Four on the clay surface, one in the base drain and three embedded in the clay. The latter three were installed prior to the clay pour, fixed to supports fastened to the base of the channel. Eight PPTs were positioned diametrically opposite in an identical orientation to monitor a typical stretch of the unreinforced clay.

The PPTs embedded in the clay were to monitor the build-up and post-construction dissipation of excess pore water pressures within the soft clay. The PPTs on the surface were intended to act as settlement gauges. Any vertical movement of the PPTs would result in a change in measured pressure. This could easily be converted into a distance - at 100g, 1 kPa change in pressure corresponds to a lmm change in depth. Any fluctuation in measured pressures due to a change in water level in the channel could be taken into account by monitoring the PPTs in the base drain.

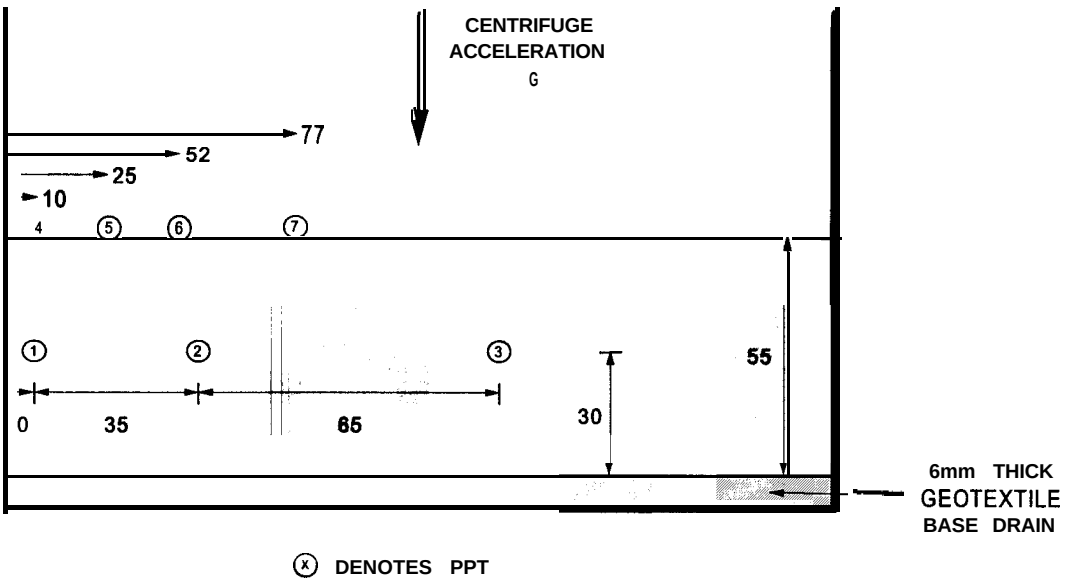

Figure 14 - PPT Locations, MEng Tests (Dimensions in mm)

7 EXPERIMENTAL PROCEDURE

Two tests were conducted at 100g (537rpm). In each test, an embankment 45mm high was constructed using the sand hopper. Construction times were 90 minutes in Test 1 and 40 minutes in Test 2.

7. I Prototype embankment

The models constructed correspond to an embankment 4.5m high at prototype scale. The model construction times correspond to prototype construction times of 625 and 278 days respectively.

7.2 *Sand hopper*

The sand hopper, shown in figures 15a - d, was developed to allow the construction of embankment models at varying rates in the mini-drum centrifuge.

It is mounted on the central turntable. Sand is introduced to the hopper via a stationary funnel in the same way as for the pouring of the clay slurry. With the hopper rotating relative to the clay in the channel, a continuous embankment is produced around the circumference.

The hopper receives power via the turntable slip-rings, driving a motor[19] which extends or retracts the hopper nozzle in-flight (via a lead screw). This enables the sand to be poured from close to the current embankment crest, giving an accurate profile. Sand poured from the nozzle at a significant distance from the existing embankment will develop a vertical component of velocity due to the lg normal gravity, which leads to an incorrect profile.

Constraints imposed by the space required for the motor and lead screw arrangement mean that the embankment must be constructed against the top wall of the channel. Direct observation of the construction is impossible in the early stages but it can be viewed indirectly by means of a mirror mounted on the hopper at an angle of 45".

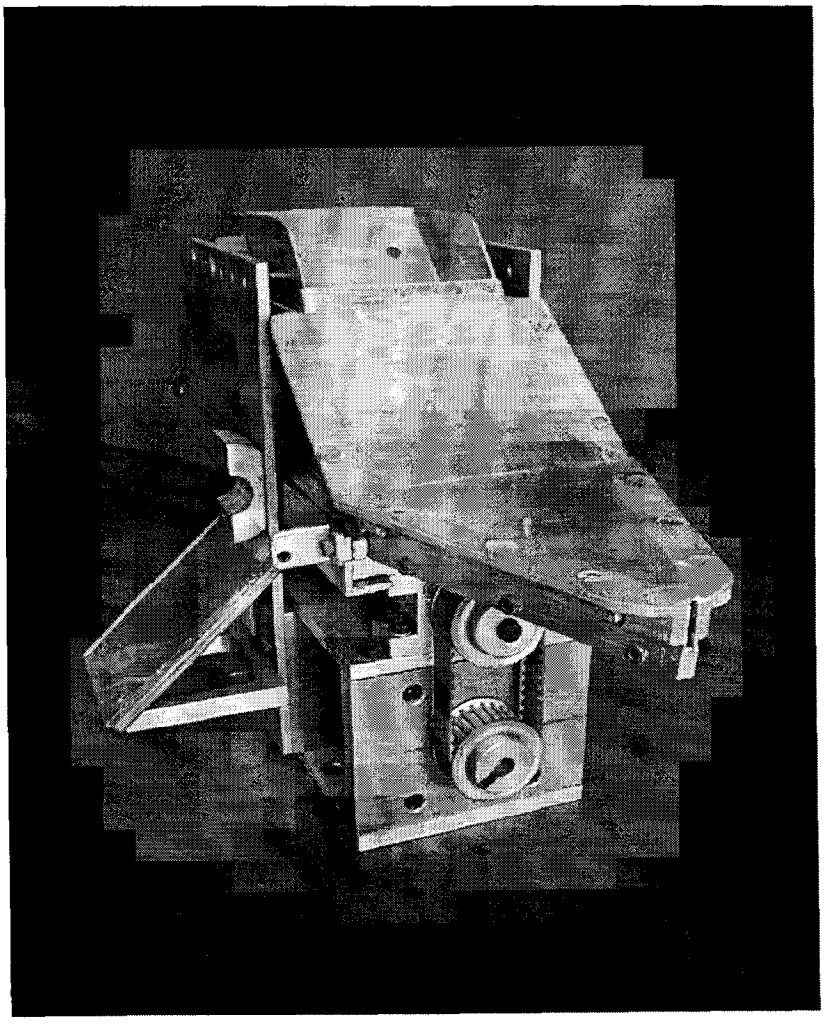

Figure 15a - Sand Hopper

[19] McLennan GM4120 30V geared DC servo motor

Figure 15b - Sand Hopper

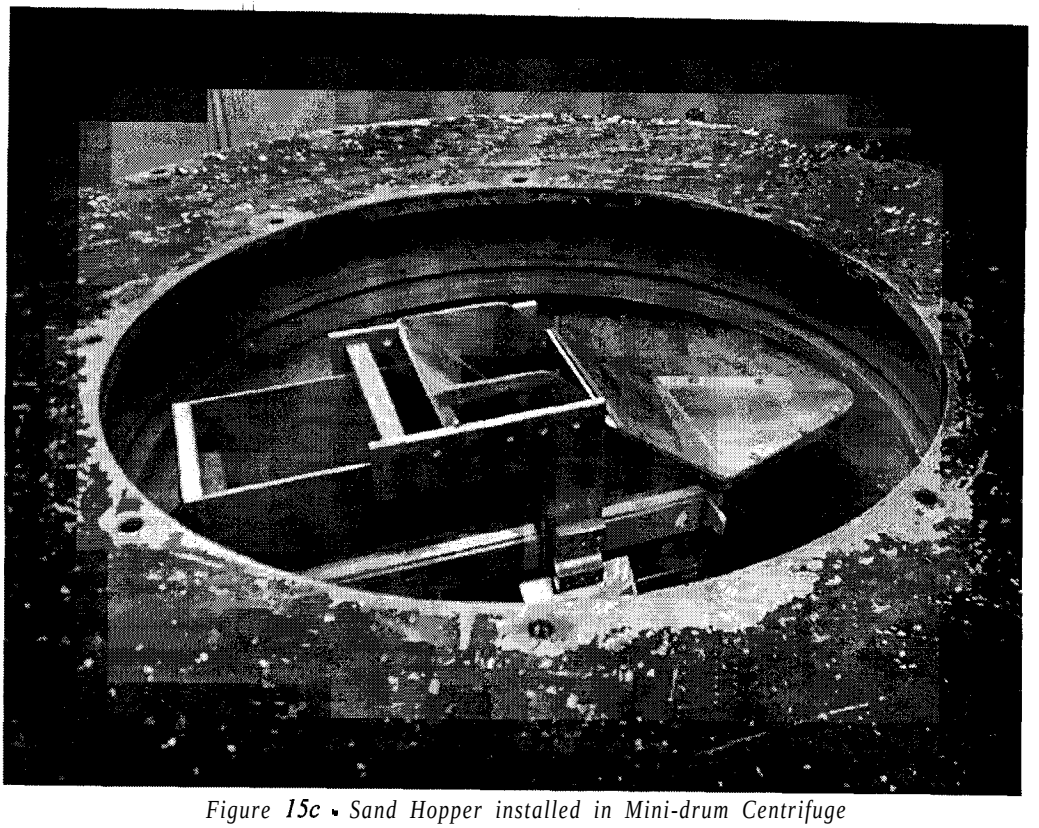

Figure 15c - Sand Hopper installed in Mini-drum Centrifuge

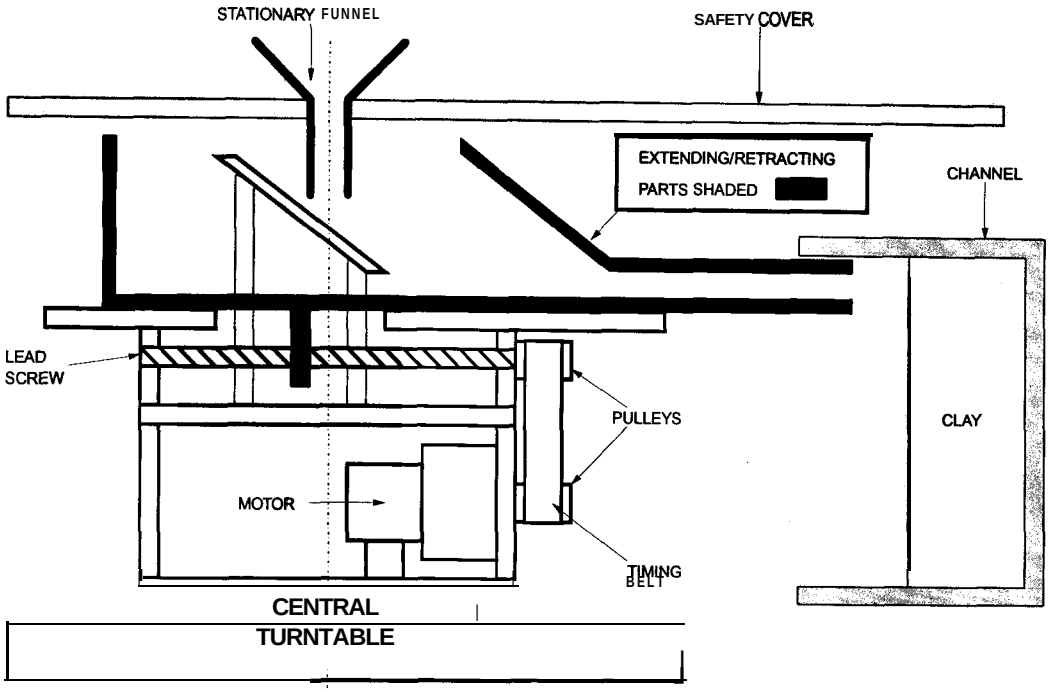

Figure 15d - Schematic Section Through Hopper

7.3 Embankment profile

The slow retraction of the hopper during sand pouring operations produces an embankment with a constant crest width of 16mm. The height of the embankment increases with time, as does the base width. The progressive embankment construction is shown in figure 16.

Inevitably, some sand will be lost from the embankment slope onto the undisturbed clay. This overspill layer had a maximum depth of lmm and so did not significantly affect the loading conditions imposed on the clay.

8 EXPERIMENTAL RESULTS

The results from the two tests are shown in figures 17a to h.

8. I Explanation of graphs

The pore pressures within the clay initially had absolute values of between 25 and 30 kPa. The graphs show the excess pore pressures within the clay, i.e. the pore pressure change from the steady-state pre-construction value due to the deposition of the embankment.

The responses of the surface PPTs have been converted into displacements (see Section 6.3). A positive displacement corresponds to an upwards movement.

The embankment for Test 2 was constructed continuously, at the maximum rate allowed by the hopper nozzle. The embankment for Test 1 was constructed using the same constraint. In order to produce the longer construction time required, the embankment was poured in a number of stages. This is the reason for the numerous maxima on the graphs of Test 1 for $T < 4000$.

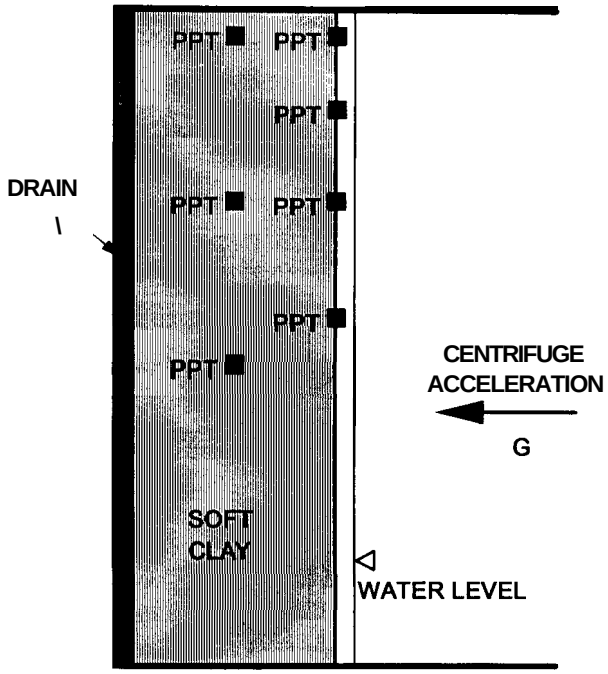

Figure 16a

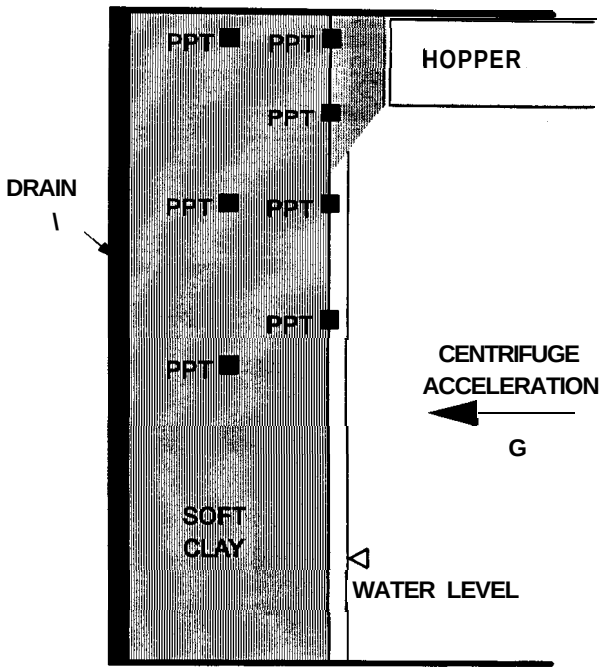

Figure 16b

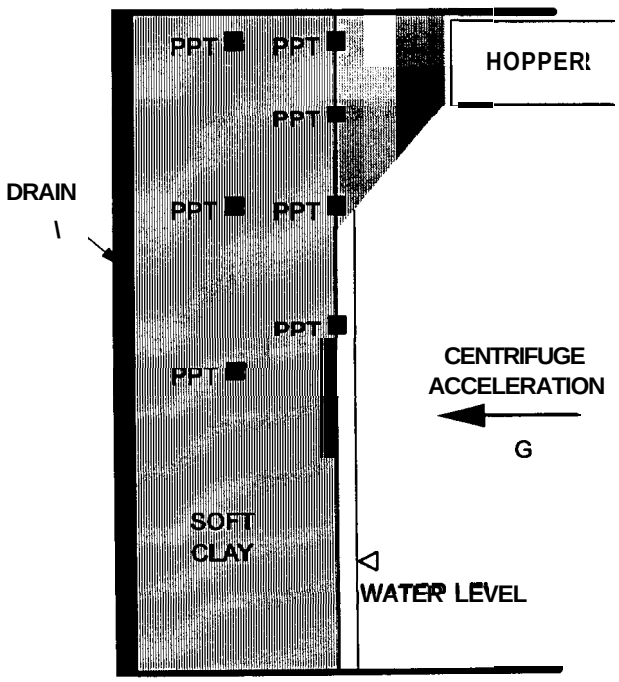

Figure 16c

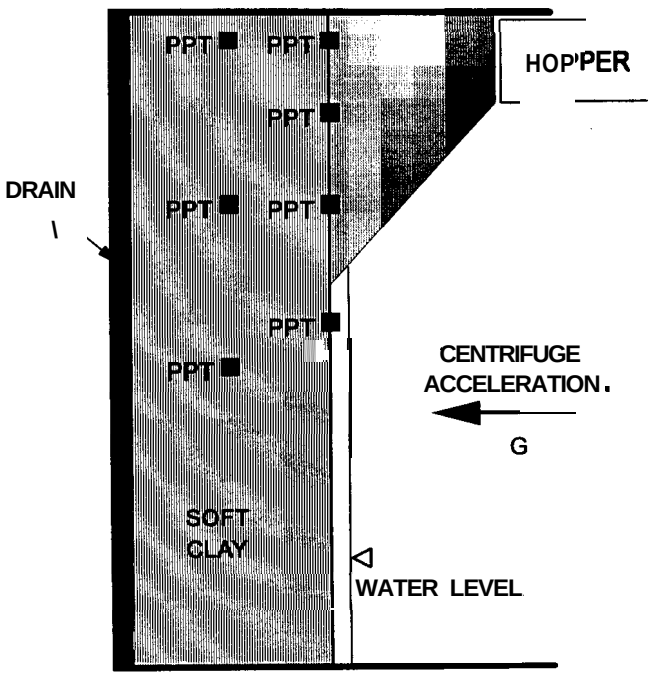

Figure 16d

Figures 16a, b, c & d - Embankment Construction Sequence

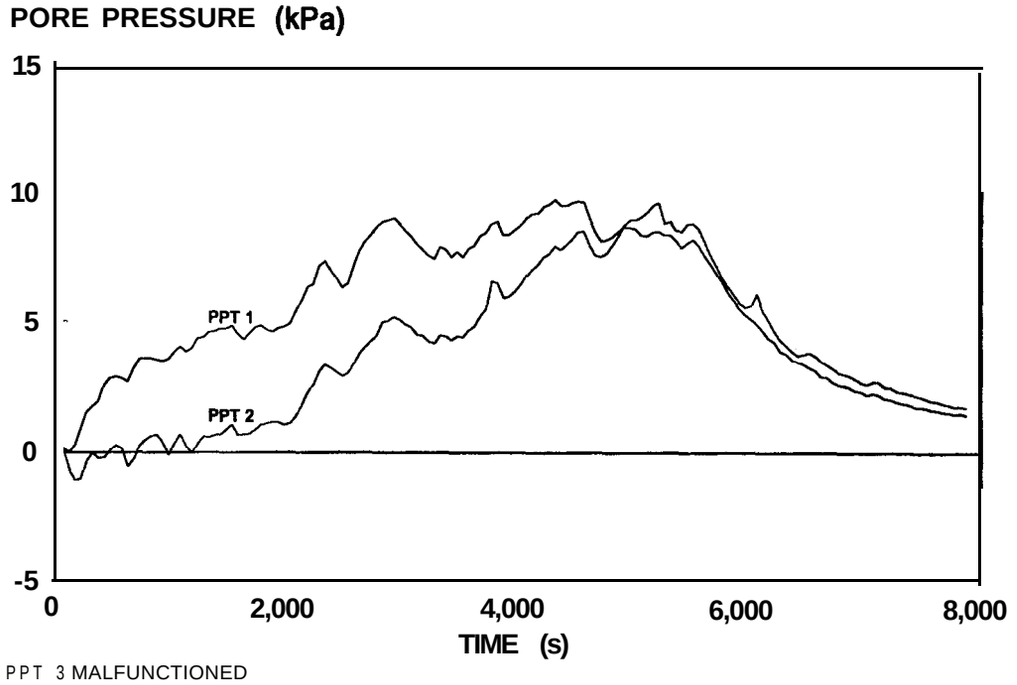

PPT 3 MALFUNCTIONED

Figure 17a - Test 1. Unreinforced Embankment. Excess Pore Pressures within Clay

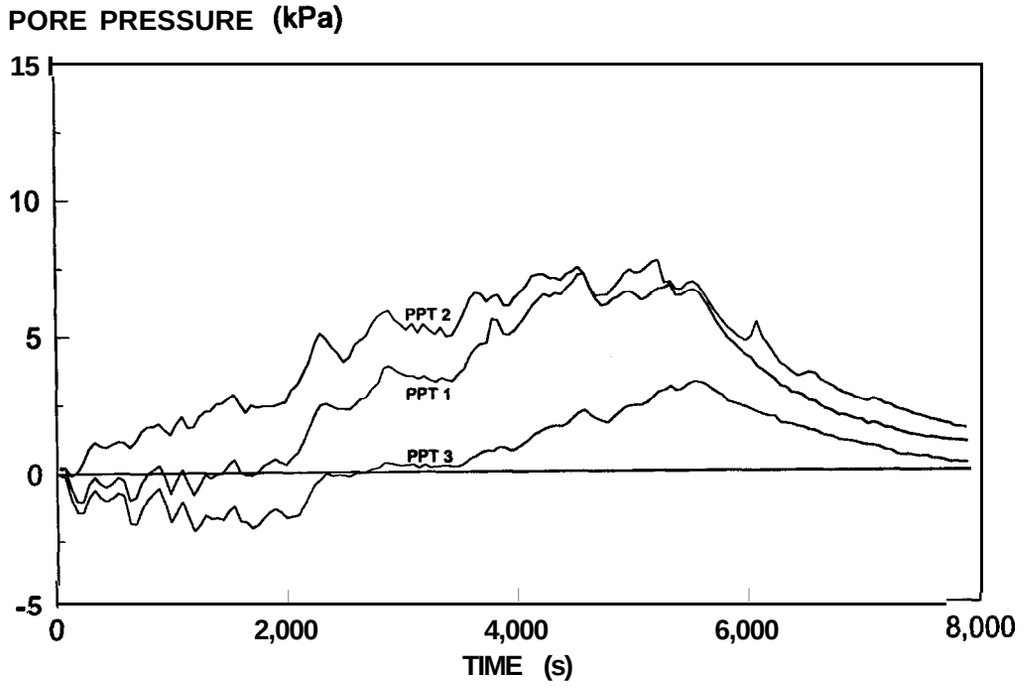

Figure 17b - Test I. Reinforced Embankment. Excess Pore Pressures within Clay

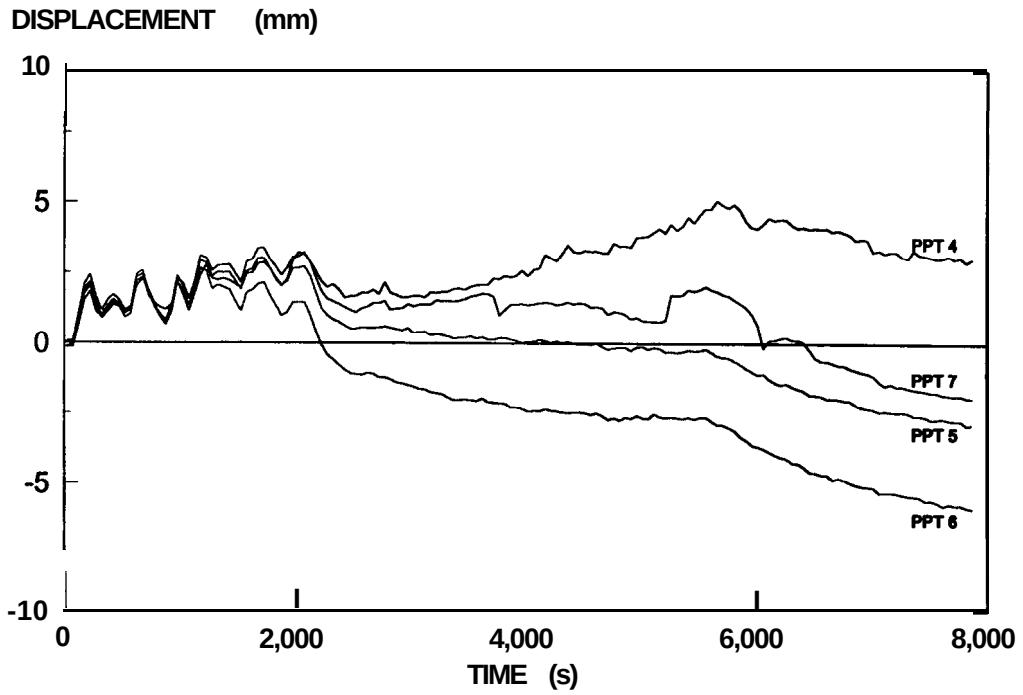

Figure 17c - Test 1. Unreinforced Embankment. Surface Settlements

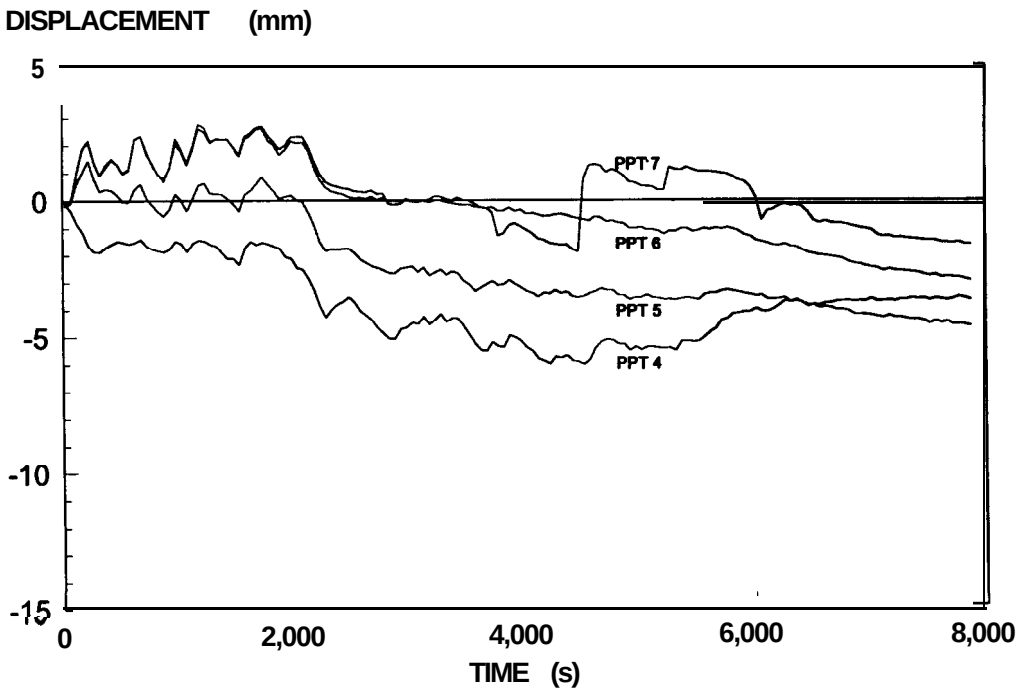

Figure 17d - Test I. Reinforced Embankment. Surface Settlements

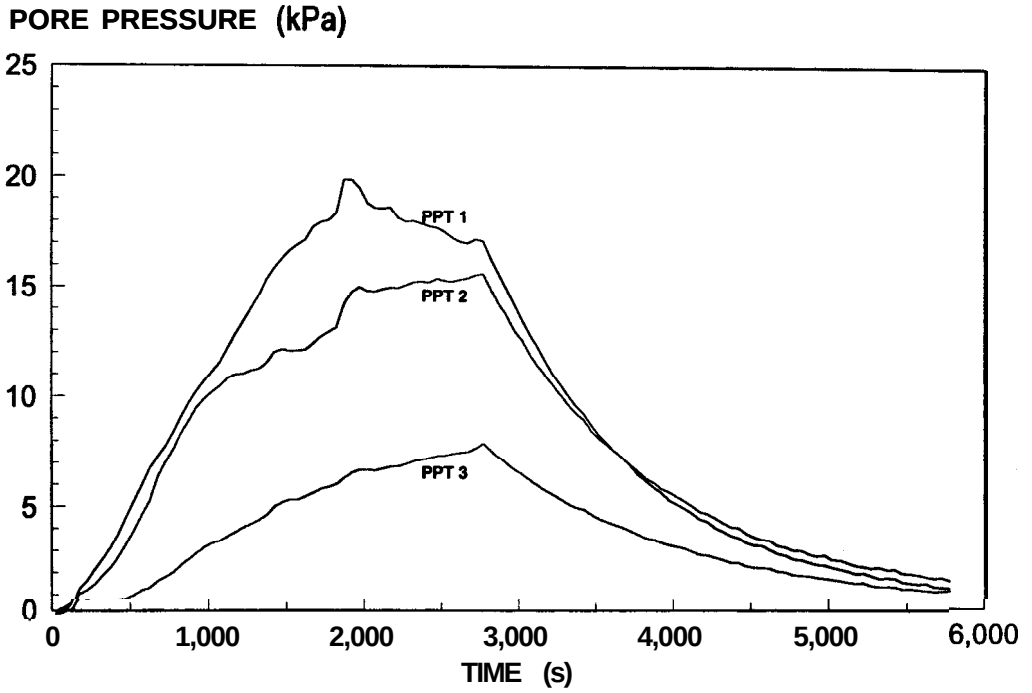

Figure 17e - Test 2. Unreinforced Embankment. Excess Pore Pressures within Clay

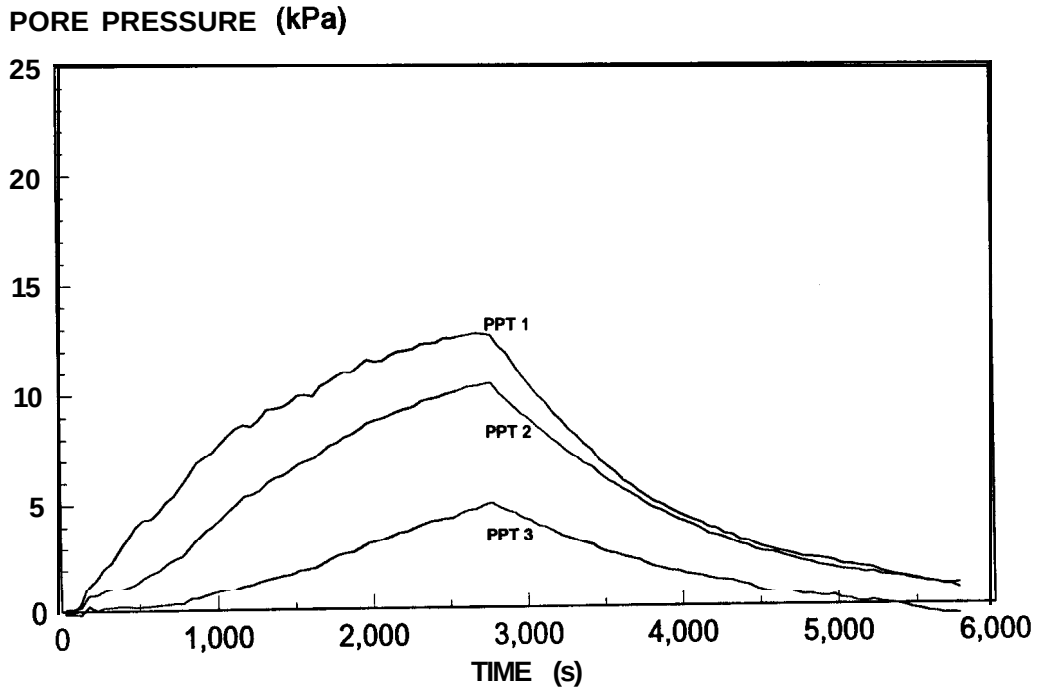

Figure 17f - Test 2. Reinforced Embankment. Excess Pore Pressures within Clay

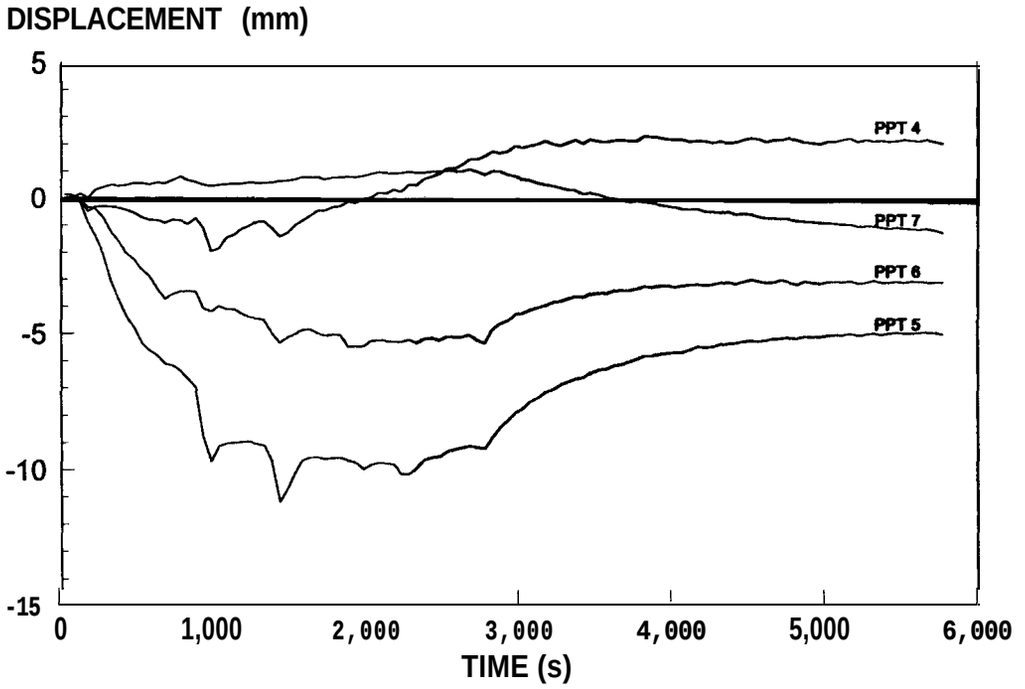

Figure 17g - Test 2. Unreinforced Embankment. Surface Settlements.

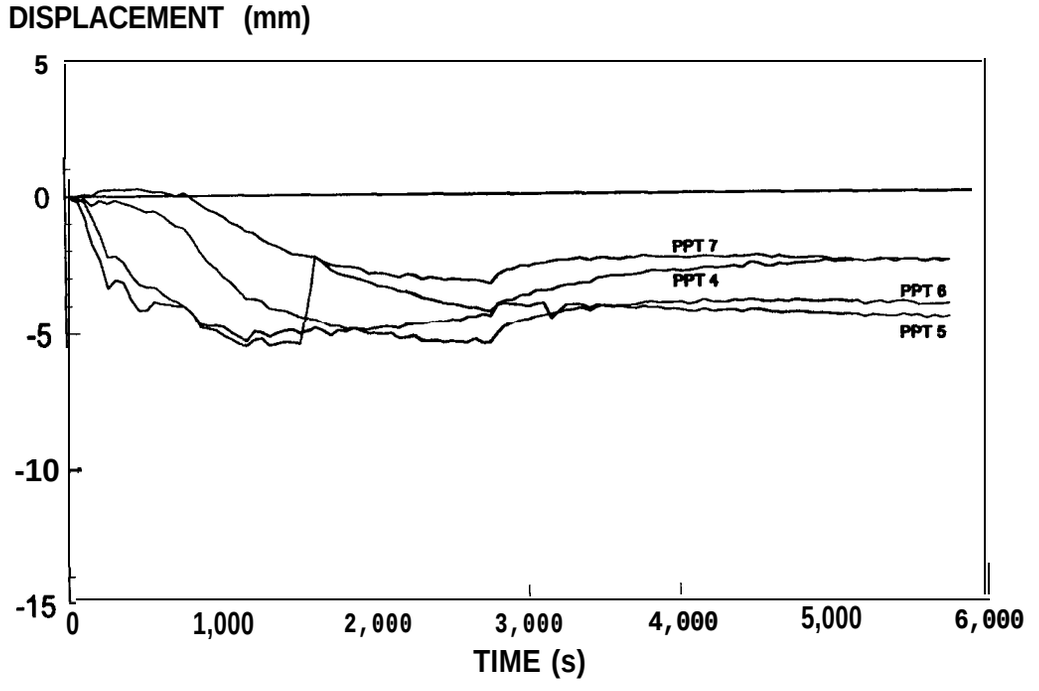

Figure 17h - Test 2. Reinforced Embankment. Surface Settlements.

8.2 Discussion of results

Discussion of the centrifuge test results, and making a comparison between them and the results from a series of finite element analyses (see Section 9) were a major part of the coursework undertaken by the MEng students. The coursework reports of one student, Nicholas Sartain of Girton College, are included in their complete form as Appendix B.

9 FINITE ELEMENT ANALYSIS

9. I General description of GeoFEAP

A finite element program, GeoFEAP, was used in the class to simulate the mini-drum centrifuge tests of embankment construction. GeoFEAP is a general purpose geotechnical FE program for static analysis of non-linear soil-structure interaction problems developed at the University of California at Berkeley (Espinoza, Bray, Taylor and Soga, 1995). The program is based on the well-validated general purpose finite element program FEAP and the earlier version of FEAP is described in Zienkiewicz and Taylor (1989, 1991). The program was modified to provide additional capabilities for solving problems of interest to geotechnical engineers. A FE analysis from pre-processing to post-processing is prescribed by a variety of macro commands, which allow the user to perform an analysis in a batch mode, an interactive mode or a combination of these modes. This flexibility allows the inclusion of a wide variety of solution schemes, which can be essential when solving problems using different non-linear stress-dependent soil constitutive models. This program structure helps the students to understand the basic concept of the finite element method. The program also includes a graphical processor to allow the analyst to readily visualise the results even during the analysis.

Four types of elements are implemented within the GeoFEAP clement library : (a) 2 node bar elements, (b) 2 node beam elements, (c) 4 node interface elements and (d) 3 to 9 node soil elements. Presently, the structural bar and beam elements are modelled as a linear isotropic elastic material. Interface elements may be used to model the non-linear behaviour of soil-structure interfaces or shear planes within a soil mass (Goodman et al., 1968; Clough and Duncan, 1969). The soil response can be represented by the non-linear stress-dependent incrementally elastic hyperbolic model (Duncan et al., 1980), the Drucker-Pragcr model assuming an elastic-perfectly plastic material, the non-linear stress-dependent clasto-plastic model (Lade, 1975) or the modified Cam-clay model (Roscoe and Burland, 1968).

Several iterative solvers can be used in GeoFEAP to solve non-linear governing equations. Commonly, the Newton-Raphson technique is used to find a solution which satisfies the global equilibrium of the analysed system. Both drained and undrained analyses can be performed. Consolidation analysis can also be performed using a linear elastic model or the modified Cam-elay model. Construction of geotechnical structures is modelled by adding elements and excavation of soils is modelled by removing elements and then by satisfying the global equilibrium of the analysed system. Initial geostatic stresses under, a complex boundary condition can be estimated using any soil model or from an input of assumed coefficient of lateral stresses. Original geometry with estimated initial stresses can be recovered at the start of the analysis by defining the displacement to be zero in specified regions.

9.2 Use of GeoFEAP in the module

In the 4th year module, the students were asked to make an input tile to model the embankment construction tested in the centrifuge tests. Most of the student used approximately 100 elements for the clay foundation and 60 elements to model the embankment. The embankment is constructed in 6 layers. The modified Cam-clay model was used for the clay foundation. The Cam-clay properties of the speswhite clay were determined by the students from the results of the undrained triaxial tests and one-dimensional consolidation tests reported by Elmes (1985). An overconsolidation ratio of 1.1 and Poisson's ratio of 0.25 were assumed. The embankment was modelled as a linear elastic material. For the reinforced embankment, bar elements were used to model the geotextile and interface elements were used between the soil and the geotextile. Students were asked to perform both drained and undrained analyses. The following section describes the general observations obtained from the students' analyses.

9.2.1 Undrained analysis of the unreinforced embankment

In undrained conditions, the embankment failed when the third or fourth layer was placed (full embankment is six layers). The displacement vectors showed that the mode of failure was quite shallow because of the effect of undrained strength increasing with depth. This type of failure mode can be different from the failure modes predicted in a conventional slope stability analysis, which commonly assumes that the undrained strength is constant with depth.

When the embankment is close to failure, the excess pore pressures predicted by GeoFEAP were about 30 kPa at PPT1, 20 kPa at PPT2 and 10 kPa at PPT3. These predicted values are larger than the actual measured values in the centrifuge tests, especially for Test 1 which was the slower embankment construction. Thus, the behaviour of the embankment during construction is partially drained conditions. In Test 3, which was the faster embankment construction, the maximum excess pore pressure was recorded to be approximately 18 kPa at PPT2. This value is slightly smaller than the excess pore pressure predicted in undrained analysis. Indeed, the embankment showed a large movement during construction in this case. In general, the students found that the measured pore pressures were the transient ones and it was not possible to use the FE results to compare directly with the centrifuge test results.

9.2.2 Drained analysis of the unreinforced embankment

The students compared the calculated vertical displacements of the embankment with the measured ones using the drained analysis. The predicted displacements were approximately 150 mm at the toe of the embankment and increasing up to approximately 450 mm at the centre of the embankment. The measured vertical displacement at the centre of the embankment was not comparable to the predicted one because the friction between the clay and the container boundary restricted the clay moving downwards freely as was assumed in the FE calculation. The other measured displacement values were quite similar to the predicted ones. The measured vertical displacements at the toe of the embankment were about 250 mm for Test 1 and 100 mm for Test 3. The vertical displacement increased toward the centre of the embankment, and the vertical displacement at PPT 5 location was approximately 500 mm. The stress paths at various locations in the embankment showed that the stress states were well below the failure line implying that the embankment is quite stable.

9.2.3 Reinforced embankment

The finite element analyses of the reinforced embankment predicted that in undrained conditions, the reinforced embankment failed at about the same height as the unreinforced case. Although the computed horizontal displacements were smaller for the reinforced case than the unreinforced case, the tension in the geotextile did not help increase the bearing capacity of the clay foundation. The FE analysis of the reinforced embankment showed a similar mode of undrained failure as the unreinforced case. However, the failure of the reinforced case was catastrophic, whereas that of the unreinforced case was more gradual.

Drained analysis also showed similar results to the undrained case. The geotextiles did not reduce the vertical displacements. Horizontal displacements were reduced by inclusion of geotextiles. But, again, this reduction was not as significant as expected.

Sharma (1994) reports the behaviour of reinforced embankments on soft clay based on centrifuge tests and CRISP finite element analysis. He concludes that reinforcing an embankment with a reinforcement of typical stiffness and strength results in only 8 to 10% reduction in the mobilised strength of the subsoil. He further comments that the magnitude of tension in the reinforcement is sensitive to the magnitude and distribution of undrained shear strength of the subsoil.

Hence, for the analysed cases, it is probable that the small increase in mobilised strength of the shallow clays by the geotextiles did not contribute much to the bearing capacity of the reinforced embankment/foundation. It is also considered that the slippage between the soil and geotextiles did not allow the geotextiles to mobilise their full tension capacity.

In all of the analyses, a linear elastic material was used to model the embankment because it was initially thought that the failure in the clay foundation was the dominant factor in terms of the stability of the embankment. Some preliminary analyses using the hyperbolic model showed quite different stress profiles within the foundation as well as the embankment. Hence, the choice of soil model for the embankment may contribute to the stability of an embankment-foundation system. This needs further investigation.

10 A CONCLUDING COMMENT ON THE A3 MODULE TEST ANALYSIS

The analytical model introduced in the MEng coursework report (Appendix B) reflects the undergraduate teaching that was given in 1995/6/7 on the theory of plasticity. The soil body is treated as if it had a strength *Cu* uniform with depth; that strength Cu is taken to be the strength at half the depth of the layer. It is a consequence of this analysis that the use of reinforcement on the upper surface of the clay layer is expected, incorrectly, to almost double the bearing capacity of the clay layer.

In earlier years undergraduate teaching on bearing capacity used to include discussion of the 'Gibson soil' (Gibson 1974) which has stiffness increasing linearly with depth. In future when our MEng students are introduced to the A3 module we need to explain to them the difference there is in behaviour between a uniform layer and a layer with strength and stiffness increasing with depth.

PART C

INTRODUCTION

This part of the report deals with further developments that have been made in the techniques for constructing embankments in-flight in the mini-drum centrifuge, subsequent to the MEng module tests described in Part B.

The air flows in the mini-drum were found to be a problem when constructing dry sand embankments at higher speeds (658 rpm (150g) and above) using the hopper, This problem and attempts at its remediation using a screening method will be described. Preliminary tests have also been conducted using a completely new method of constructing embankments in-flight - one which allows for the embankment to be constructed at any position on the clay surface, and at much faster rates that those permitted by the original hopper. This new method and the preliminary tests are described.

11 AIR FLOWS IN THE MINI-DRUM CENTRIFUGE

11. I Introduction

Four tests were in fact conducted for the MEng module; 2 each at 100g and 150g. Both of the 150g tests were unsuccessful. One of the turntable slip-ring brushes broke as the first 150g test began, preventing the hopper from being retracted. In the second 150g test, visibility was rapidly reduced by a layer of dirt accumulating on the underside of the polycarbonate safety screen. The responses from the transducers were not as expected and subsequent inspection of the model showed that the embankment had not formed as desired. Sand was distributed almost evenly across the entire clay surface, and only approximately 40% of the sand poured into the hopper had actually finished up on the clay. The remainder was deposited on the floor of the safety cylinder, beneath the face plate. The accumulated dirt on the safety screen was finely ground sand.

These problems (visibility and sand distribution) had not occurred in the 1995 MEng module tests. The difference between the two series of tests was that the 1995 embankments had been poured with the water level in the channel being gradually raised such that the embankment crest was always just submerged. It was postulated that the problems in 1996 were arising due to the air flows within the mini-drum blowing the newly constructed embankment away.

Il.2 Source of turbulence

The mini-drum is housed within a stationary safety cylinder. Below the ring channel itself lies the structural support which connects the channel to the face plate and the drive shaft. The arrangement of this supporting structure is shown in figure 18. In addition to this structure, there are a number of irregularly-shaped attachments mounted below the face plate. These objects, rotating at high speeds past the stationary safety cylinder give rise to turbulent air flows within the mini-drum. Flows of air directly up into the vicinity of the ring channel are possible through the gaps in the support structure.

I I. 3 Turbulence screens

Turbulence screens, 1.2mm thick Dural plates bent to the appropriate curvature, were fastened to the basic mini-drum structure as shown in figure 19. Three screens were used to cover the circumference. The gaps between the individual screens were sealed using heavy duty waterproof cloth ('gaffer') tape, creating an unbroken surface.

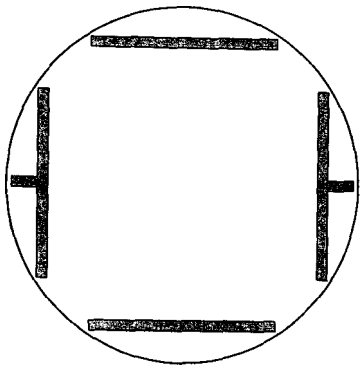

Figure 18 - Ring Channel Support Structure

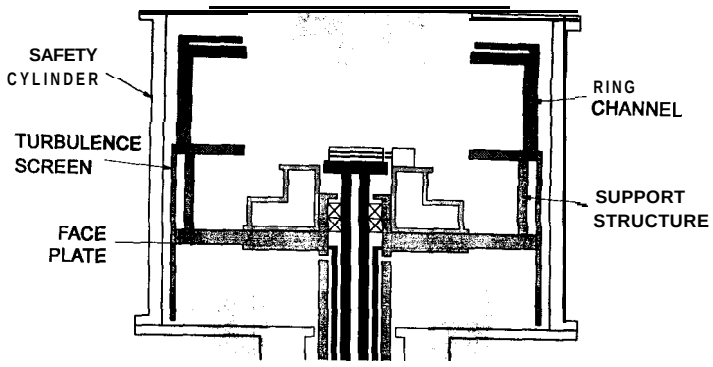

Figure 19 - Section Through Mini-drum with Turbulence Screens Installed

The aim of the screens was to reduce the turbulent air flows in the mini-drum and more specifically those within the vicinity of the ring channel. While there is still a large speed differential between the mini-drum and the safety cylinder, the screens prevent air flows up between the support structure and their profile will produce a more regular air flow pattern.

11.4 Repeat MEng module tests A35 and A36

11.4.1 Test A35

This test was identical to the 150g MEng tests except that the turbulence screens were in place. This test saw the first occurrence of the current threshold being exceeded, during the rapid acceleration to 150g and back at the start of the consolidation procedure. The centrifuge executed an emergency stop and the unconsolidated clay slurry fell from the ring channel into the main body of the mini-drum. The test was abandoned pending an investigation of the current problem - see Section 11.5.

11.4.2 Test A36

This test was again almost identical to the 150g MEng tests. The screens were not installed for this test. Instead, a modification to the hopper was made. This involved enclosing the delivery plate onto which the sand was poured[20]. This modification was made with the intention of reducing any bouncing of sand particles out of the hopper that might occur on impact with the rotating delivery plate.

[20] The plate used to cover and enclose the delivery plate can be seen in the photographs in Section 7, figures 15a-c, which were taken after the modification had been made. It has been omitted from the schematic diagram of figure 15d.

This modification did improve the sand-pouring operation to the extent that the embankment profile was closer to that which was desired. However, there remained a lot of sand beyond the nominal toe of the embankment and the visibility problems due to dust build-up on the safety screen were still encountered.

What data exists from test A36 will not be reproduced in this report: one of the base drain PPT cables became loose during the course of the embankment construction and came into contact with the safety cylinder. The cable was frayed through, short-circuiting the channel in question and consequently the power supplies to the doughnut ring as a whole.

11.5 Increased drag due to turbulence screens and current overloadproblems

Following the test A35, aborted due to a current overload, an investigation was carried out into the effect of the turbulence screens on the current required by the face plate motor. A variety of acceleration and deceleration patterns were studied, along with other common experimental operations (standpipe operation, turntable control, etc.).

In early tests with the turbulence screens, there were several instances of the current safety threshold being exceeded during acceleration to higher rpm values and the machine executing an emergency stop. There were also occurrences of this at steady speeds several seconds after the standpipe had been lowered and drainage of water from the channel had begun.

In various investigative trial runs, the maximum current monitored during acceleration to 700rpm was in the range 11.4 to 12.3 A rms.[21]. While this is higher than the range normally experienced during the same acceleration without the screens (10 to 11 A rms.) it is still short of the safety threshold of 20 A rms.

The problem appears likely to be caused not by increased air resistance but by the bottom of the screens dragging in sand and water which has accumulated on the floor of the safety cylinder. If the drainage holes become partially or completely blocked, water can build up, especially during rapid drainage from the ring channel.

To avoid this problem it is recommended that whenever the screens are used:

- they are removed after each test and cleaned, along with the floor of the safety cylinder;
- the drainage pipes are thoroughly cleaned prior to each test;
- the current to the Digiplan ZX640 face plate motor is monitored. This may help to give advance warning of any possible problems during accelerations.

[21] The currents measured fluctuated by as much as 0.5A at any one time. The values given are the maximum observed during the period in question, as this is the relevant value ▪ the safety threshold works in terms of absolute values, not time-averaged ones.

12 NEW SAND POURING TECHNIQUE

12. I Introduction

The Primary limitations to the use of the hopper are its maximum embankment construction rate and the space it sweeps through whilst rotating. The latter constraint places size and location restrictions on any other instrumentation or equipment which may be required to be mounted. The embankment location is also fixed with the hopper - at the top of the channel.

A different method of Pouring sand embankments was required - one in which these problems were addressed and solved.

12.2 Preliminary tests

12.2.1 Initial designs

The basic idea which was settled upon was to pour sand in a similar manner to that used to introduce clay slurry to the channel. The sand would be introduced via a funnel and column and would then be distributed radially. If the distribution equipment could be set at different vertical heights, this would allow for embankment construction at any position in the channel.

12.2.2 Sand base layer

All of the preliminary tests were carried out with a 55mm deep layer of LB 100/170 sand as the foundation, rather than kaolin clay. This was done to save preparation time. The sand base layer was prepared in the same manner as the Evans (1994) clay layers - using the paddle system to introduce the sand to the channel at 170rpm with the axis of rotation horizontal. The mini-drum was then rotated to bring the axis vertical and the sand was saturated with water from the base upwards. When the water level was above the sand, giving near-complete (and sufficient) saturation, the standpipe was fully lowered and the water was allowed to drain away. The sand was left in this condition for 10 minutes before the centrifuge was stopped. The negative pore water pressures hold the sand in place, allowing the various pieces of equipment to be installed before the proper testing begins. This method of foundation layer preparation takes no more than 30 minutes, compared to the more than five hours required for E-grade kaolin.

12.2.3 Test with spreader apparatus /friction problem

One test was carried out initially using the existing clay spreader equipment. One problem became immediately apparent during this test - that caused by friction. The rotating vertical column used to introduce the sand quickly became almost completely blocked up by sand.

Near to the axis of rotation, the centripetal acceleration, $\omega^2 r$, experienced by the rotating particles becomes less and the normal, constant gravitational acceleration Of $9.81 ms^{-2}$ becomes more significant. The resultant acceleration becomes $\sqrt{(\omega^4 r^2 + 96.24)}$ ms^{-2} inclined at an angle of $\tan^{-1}\left(\frac{9.81}{\omega^2 r}\right)$ to the horizontal.

Sand resting against the side of the vertical column will do so with a slope angle of a, given by $\phi = \tan^{-1}\left(\frac{9.81}{\omega^2 r_1}\right)$, where ϕ is the angle of friction of the sand. As the sand builds up, the surface will be at a lower radius. The radius at which no sand can rest is given by $\frac{9.81}{\omega^2 \tan\phi}$ and hence a profile will develop as shown in figure 20.

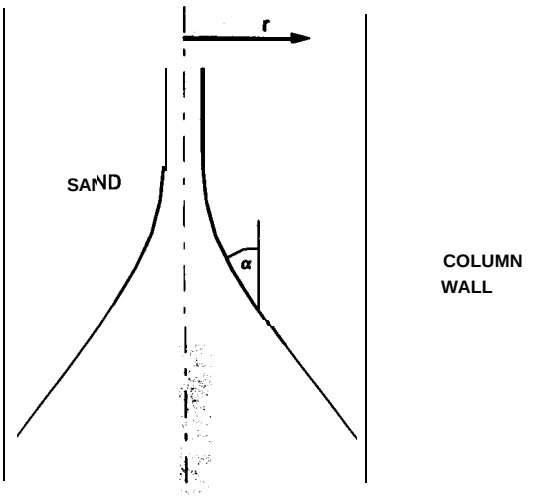

Figure 20 - Sand Profile in Vertical Rotating Column

This results in significant blockage of the column, especially at higher speeds of rotation. The problem can be eliminated by using a stationary vertical column to introduce the sand.

12.3 Twin Plates

12.3. I Description

Instead of using rotating distribution equipment, such as the original hopper or the clay spreader, it was decided to use twin parallel circular plates. If sand is introduced between the centres of the plates, it will be evenly distributed radially. These plates prevent the need for any components to be rotating relative to the clay and allow for additional instrumentation and equipment to be mounted on top of them. The operation of the plates is shown in figure 21.

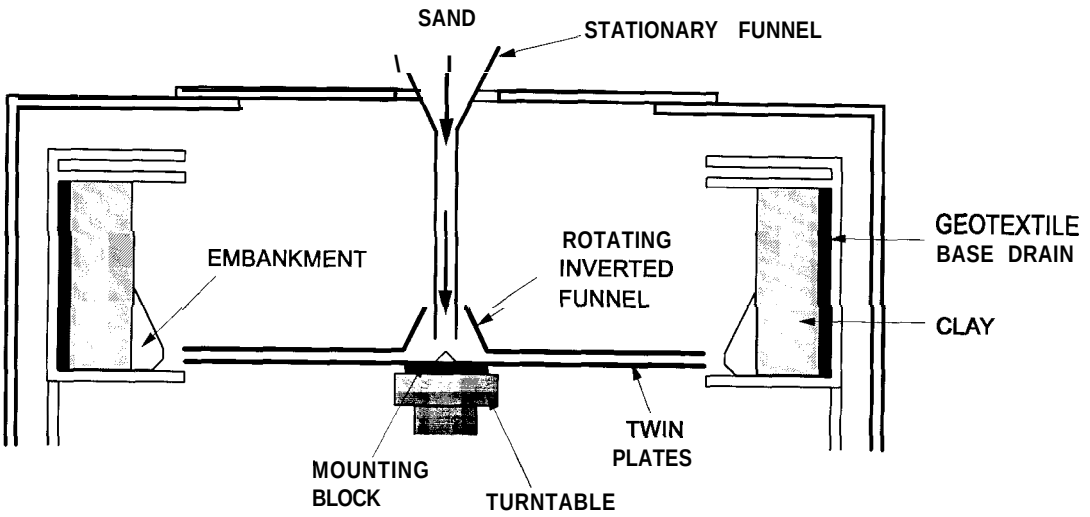

Figure 21 - Section Through Twin Plate Equipment installed in Mini-drum

The mounting block shown is a solid piece of Dural plate. The height of this block and the length of the supply column can easily be adjusted to give embankment construction at any desired height. The stationary column overcomes the problem described in Section 12.3.2. The inverted funnel on top of the plates prevents spillage of sand. The funnel walls are at an angle greater than the angle of friction of the sand. The plates themselves are made from Dural. The top and bottom plates are 3.5mm and 5mm thick respectively. They are held 5mm apart by brass tubing spacers. Their radii are both 248mm, to enable them to be installed inside the ring channel, which has a radius of 250mm.

The complete assembly is shown in figures 22a & b. The conical protrusion visible in the centre of the bottom plate in figure 22a is in fact the end of the bolt fastening the bottom plate to the mounting block. Its shape is designed such that it does not interfere with the uniform radial distribution of the sand.

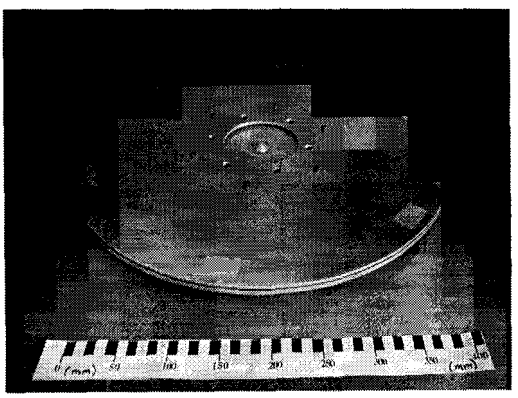

Figure 22a - Twin Plates without Funnel

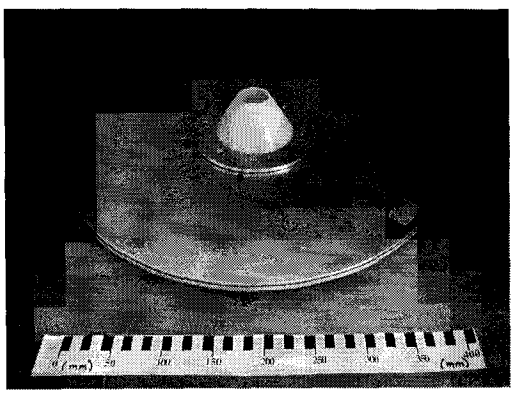

Figure 226 - Twin Plates with Funnel

12.3.2 Experimental considerations

12.3.2.1 Introduction

The twin plate method differs from the hopper method in that the plates are obviously unable to release the sand a short distance from the current embankment crest. Sand distributed radially by the twin plates will have to travel a finite distance after leaving the plates before arriving at the embankment. This necessitates a consideration of two factors. Firstly, the influence of normal gravity on the sand trajectory and hence the embankment position, and secondly, the impact velocity of the sand relative to the embankment or clay foundation, and the effect of this relative velocity.

12.3.2.2 Sand velocities

Before any calculations can be made regarding the motion of the sand after it leaves the twin plates, its motion whilst still between the plates must be considered. The sand starts at the centre of the plates with zero velocity. Contact with the base plate causes the sand to start rotating and the subsequent centripetal acceleration it experiences causes it to travel radially outwards. There will inevitably be a certain degree of bouncing between the plates, and slipping, both radially and tangentially. To arrive at a definitive value for the velocity of the sand as it reaches the edge of the plates is thus beyond the scope of this simple analysis. The effect of varying the initial tangential and radial velocity values will be examined to give an indication of the magnitude of their respective importance.

12.3.2.3 Impact velocities

It can be shown[22] that in a general case, the impact velocity ('NV') normal to a rotating (clay) layer (at a radius R_2) of a particle released at a smaller radius (R_1) is given by:

$$\mathrm{NV} = V_1\sqrt{1+\left(\frac{R_1}{R_2}\sin\theta\right)}, \tag{19}$$

and the impact velocity tangentially (the sliding velocity 'SV') is given by:

$$\mathrm{s\ v} = \omega R_2 - \frac{V_1 R_1}{R_2}\sin\theta, \tag{20}$$

$$\text{where } V_1 = \sqrt{(V_r)^2 + (\omega_p R_1)^2}, \tag{21}$$

$$\text{and} \qquad \theta = \tan^{-1}\left(\frac{\omega_p R_1}{V_r}\right), \tag{22}$$

[22] Barker (1997)

and ω_p is the angular velocity of the particle at release, ω is the angular velocity of the rotating layer and V_r is the radial velocity of the particle at release.

Rewriting $\omega_p = \alpha\omega$, and keeping R_1 and ω constant (248mm and $68.9s^{-1}$ respectively), the effect of varying the three parameters R_2, a and V_r on the impact velocities can be examined for the case of the twin plate equipment at 658rpm.

V_r was varied from 0 to 1 $0ms^{-1}$, a from 0 to 1. Two values of R_2 were examined, 260mm and 320mm. The results are shown in figures 23a-f.

It can be seen from these results that variation of the three parameters will have some effect on the impact velocities, but the overall impact velocity will always be of the order of $15ms^{-1}$ or higher. Velocities of this order of magnitude will lead to a large amount of scattering of sand during embankment construction using the twin plate equipment.

12.3.2.4 Preliminary test results and conclusions

The scattering of sand was indeed found to be a large problem when pouring embankments in preliminary tests. The impact velocities are of such a large magnitude that it will be impossible to pour embankments with the twin plate equipment in the same manner as the hopper.

Any embankments poured using the twin plate equipment have to be poured with water above the clay layer. This reduces the impact velocities substantially but will obviously lead to the loading being that due to the buoyant unit weight of the sand rather than the dry unit weight. This embankment construction under water worked well in preliminary tests; the desired embankment profiles were produced and the scatter was negligible - substantially less than that achieved using the hopper - as was predicted, given that the lg normal gravity is hindering rather than aiding scatter beyond the toe when the embankment is constructed at the bottom of the ring channel. There was negligible deformation of the sand foundation layer in each case, allowing it to be scraped clean and used again, provided that the water table had been lowered sufficiently each time before the centrifuge was stopped, generating the required negative pore pressures.

Following these preliminary tests on sand foundations, a test on a fully instrumented clay layer was conducted, test HB04.

23d: SLIDING VELOCITY SV

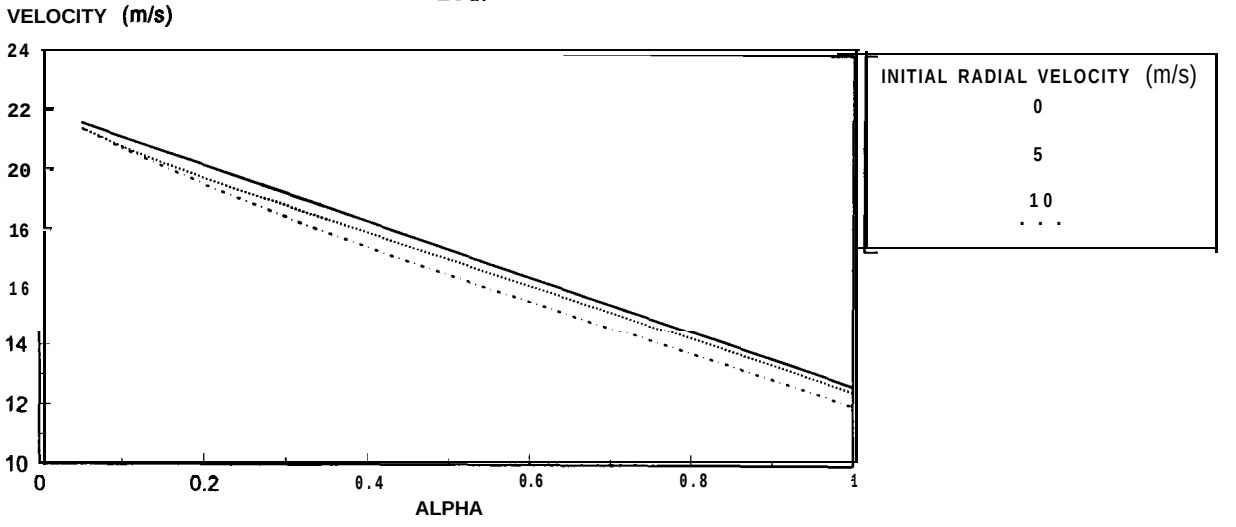

23e: IMPACT VELOCITY NV

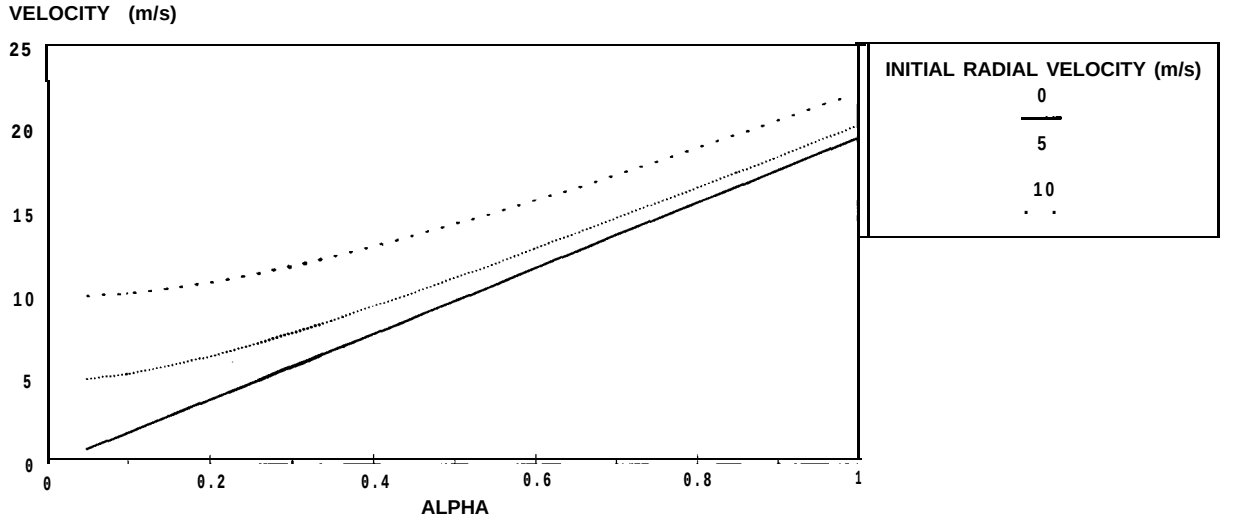

23f: OVERALL IMPACT VELOCITY

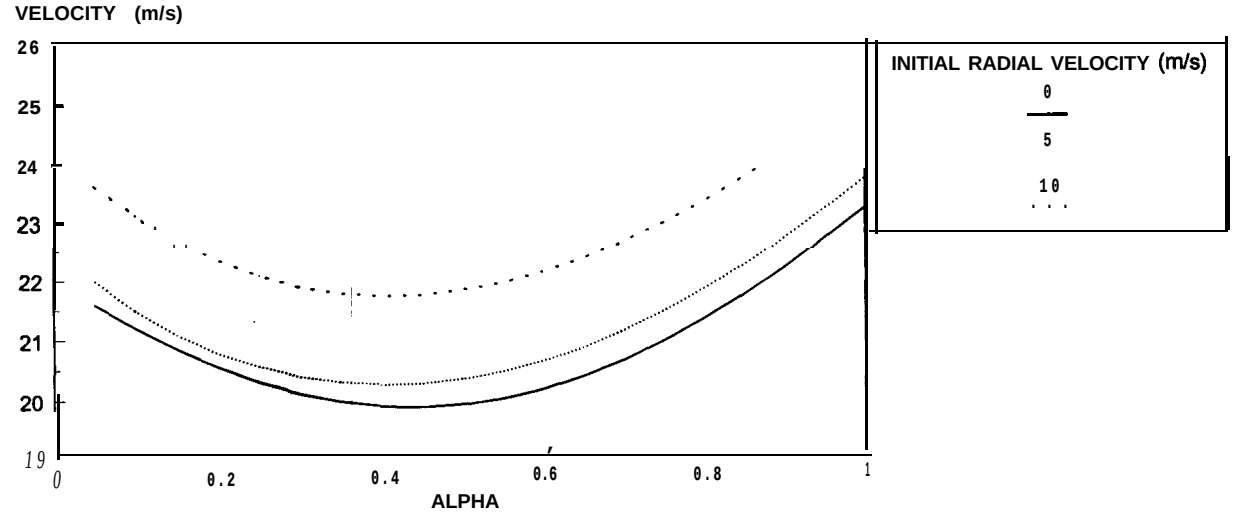

Figure 23d, e & f . Variation of Impact Velocities with Alpha and Initial Radial Velocity for Impact Radius of 320mm

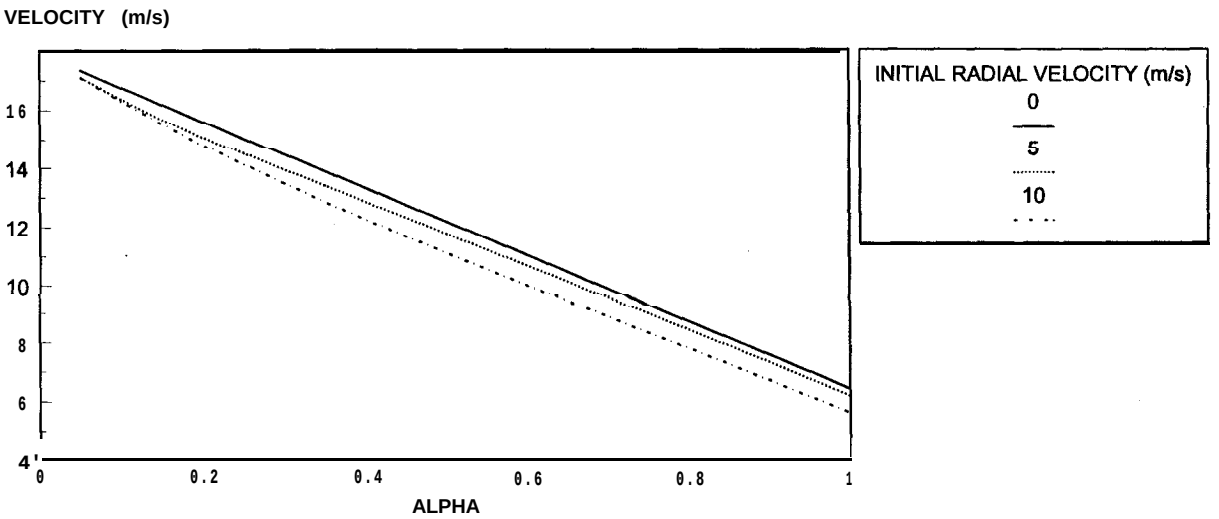

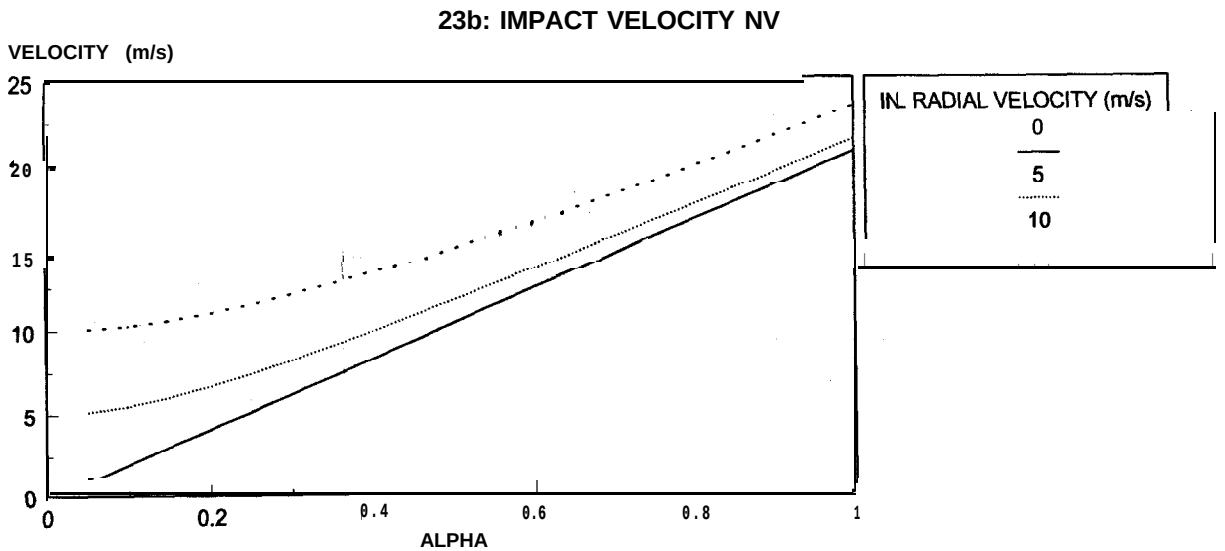

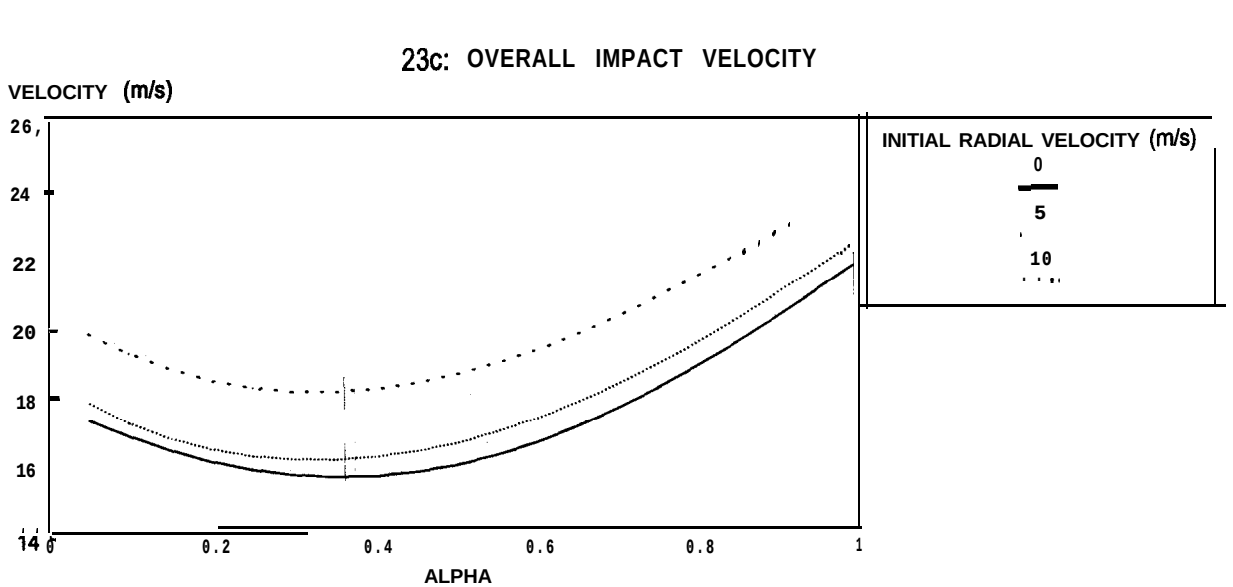

Figure 23a, b & c - Variation of Impact Velocities with Alpha and Initial Radial Velocity for Impact Radius of 260mm

13 TWIN PLATE TEST HB04

13. I Introduction

Following the successful structural and conceptual proof tests of the twin plate equipment, a test was carried out on a fully instrumented clay foundation layer. The test, HB04, was very similar to the MEng tests in that it involved constructing an embankment of LB 14/25 sand on a speswhite kaolin foundation layer, one section of which was reinforced in the same manner as for the MEng tests. The test was conducted at 150g.

As well as the obviously different method of embankment construction, HB04 differed from the MEng tests in the following ways:

- the embankment was poured at the bottom of the ring channel instead of the top;
- the embankment did not have a crest - its profile was as shown in figure 24;
- the rate of construction was significantly faster than for the MEng tests;
- the embankment was poured entirely under water. This had the effect of surcharging the clay with the buoyant weight of the sand embankment instead of its dry weight.

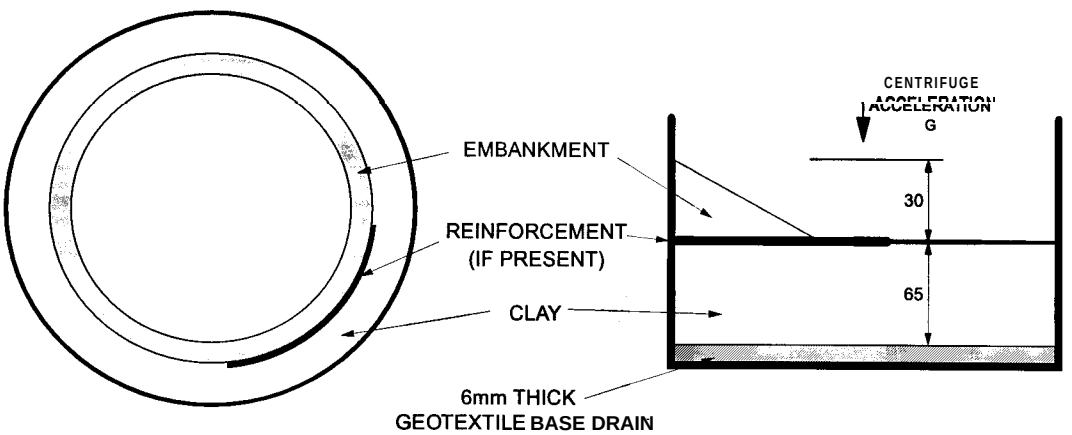

Plan View *Typical Reinforced Section*

Figure 24 - Basic Test Geometry, Test HB04

13.2 Model preparation

The PPTs to monitor pressures within the clay were mounted and installed prior to the clay pouring operations, as for the MEng tests. 48.1kg of speswhite kaolin clay slurry was then poured at a moisture content of 120%, in the manner described in Section 3. This produced a clay layer 65mm deep , following near-complete consolidation at 658rpm (150g) at the end of the standard two-day consolidation procedure for speswhite kaolin.

With the centrifuge stopped, the reinforcement was installed[23] and the PPTs were positioned on the surface of the clay. One of the 16 data acquisition channels had malfunctioned the previous day, and with not enough time available to investigate the problem, it was decided to alter the instrumentation arrangement slightly and proceed with only three surface PPTs on each instrumented section. The final instrumentation arrangement is shown in figure 25.

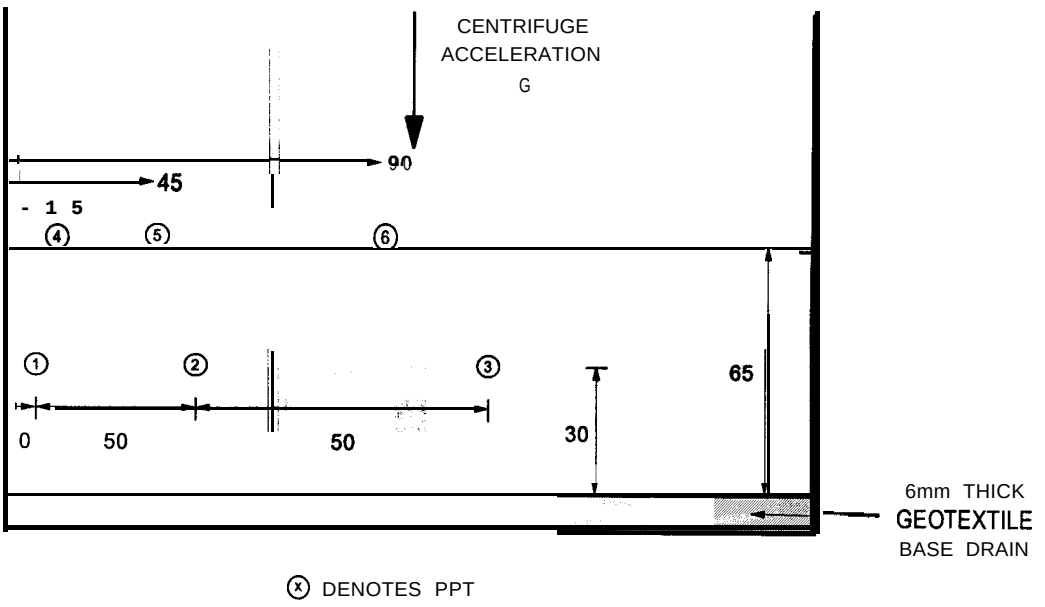

Figure 25 - PPT Locations, Test HB04 (Dimensions in mm)

13.3 Test procedure

On the day of the test, the twin plates were installed and the centrifuge was accelerated to 658rpm (150g) in 25g increments. Full re-consolidation was allowed to occur at this speed. The water level was raised so as to be at the top of the channel.

When steady-state conditions had been reached, the embankment construction began. 6.45kg of LB 14/25 sand was poured in 11 minutes, corresponding to 187.5 days at prototype scale. This was substantially more than had been calculated as being required to produce an embankment of height 30mm with the desired profile (approx. 3kg).

When steady-state pore water pressure conditions had been reached again within the clay, the water level in the channel was lowered. The centrifuge was stopped following 30 minutes in this condition. It was hoped that the final sand profile would remain intact when the centrifuge was stopped due to the negative pore pressures thus generated. This did not prove to be entirely the case, although enough sand did remain in place for a good impression to be gained of its in-flight profile.

[23] Using Option **B,** as described in Section 6.2

13.4 Results

13.4.1 PPT data

The data from the pore pressure transducers used is shown overleaf in figures 27a - d. Embankment construction started at time T=35 and finished at time T=695.

13.4.2 Clay profiles

Post-test surface profiles of the clay were taken for both the reinforced and unreinforced areas. Two profiles were taken of reinforced sections and three profiles were taken of unreinforced sections well away from the areas affected by the reinforcement. These are shown below in figure 26.

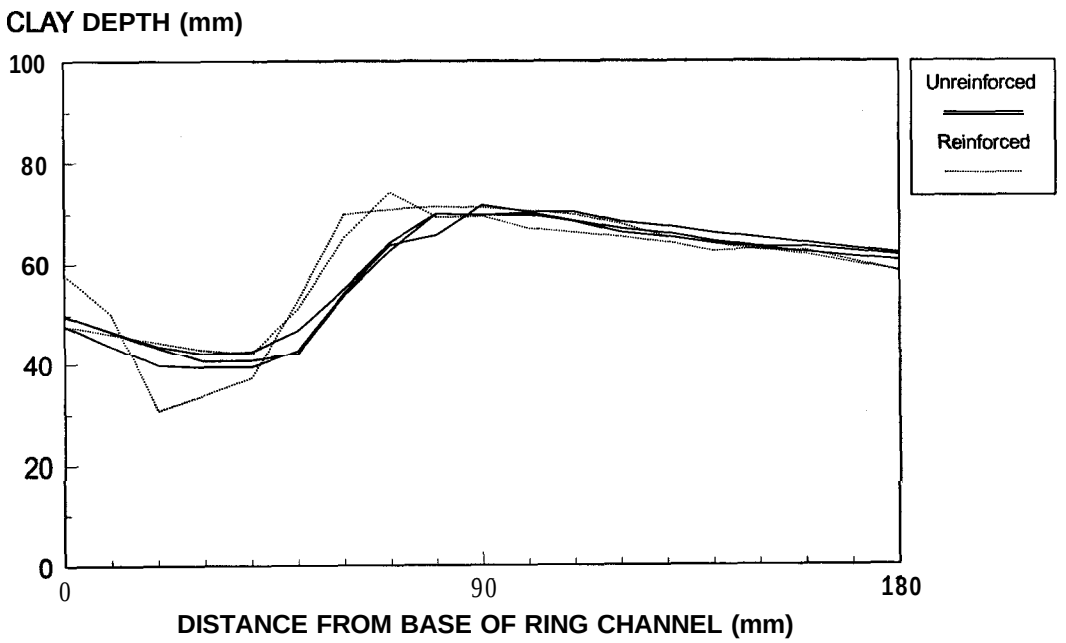

Figure 26 - Post-construction Clay Surface Profiles for Reinforced ***and Unreinforced Sections.***

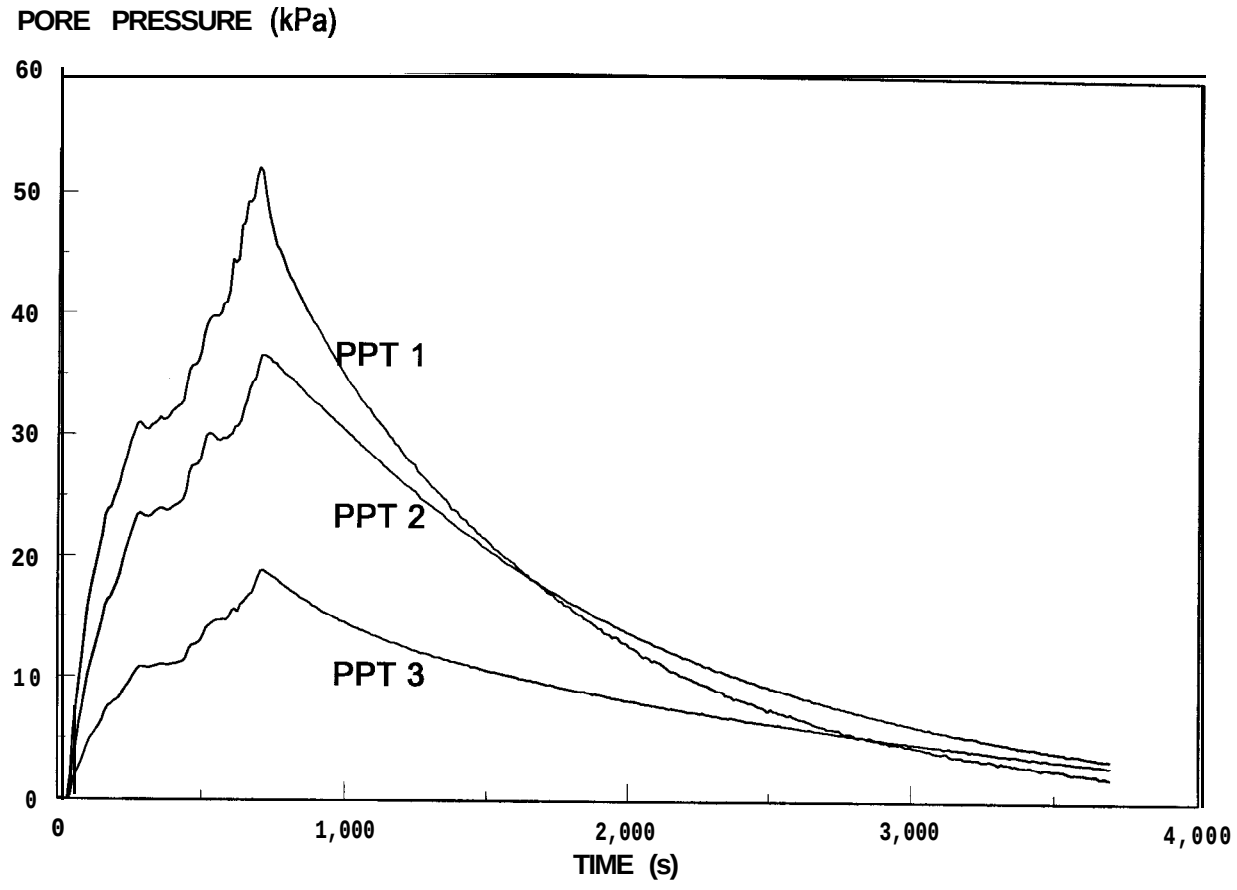

Figure 27a • Test HB04. Reinforced Embankment, Excess Pore Pressures within Clay

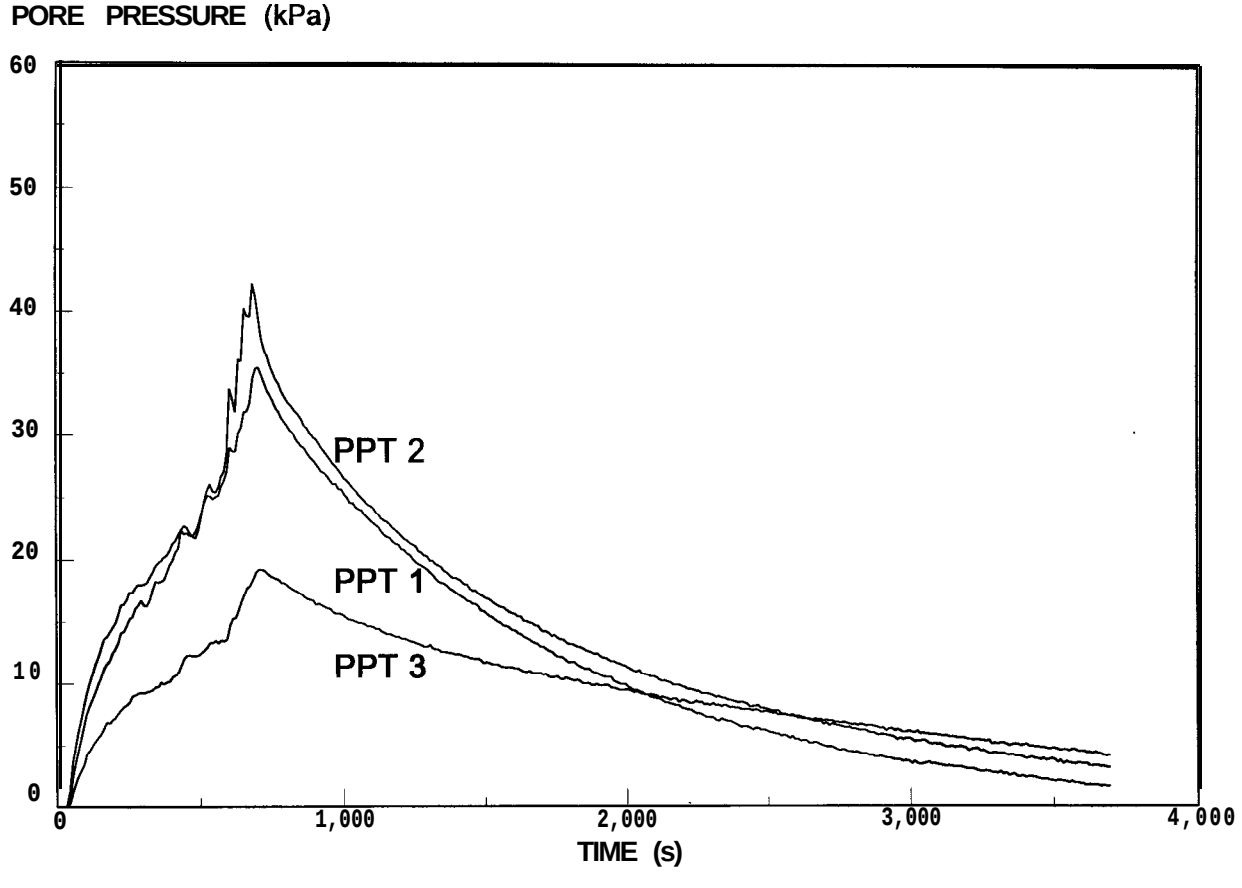

Figure 27b • Test HB04. Unreinforced Embankment. Excess Pore Pressures within Clay

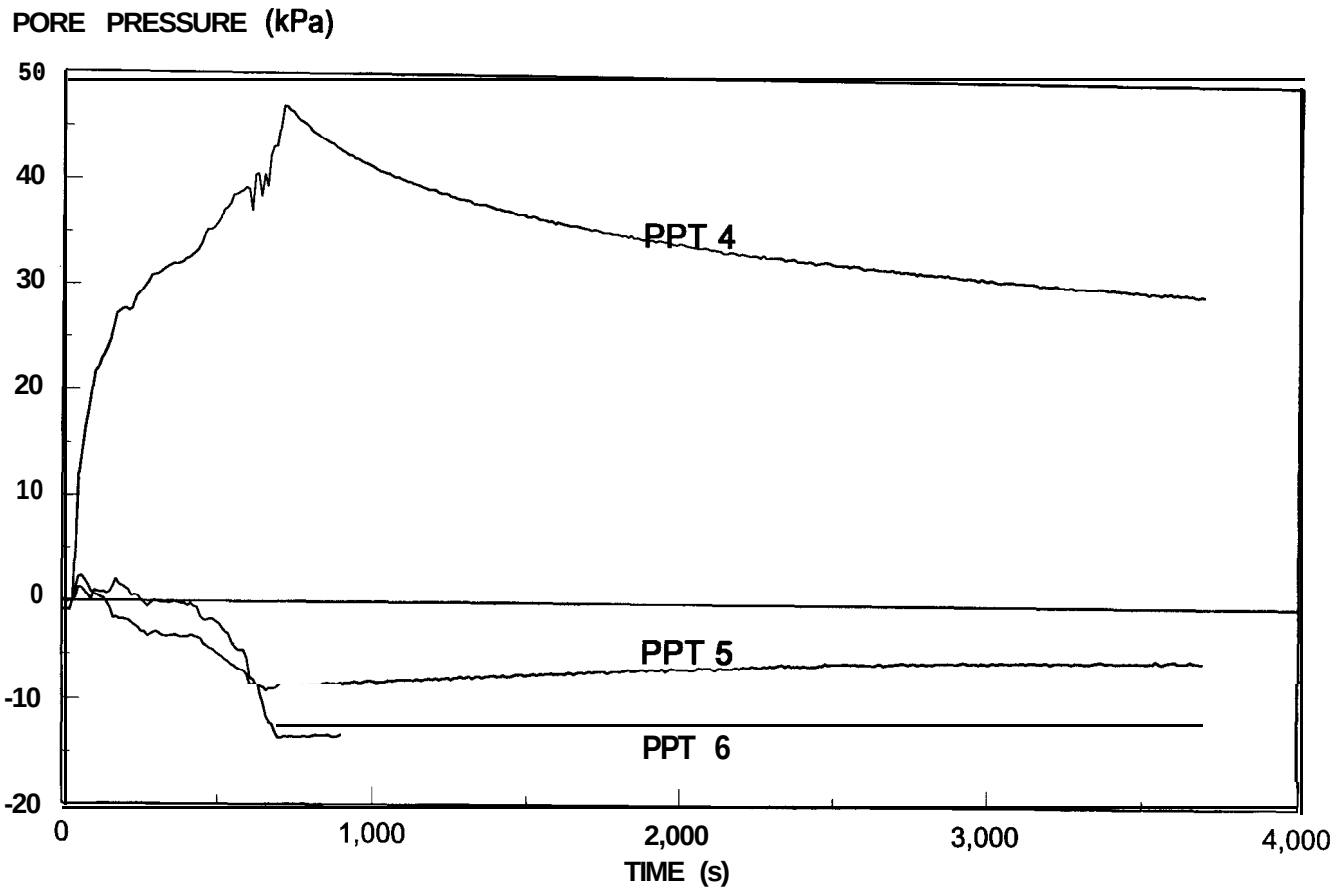

Figure 27c - Test HB04. Reinforced Embankment. Surface Pore Pressure Transducers.

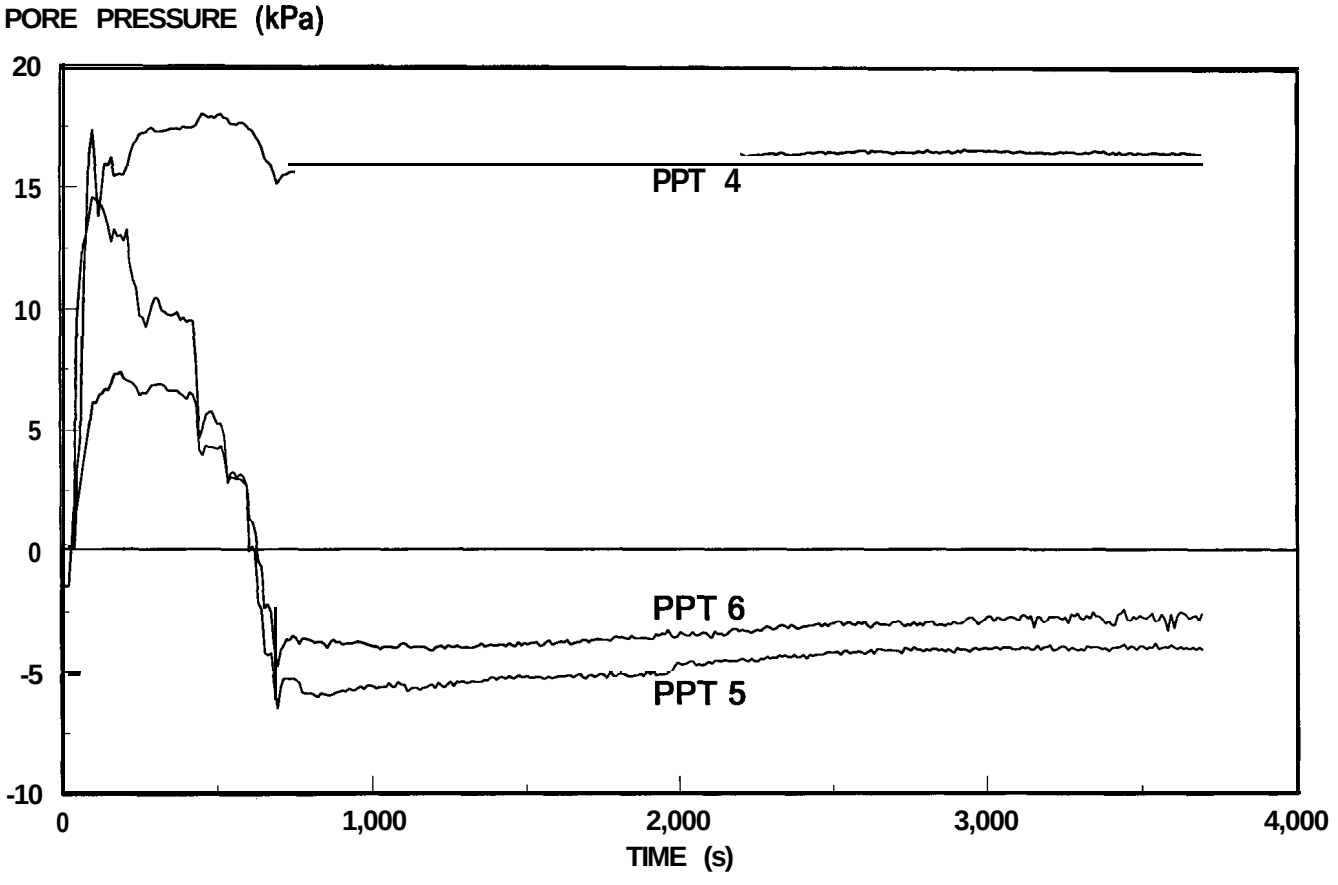

Figure 27d - Test HB04. Unreinforced Embankment. Surface Pore Pressure Transducers.

13.4.3 Photographs

A number of photographs were taken following the test which show various features. They were all taken prior to the removal of the sand to allow profiling of the clay surface. They are summarised below:

- figure 28a shows the step in the clay profile, typical of all the unreinforced clay areas;
- figure 28b shows the difference between the reinforced and unreinforced areas, and the transition between them;
- figure 28c shows the other end of the reinforced section. PPT 6 can be seen, displaced from its original position;
- figure 28d shows a close-up view of a typical reinforced section. The original position of the reinforcement on the clay can be seen.

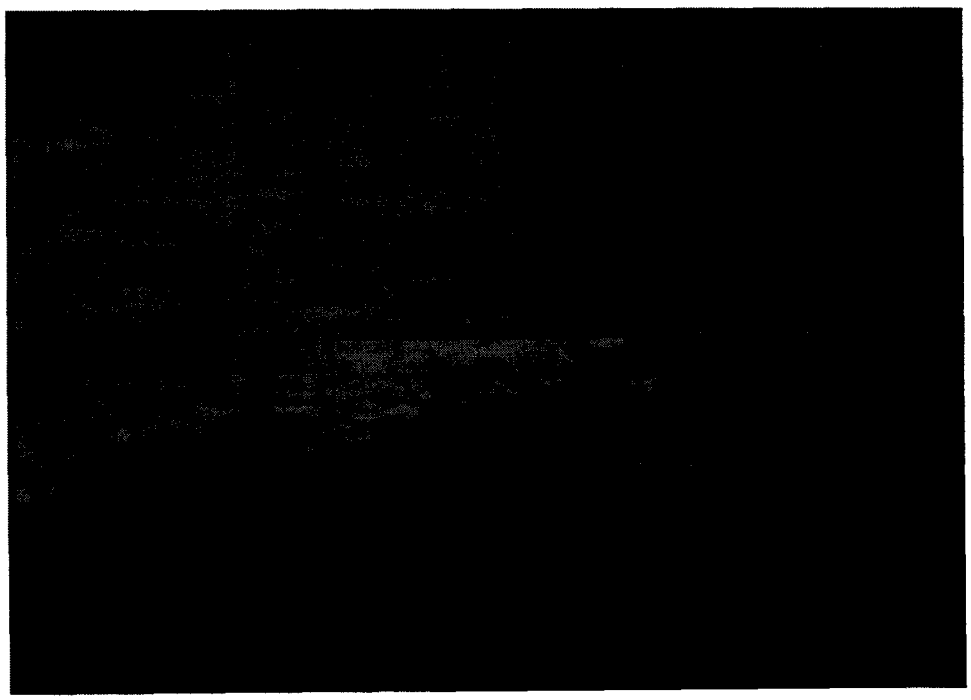

Figure 28a

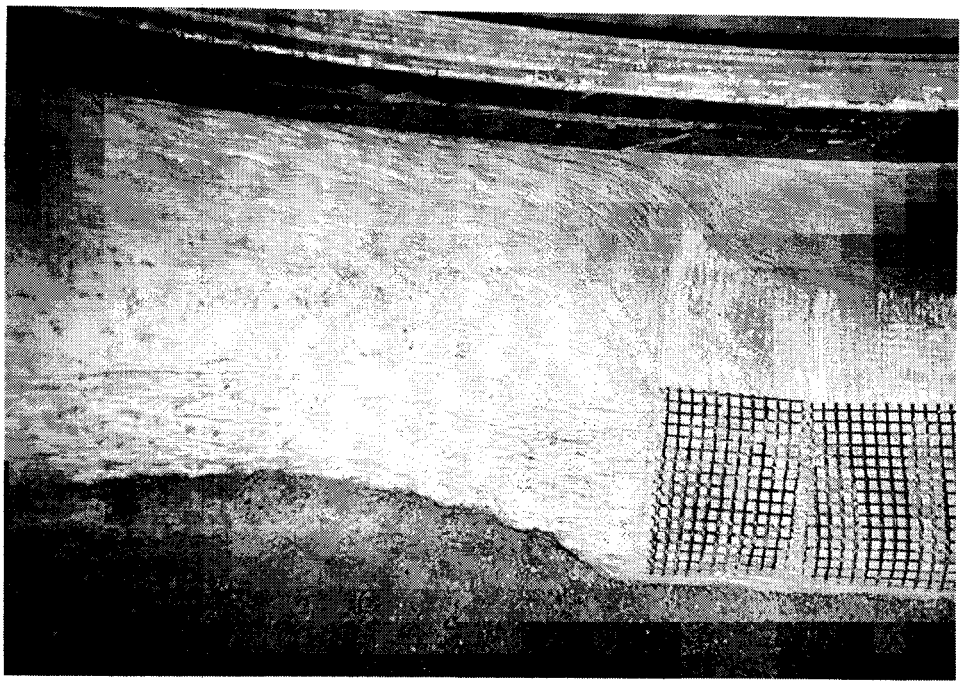

Figure 28b

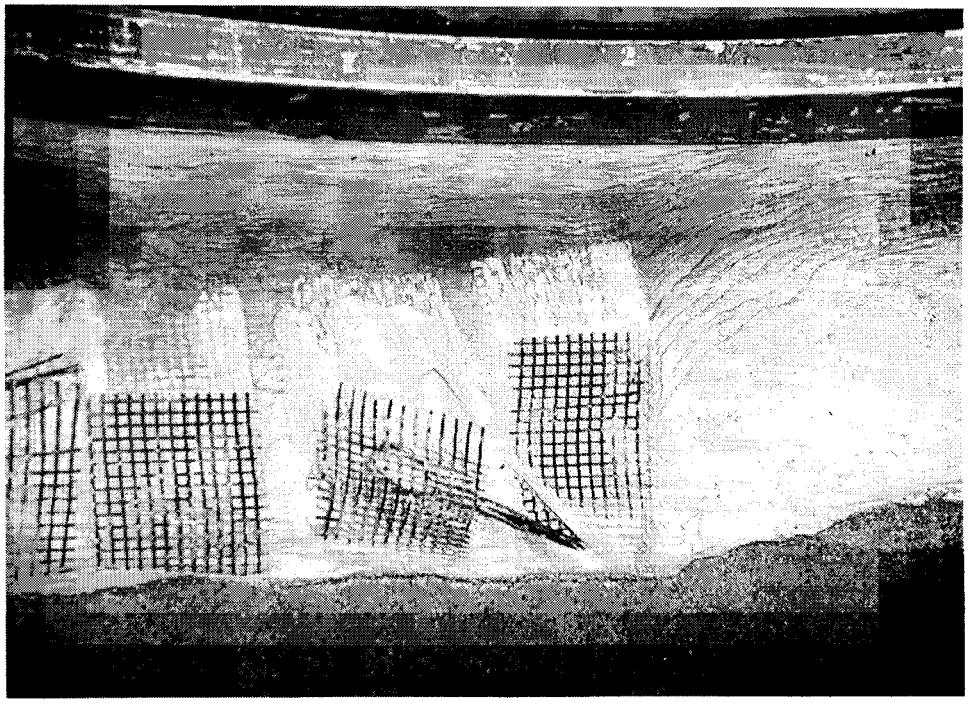

Figure 28c

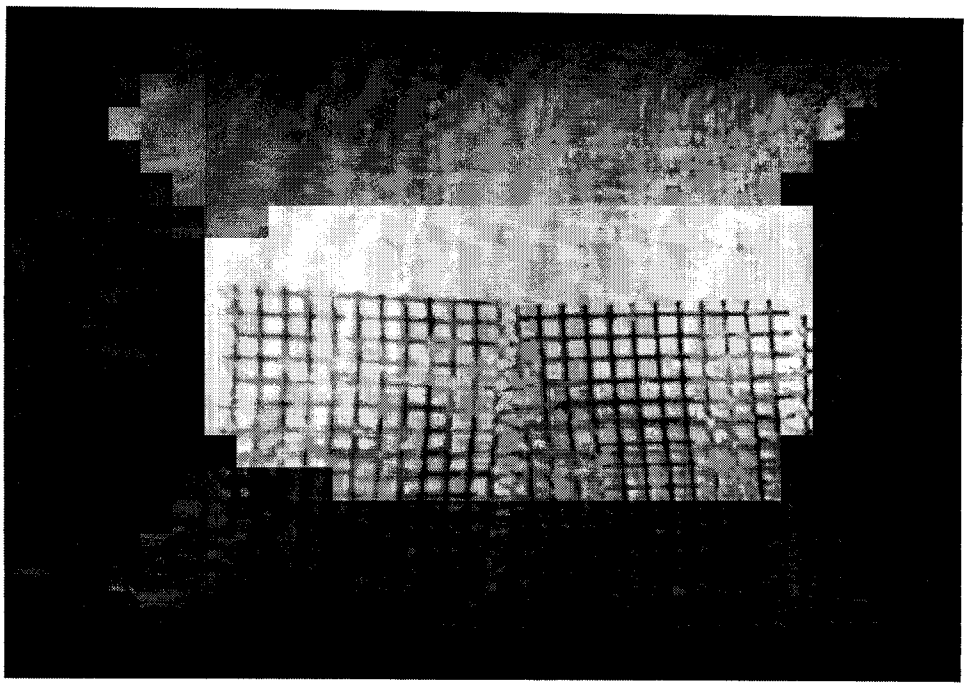

Figure 28d

13.5 Discussion of results

For a comparison of the experimental results to those predicted using FE analysis and a full discussion of the test, the reader is referred to Barker (1997). This section will be limited to a brief summary of the physical events of the test.

The results clearly show a difference in behaviour between the reinforced and unreinforced sections of the clay surface for this rapid embankment construction. Figures 26, 28b & 28c show that the displacement of the clay in the unreinforced cases is generally shallower but to a greater horizontal extent than in the reinforced areas. The reinforcement hindering horizontal motion of the clay at shallow depths (and spreading of the surcharging sand with it) would account for the greater generation of excess pore water pressures under the reinforced embankment as shown in figures 27a & b.

The deformations were large, and there are obviously boundary effects at the walls of the channel (the centre of the prototype embankment). Further consideration must be given to the method of anchoring the reinforcement, and to this boundary in general, if deformations on this scale are to be modelled.

Considerably more sand was required to produce an embankment 30mm above the original clay surface than had been predicted (see Section 13.3). The profiles of figure 26 show clearly why this was the case. The cross-sectional area of the region in which clay has been displaced by sand is of the same order of magnitude as the desired cross-sectional area of the embankment itself.

14 CONCLUSIONS

A second method for pouring sand embankments on soft clay foundations has been successfully developed. It has advantages over the original hopper in that:

- construction rates can vary over a very large range;
- instrumentation can be mounted on top of the plates to monitor the clay and sand profiles during the course of the experiments;
- it can be used on mini-drum centrifuges which do not possess a central turntable capable of rotating relative to the face plate;
- the position of the embankment can be varied.

However, impact velocities on the foundation surface mean that embankments poured using this method must be poured under water - a constraint which the original hopper does not have.

Further developmental work with the twin plate equipment will include trial tests with construction in the middle of the clay layer, modelling a complete prototype embankment and eliminating the boundary effect problem at the centre of the embankment.

15 ACKNOWLEDGEMENTS

The support of EPSRC in funding the first author's PhD research is gratefully acknowledged.

Thanks go to Dr Gopal Madabhushi for his help in demonstrating during the MEng A3 module tests described in this report.

The assistance of the technical staff in the Geotechnical Group at the Engineering Department must also be acknowledged. Thanks to Tim Ablett for his help in producing and preparing the photographic images in this report, Steve Chandler, John Chandler and Paul Ford for producing many of the pieces of equipment used and for practical help both before and during the tests, Stuart Driver and Chris McGinnie for their help with all things electrical, and to Stuart for his company on the cold early morning starts.

The last word of thanks must go to Chris Collison, Chief Technician at the Geotechnical Centrifuge Centre. Without his knowledge and experience, and his ability to turn conceptual designs into functioning reality, the practical work described in this report would have been immeasurably more difficult and as a result, the development of the mini-drum centrifuge as an experimental tool would not be as far advanced as it currently is.

16 REFERENCES

Al-Tabbaa, A. (1987) Permeability and stress-strain response of speswhite kaolin. PhD Thesis, University of Cambridge.

Barbosa, M.C., Lynch, R.J. & McKinley, J.D. (1995). Migration of Aqueous Acetone and KC1 through E-Kaolin: Minidrum Test CBLC1. Technical Report [284], University of Cambridge Engineering Department, Soil Mechanics Group.

Barker, H.R. (1996). Data acquisition on the mini-drum centrifuge. Internal note, Geotechnical Centrifuge Centre, CUED.

Barker, H.R. (1997). Forthcoming PhD Thesis.

Bolton, M.D. & Chin, C.Y. (1994). Soil Grouting in the Mini-Drum Centrifuge. Technical Report [266], University of Cambridge Engineering Department, Soil Mechanics Group.

Bolton, M.D. & Sharma, J.S. (1994). Embankments with base reinforcement on soft clay. *Centrifuge* '94, pp587-592. Balkema, Rotterdam.

Chin, C.Y. (1996). An experimental study of hydrofracture in soils. PhD Thesis, University of Cambridge.

Clegg, D.P. (198 1). Model piles in stiff clay. PhD Thesis, University of Cambridge.

Clough, G.W. & Duncan, J.M. (1969). Finite element analysis of Port Allen and Old River Locks, Report No. TE-69-3, Department of Civil and Environmental Engineering, University of California at Berkeley.

Duncan, J.W., Bryne, P., Wong, K.S. & Mabry, P. (1980). Strength, stress-strain and bulk modulus parameters for finite element analyses of stresses and movements in soil masses. Report No. UCB/GT/80-0 1, Department of Civil and Environmental Engineering, University of California at Berkeley.

Elmes, D.R. (1985). Creep and viscosity in two kaolin clays. PhD Thesis, University of Cambridge.

Espinoza, R.D., Bray, J.D., Taylor, R.L. & Soga, K. (1995). GeoFEAP : Geotechnical Finite Element Analysis Program. Report No. UCB/GT/95-05, Department of Civil and Environmental Engineering, University of California at Berkeley.

Evans, D.C., Savvidou, C. & Schofield, A.N. (1993). Contaminant Migration through Clay in a Mini-Drum Centrifuge. Technical Report [257], University of Cambridge Engineering Department, Soil Mechanics Group.

Evans, D.C. (1994). Contaminant migration through intact and damaged clay liners. PhD Thesis, University of Cambridge.

Fowler, J. (1981). Design, construction and analysis of fabric reinforced embankments ▪ test section at Pinto Pass, Mobile, Alabama. Technical Report EL-81-8, UEAE Waterways Experiment Station, Vicksburg, Mississippi.

Gibson, R.E., England, G.L. & Hussey, M.J.L. (1967). The theory of 1-D consolidation of saturated clays I. Finite non-linear consolidation of thin homogeneous layers. *Géotechnique* Vol. 17, pp 261-273.

Gibson, R.E. (1974). The analytical method in soil mechanics. *Géotechnique* Vol. 24:2, pp115-140.

Goodman, R.E., Taylor, R.L. & Brekke, T.L. (1968). A model for the mechanics of jointed rocks, JSMFE, ASCE, Vol. 94, No. SM4, pp. 637-659

Hsu, Y.S. (1997). Forthcoming PhD Thesis, University of Cambridge.

Lee, K. & Sills, G.C. (1981). The consolidation of a soil stratum, including self-weight effects and large strains. *International Journal for Numerical and Analytical Methods in Geomechanics*, Vol. 5, pp 405-428.

Liu, L.Y., Wang, M.R. & Ding, E.R. (1991). Centrifugal tests of mechanism of geotextile reinforced soft foundation under breakwater. *Centrifuge '91*, pp3 19-324. Balkema, Rotterdam.

McBride, I. (1996). A study of reinforced embankments by centrifuge modelling. MEng project report, University of Cambridge Engineering Department.

McKinley, J.D., Price, B.A. & Schofield, A.N. (1996). Technical Report [301], University of Cambridge Engineering Department, Soil Mechanics Group.

Olivera, A. (1982). Use of nonwoven geotextiles to construct a deep highway embankment over swamps. *Proc. 2nd Int. Conf. on Geotextiles, Las Vegas:* Vo13, pp63 l-634

Pokrovsky, G.I. & Fyodorov, I.S. (1936). Studies of soil pressures and soil deformations by means of a centrifuge. *Proc. 1st ICSMFE*, Vol 1, No. 70

Potter, L.J. (1996). Contaminant migration through consolidating soils. PhD Thesis, University of Cambridge.

Roscoe, K.H. & Burland, J.B. (1968). On the generalised stress-strain behaviour of wet clays. Engineering Plasticity, Cambridge University Press, pp. 535-609

Sasakura, T. (1996). Suction enhanced fixity of jack-up foundations. MPhil Thesis, University of Cambridge.

Schofield, A.N. (1980). Cambridge University geotechnical centrifuge operations. *Géotechnique*, Vol. 30:3, pp227-268.

Sekiguchi, H. & Philips, R. (1991). Generation of water waves in a drum centrifuge. *Centrifuge* '91, Balkema, Rotterdam.

Sharma, J.S. (1994). Behaviour of reinforced embankments on soft clay. PhD Thesis, University of Cambridge.

Sharma, K.G., Varadarajan, A. & Mahmoud, A.A.Aly (1994). Analysis and design of a reinforced embankment on soft clay. *Proc. 13th ICSMFE*, Vol. 2, pp739-742

Springman, S.M., Bolton, M.D., Sharma, J.S. & Balachandran, S. (1992). Modelling and instrumentation of a geotextile in the geotechnical centrifuge. *Proc. Int. Symp. on Earth Reinforcement Practice, Kyushu:* pp 167- 172. Balkema, Rotterdam.

Taylor, D.W. (1948). Fundamentals of soil mechanics. Wiley, NY.

Taylor, R.N. (Ed) (1995). Geotechnical Centrifuge Technology. Blackie Academic and Professional.

Terashi, M. & Kitazume, M. (1988). Behaviour of a fabric reinforced clay ground under an embankment. *Centrifuge* '88, pp243-252. Balkema, Rotterdam.

Tsukamoto, Y. (1994). Drum centrifuge tests of three-leg jack-ups on sand. PhD Thesis, University of Cambridge.

Yan, L. & Byrne. P.M. (1989). Application of hydraulic gradient similitude method to small-scale footing tests on sand. *Canadian Geotechnical Journal,* Vol. 26, pp 246-259.

Zelikson, A. (1969). Geotechnical models using the hydraulic gradient similarity method. *Géotechnique,* Vol. 19, pp495-508.

Zelikson, A. (1978). Rigid piles in sand under inclined forces; model tests using the hydraulic gradient similarity method. *Journal de Mécanique Appliquée,* Vol 2:2, pp 153- 165.

Zienkiewicz, O.C. & Taylor, R.L. (1989, 1991). The Finite Element Method, Vol. I and II, McGraw-Hill Book.

17 LIST OF FIGURES

APPENDIX A

VARIABLE ACCELERATION FIELD IN THE MINI-DRUM CENTRIFUGE

A. I Introduction

The radial dimensions in the mini-drum centrifuge are an order of magnitude smaller than those in a typical beam centrifuge. The effect of this reduction will be examined. The basic principles of centrifuge scaling (Schofield 1980) are reproduced here to define the variables used in the subsequent analysis.

A.2 Basic principles

The centripetal acceleration experienced by a particle in a centrifuge is given by

$$A = \omega^2 r\,, \tag{A.1}$$

(where ω is the angular velocity of the centrifuge and r is the radius at which the particle is rotating).

Soil models in a centrifuge exist between two finite radii. For the purposes of scaling, the whole model is assumed to experience a constant acceleration and a nominal value of radius is selected between the two extremes to calculate this acceleration,

$$\text{i.e. } A = \omega^2 (R + x), \tag{A.2}$$

(where R is the radius to the surface of the model and x is a chosen (constant) depth below the surface)

The scaling factor, n, is given by

$$n = \frac{\omega^2 (R + x)}{g}\,. \tag{A-3}$$

Assuming constant density, the prototype vertical stress, σ_{vp}, varies linearly with depth as $\rho g z_p$, where z_p is the depth below the surface. This corresponds to a stress profile in the centrifuge model which varies linearly with depth:

$$\sigma_v = \rho g z n\,; \tag{A.4}$$

using (A.3),

$$\sigma_v = \rho z \omega^2 (R + x). \tag{A.5}$$

In the model, the incremental stress $\delta\sigma_v$ due to an element of material of depth δz is given by

$$\delta\sigma_v = \rho\omega^2 r'\delta z, \tag{A.6}$$

(where r' is the radius to the element);

r'can be re-written as $(R+z)$, where R is the radius to the surface of the model, and z is the depth of the element below the surface. The vertical stress at a depth z below the surface in the model is given by

$$\sigma_v = \sum_0^z \rho\omega^2 (R+z)\delta z, \tag{A.7}$$

which gives

$$\sigma_v = \rho\omega^2 Rz + \frac{\rho\omega^2 z^2}{2}. \tag{A.8}$$

The two stress profiles are shown in figure Al.

The prototype and model stresses are only equal at the surface, $z=0$, and at one other depth, $z=H'$, where the two curves intersect, which is dependent upon the gradient of the prototype curve and the scaling factor used, n. At all points above this intersection, there is a stress deficiency in the model and at all points below, there is overstress in the model.

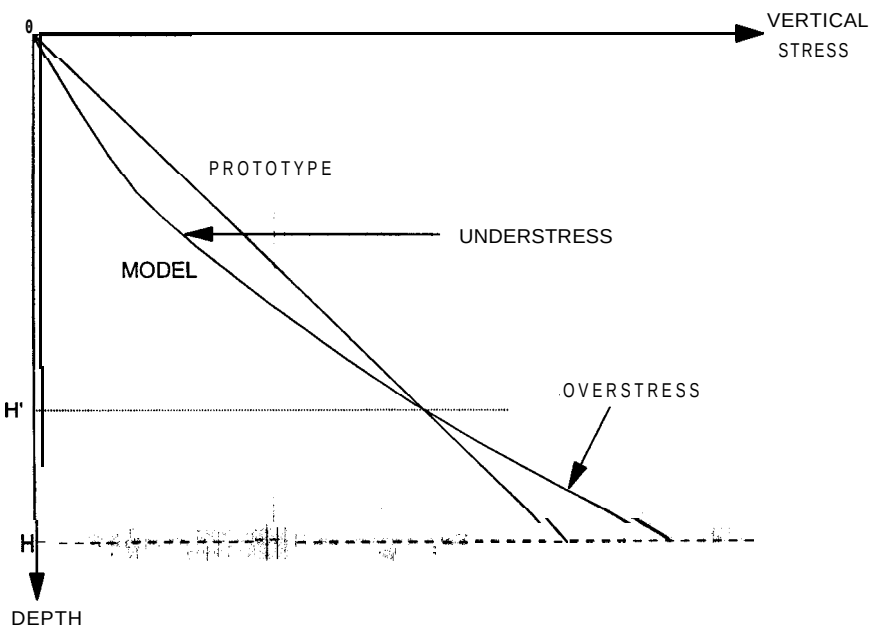

Figure Al • Model Stress Error

Pokrovsky & Fyodorov (1936) stated that the errors could be neglected provided that the radius occupied by the model was less than 15% of the effective radius of rotation. Schofield (1980) considered the under and overstress errors. Setting H', the depth at which the stresses are correctly modelled, to 2H/3, he calculated that the errors in the model , given by

$$\left| \frac{Correct\ \ Stress}{Model\ \ Stress} - 1 \right|$$

are:

$$\frac{a}{(4-3a)}\ ,\ \text{at a depth of}\ \frac{H'}{2}\ \text{(understress)}$$

$$\text{and}\ \frac{a}{(4-a)},\ \text{at a depth of}\ \frac{3H}{2},\ \text{i.e. H (overstress),}$$

where a is the ratio of the depth of the understressed part of the model to the radius at which the stresses are correctly modelled, i.e. H'/(R+H') in the notation previously used.

For a typical beam centrifuge in which the model depth extends over 10% of the radius, setting H'=2H/3 gives a=1/15. The understress and overstress errors in the model are therefore 1/57 and 1/59 respectively, a little under 2%.

In the Mk II mini-drum centrifuge, a has a typical value of 80/(250+80), i.e. 8/33. This value of a gives under and overstress errors of 2/27 and 2/31 respectively. These errors of 7.4% and 6.4% in the mini-drum centrifuge are much more significant than those in the beam centrifuge and warrant a further more complete analysis of the subject.

Two questions must be answered:

1) What scaling factor n should be used for a particular model, i.e. at what depth x below the surface of the model should the nominal acceleration for the whole model be calculated?

2) What magnitude of error does this nominal acceleration introduce into the modelling of the prototype stresses?

A. 3 Nominal accelerations and stress errors

Six different approaches to determining the required nominal acceleration (at a depth x) and minimising the subsequent errors introduced will be discussed and compared.

1) $x = H'$, i.e. the intersection of the two curves. This is the approach used by Schofield (1980). It is a more complicated calculation in the case of the mini-drum centrifuge as the gradient of the prototype line is also dependent on x.
2) x chosen such that the area between the two curves is minimised. (The shaded area in figure A2a).
3) x chosen such that the area between the two curves is equal on either side of the point of intersection
4) x chosen so as to minimise the absolute error between the two curves (D in figure A2b).
5) x chosen so as to minimise the percentage error between the two curves
6) x chosen so as to produce a least squares optimisation to the two curves.

A.3.1 $x = H'$

The nominal depth is chosen such that $x = H'$, the point of intersection of the two curves.

For the two curves to intersect at a depth H',

$$\rho\omega^2 RH' + \frac{(\rho\omega^2 H'^2)}{2} = \rho\omega^2 H'(R + H'). \qquad \text{(A.9)}$$

$$\therefore \; H' = 0$$

i.e. it is not possible to find a nominal depth such that the prototype and model stresses are equal at this depth, unless the surface is chosen.

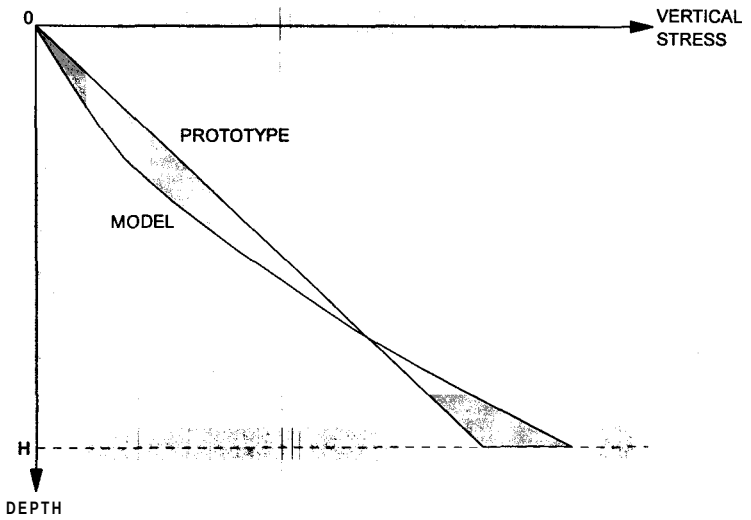

Figure A2a - Minimisation of Area between Curves

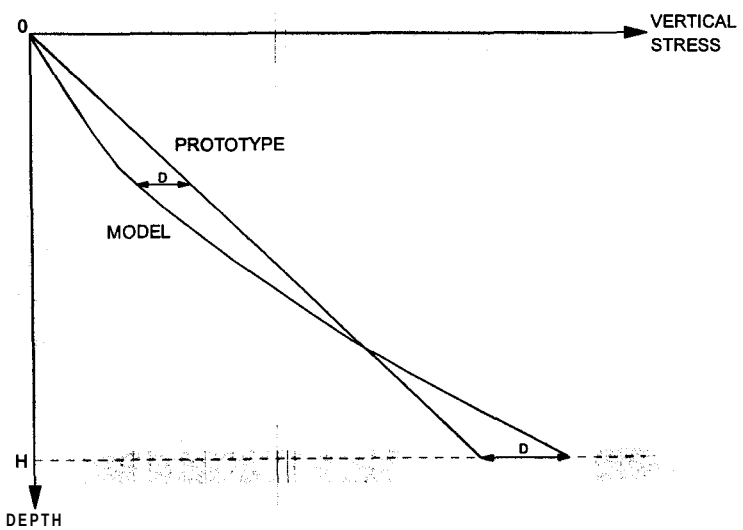

Figure A2b - Minimisation of Absolute Error

A.3.2 Area minimisation

At the point of intersection of the two curves

$$\rho\omega^2 Rz + \frac{(\rho\omega^2 z^2)}{2} = \rho\omega^2 z(R+x). \tag{A.lO}$$

$$\therefore z = 2x$$

Between depths of 0 and 2x, area between curves is

$$A_T = \int_0^{2x} \left(\rho\omega^2 zx - \frac{(\rho\omega^2 z^2)}{2} \right) dz \tag{A.1 1}$$

$$= \frac{2\rho\omega^2 x^3}{3}. \tag{A.12}$$

Between depths of 2x and *H*, area between curves is

$$A_n = \int_{2x}^{H} \left(\frac{\rho\omega^2 z^2}{2} - \rho\omega^2 zx \right) dz \tag{A.13}$$

$$= \frac{\rho\omega^2 H^3}{6} - \frac{\rho\omega^2 H^2 x}{2} + \frac{2\rho\omega^2 x^3}{3}, \tag{A.14}$$

From (12) and (14), total area is given by

$$A = A_T + A_B = \frac{\rho\omega^2 H^3}{6} - \frac{\rho\omega^2 H^2 x}{2} + \frac{4\rho\omega^2 x^3}{3}. \tag{A.15}$$

$$\frac{dA}{dx} = 4\rho\omega^2 x^2 - \frac{\rho\omega^2 H^2}{2}. \tag{A.16}$$

Minimising this gives

$$\underline{x = H/(2\sqrt{2}) = 0.354H}$$

A. 3.3 Equating areas

For equal areas either side of the point of intersection, from (A.12) and (A.14)

$$\frac{\rho\omega^2 H^3}{6} - \frac{\rho\omega^2 H^2 x}{2} + \frac{2\rho\omega^2 x^3}{3} = \frac{2\rho\omega^2 x^3}{3}. \tag{A.17}$$

$$\therefore \frac{H^3}{6} = \frac{H^2 x}{2},$$

$$\therefore \underline{x = H/3 = 0.333H}$$

A. 3.4 Minimising absolute error

Error at bottom, depth H

$$E_B = \frac{\rho\omega^2 H^2}{2} - \rho\omega^2 Hx. \tag{A.18}$$

Error in top

$$E_T = \rho\omega^2 zx - \frac{\rho\omega^2 z^2}{2} \tag{A.19}$$

For a fixed x, maximum error in the top must occur at $z = x$

$$\text{i.e.} \quad E_{T=}\frac{\rho\omega^2 x^2}{2}. \tag{A.20}$$

For equal absolute errors,

$$E_T = E_B.$$

$$\frac{\rho\omega^2 H^2}{2} - \rho\omega^2 Hx = \frac{\rho\omega^2 x^2}{2}. \tag{A.2 1}$$

$$\therefore x = (\sqrt{2} - 1)H = 0.414H$$

A. 3.5 Minimising percentage error

The percentage error between the two curves is given by

$$E_{\%} = \frac{\left|\rho\omega^2 zx - \frac{\rho\omega^2 z^2}{2}\right|}{\rho\omega^2 z(R+x)}. \tag{A.22}$$

$$\text{or} \quad E_{\%} = \frac{\left|x - \frac{z}{2}\right|}{(R+x)}. \tag{A.23}$$

This analysis is the only one of the six considered which is dependent upon the dimensions of the model, i.e. R & H.

The percentage error is 0 at a depth of $z=2x$. Above this point, the worst error is near the surface, as $z \rightarrow 0$. It is perhaps more useful to consider the error at $z=x$, the depth of the maximum absolute error, the approach used by Schofield (1980).

$$E_{\%\ MAX-(z=x)} = \frac{x/2}{R+x}. \tag{A.24}$$

Below $z=2x$, the worst error is at the base.

$$E_{\%MAX\text{-}BASE} = \frac{\frac{H}{2}-x}{R+x}. \qquad (A.25)$$

Equating these two gives

$$\therefore \; x = H/3 = 0.333H$$

The dependence of this error on the dimensions of the model is shown in figure A3.

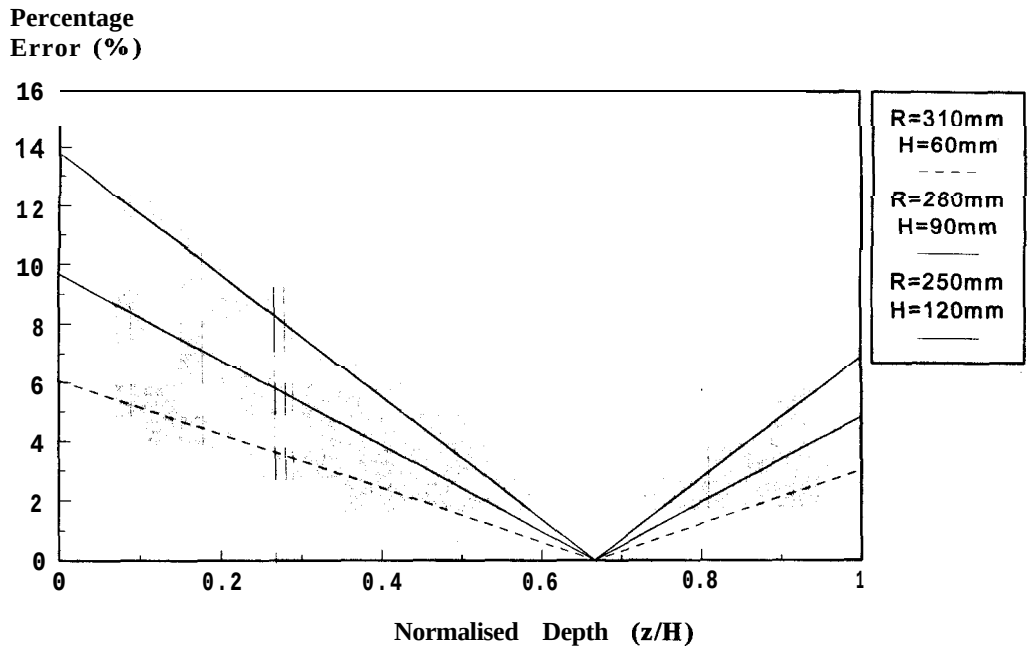

Figure A3 - Percentage Error vs Normalised Depth

A.3.6 Least squares optimisation

Difference between two curves is

$$\rho\omega^2 zx - \frac{\rho\omega^2 z^2}{2}. \qquad (A.26)$$

Difference squared over the whole depth is

$$\int_0^H \left(\rho\omega^2 zx - \frac{\rho\omega^2 z^2}{2}\right)^2 dz. \qquad (A.27)$$

This gives

$$\therefore \quad \underline{x = 3H/8 = 0.375H}$$

A. 3.7 Summary

The results are summarised in figures A4a and A4b below

Method	x
$x = H'$	-
Area Minimisation	0.354H
Equating Areas	0.333H
Absolute Error	0.414H
Percentage Error	0.333H
Least Sauares	0.375H

Figure A4a - Summary of Variable Acceleration Analysis

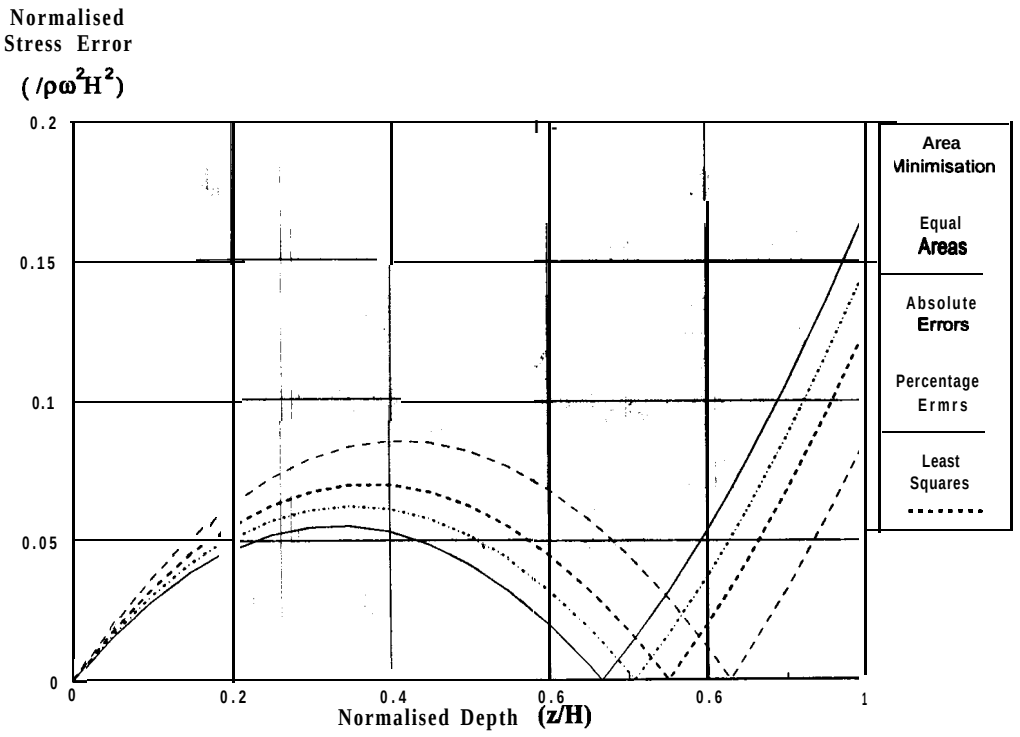

Figure A4b - Normalised Errors vs Normalised Depth

A.4 Practical modelling considerations

The analysis of section A.3 was concerned with the stress errors throughout the depth of the mini-drum channel.

There will be errors introduced into most modelling work by the effect of the rigid boundary at the base of the model. For this reason, the lower 5-10mm of the model would normally be ignored for practical modelling purposes. In addition to this, most models are underlain by a 6mm thick base drain.

With the Mk II mini-drum channel depth of 120mm, this means that the lowest 10% of the channel can be ignored for most modelling, and the effect of this on the error analysis will now be examined. Equations (A. 10) to (A.27) can be re-written, simply substituting 0.9H for H. The results thus obtained are shown in figures A5a and A5b below.

Method	*x*
Area Minimisation	0.318H
Equating Areas	0.300H
Absolute Error	0.373H
Percentage Error	0.300H
Least Sauares I	0.338H

Figure A5a - Summary of Variable Acceleration Analysis - 0.9H as Lower Limit

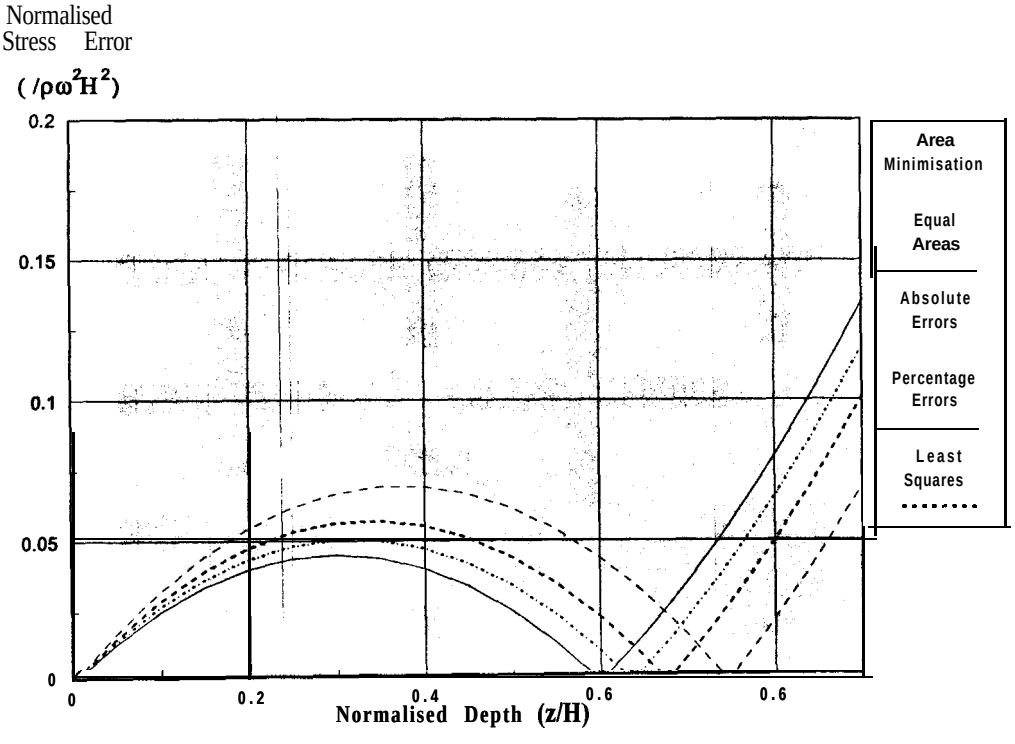

Figure A5b - Normalised Errors vs Normalised Depth - 0.9H as Lower Limit

A.5 Choice of x and hence H'

Clearly, the different approaches to error minimisation lead to different optimum values of x and hence H', the depth at which stresses are correctly matched. The variation of maximum understress and overstress errors with H' is shown in figure A6. The lowest 10% of the channel depth has been discounted.

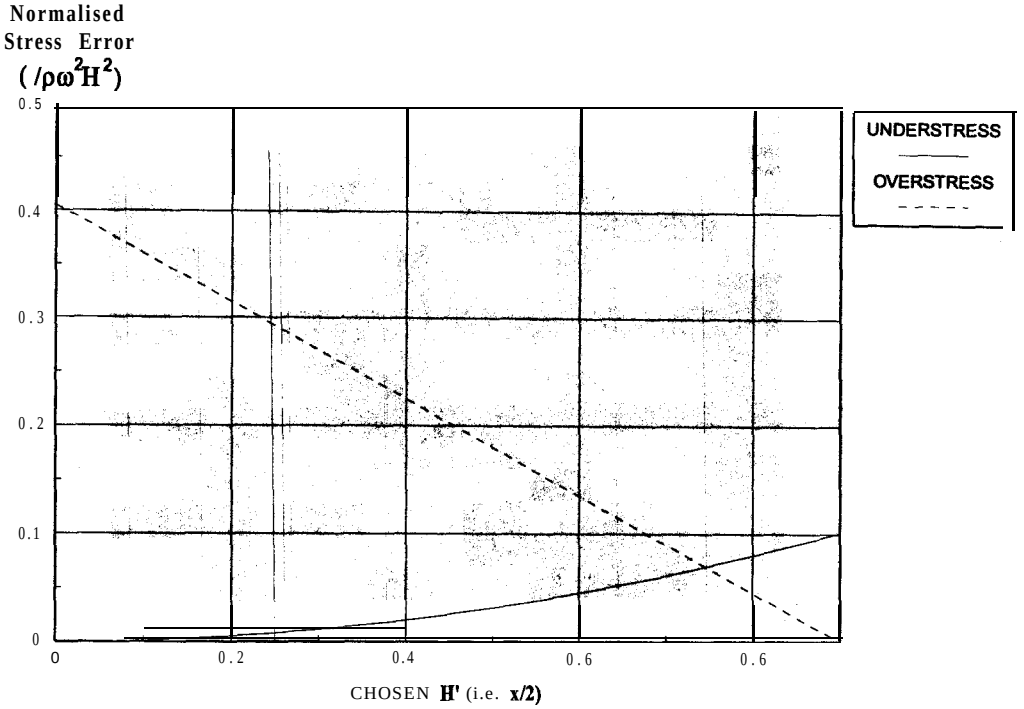

Figure A6 - Variation in Understress and Overstress with Chosen H' Values

A. 6 Conclusions

- It has been shown that it is not possible to select a radius for calculation of a nominal acceleration to be applied to the whole model, at which the model and prototype stresses are identical.

- Different methods of error analysis and minimisation lead to quite similar optimum values of x: between $0.333H$ and $0.414H$ if the full depth of the channel is considered, or between $0.300H$ and $0.373H$ if the lowest 10% is discounted.

A. 7 Recommendations

There are two options open to workers using the mini-drum centrifuge:

(i) Perform all calculations and analysis taking account of the varying g-level and hence self-weight with depth.

(ii) Choose one nominal value of acceleration for the whole model, minimising the stress errors thus introduced.

(ii) is more practical in most situations. The conventional choice for the depth at which stresses are identical in prototype and model, 2H/3, as proposed by Schofield (1980), is little different from other values suggested by the various methods of error analysis and this is recommended. The nominal radius which must therefore be chosen lies at depth of H/3 within the model.

APPENDIXB

COURSEWORK REPORTS OF NICHOLAS SARTAIN

PART IIB A3 GEOTECHNICAL MODELLING

COURSEWORK 1: CENTRIFUGE TEST DATA REPORT

NICHOLAS SARTAIN, GIRTON

0.0 Four model sand embankments were constructed on a clay foundation in a centrifuge test. They were constructed at different rates and some had a geotextile reinforcement. This report looks at data collected from the test from pore pressure transducers (ppts) located in the clay.

1.0 The prototypes modelled in each of the tests were all identical and are shown in fig. 1. The model dimensions varied, but when multiplied by the appropriate scaling factor (the g-level that the test was run at) they each represent the same prototype.

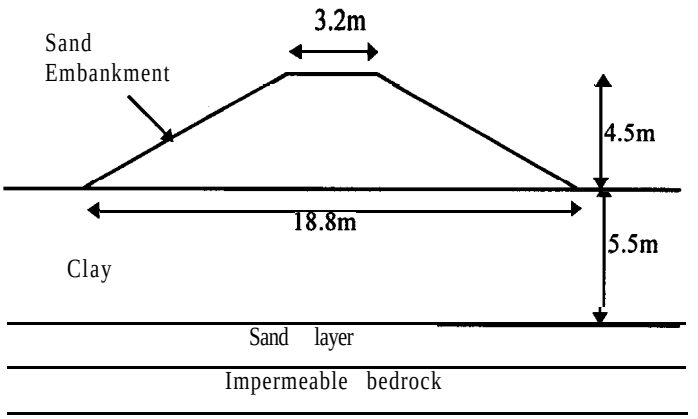

Figure 1. Prototype modelled in centrifuge tests

Only half of the prototype was modelled as it was assumed to behave symmetrically as only loading due to self weight was considered. The base drain of the model represents by a sand layer of high permeability in the prototype.

2.0 Initially, the clay was poured into the drum under water and was then allowed to consolidate. This corresponds to the natural deposition and consolidation of soil in the field. The construction of the embankment by pouring the sand represents the real life construction of such a soil structure. What is not modelled is the compaction such a structure would receive were it real. As the embankment grew, the pore pressures in the clay increased due to the low permeability of the clay. Sudden blips in the pore pressure traces indicate local failure occurring in the clay and are due to the clay temporarily losing its strength, and transferring load to the pore water. This is as would be found in the prototype.

2.1 At the end of construction the excess pore pressures dissipate slowly and settlement occurs. Again, this is as would be expected in the prototype when it is completed.

3.0 At the beginning and at the end of each test, it can be assumed that the model has reached its steady state, i.e. excess (transient) pore pressures have dissipated. The pore pressures measured relative to the drain at these times can be used to measure vertical displacement as their value is only dependent upon their depth. Table 1 shows these relative pore pressures for tests 1 and 3, the change in pore pressure, and hence the settlement (p) of the model at these locations to the nearest 5 mm. The table also shows relative pore pressures recorded at the end of the embankment construction. The pore pressures will be transient at this point, but because the ppts are very close to the clay surface it may be assumed that dissipation of excess pore pressures occurs instantaneously. This assumption will be studied later in the report.

		ppt4			ppt5			ppt6			ppt7		
		u (kPa)	Δu (kPa)	ρ (mm)	u (kPa)	Δu (kPa)	ρ (mm)	u (kPa)	Δu (kPa)	ρ (mm)	u (kPa)	Δu (kPa)	ρ (mm)
test	**init'**	70.0	-	-	70.0	-	-	65.0	-	-	72.5	-	-
1	eoc	74.5	-4.5	-460	68.0	2.0	205	65.0	0.0	0.0	73.0	-0.5	-50
unrf	**final**	73.0	-3.0	-305	65.2	4.8	490	63.0	2.0	**205**	70.2	2.3	235
test	**init'**	65.5	-	-	67.0	-	-	67.5	-	-	70.5	-	-
1	eoc	61.0	4.5	460	63.0	4.0	410	67.0	0.5	50	72.0	-1.5	-155
rf	**final**	62.5	3.0	305	62.5	4.5	460	65.0	2.5	255	69.5	1.0	100
test	**init'**	71.0	-	-	72.0	-	-	71.0	-	-	72.0	-	-
3	eoc	73.0	-2.0	-205	62.0	10.0	1020	66.0	5.0	510	71.0	1.0	100
unrf	**final**	73.2	-2.2	-225	67.0	5.0	510	68.5	2.5	255	71.2	0.8	80
test	**init'**	76.2	-	-	75.0	-	-	73.0	-	-	73.0	-	-
3	eoc	72.0	4.2	430	70.0	5.0	510	68.2	4.8	490	71.5	1.5	155
rf	**final**	73.5	2.7	275	70.5	4.5	460	69.5	3.5	360	70.5	2.5	255

init' : initial value eoc : end of construction final : final value
unrf : unreinforced **rf** : reinforced positive displacements are down

Table 1. Settlement of the models from pore pressure measurements.

4.0 Test 1 was constructed in 90 minutes (=625 days prototype time). Test 3 was constructed in 40 minutes (=278 days prototype time). Fig 2 is a plot of the pore pressures recorded in the middle of the clay. It is taken from the main results and is only to show the trends as it is not an accurate plot. It can be seen clearly from fig 2 that the faster construction leads to much higher excess pore pressures in the clay than slower construction for both the unreinforced and reinforced cases. Construction was finished after 5400s in test 1 and after 2400s in test 3. It can be seen that the excess pore pressures in both cases reach their maximum just after construction is completed.

4.1 Referring now to table 1 it can be seen that, with the exception of the readings from ppt 4, the displacements in test 3 (the faster test) are larger than those in test 1. This is the case whether the embankment is reinforced or not. These results complement those of fig 2 well. Excess pore pressures cause a reduction in the effective stress of a soil which therefore reduces its shear capacity, or strength. Therefore, high excess pore pressures are associated with larger settlements than low excess pore pressures

as the soil is more likely to fail (even if only locally) if there are high pore pressures present. It is interesting to note that often the settlement appears to be greater at the end of construction than at the end of the test. This is probably because the pore pressures are transient at the end of construction so are larger than they would be at equilibrium. Because we are plotting relative pore pressures, this gives a reading of greater displacement than has actually occurs. This shows that the assumption that the pore pressures would dissipate immediately from the top of the clay is invalid.

5.0 Fig 2 shows that the rate of pore pressure build up is less for the reinforced models and that it tends to peak at a lower value as well. A comparison of the raw data also shows much smoother variations of pore pressures with time for the reinforced tests indicating that less local failures and slips are occurring here. This is particularly noticeable in test 3 where the unreinforced model has very erratic plots indicating failure. The settlements recorded in this model are also very large. More importantly, the differences in settlement from point to point are very large and are enough to assume that failure had occurred.

5.1 Reinforcement does not seem to reduce the overall settlement of the embankment. This is not surprising as the total load applied to the soil is the same in both unreinforced and reinforced cases so the total settlement should be the same. It does however appear to **redeuce** differential settlement across the base as shown in fig 3. This is because the reinforcement reduces the amount of pore pressure build up in the clay so local slipping and failure do not occur and hence neither do variations in settlement. There is a horizontal load on the clay produced by the sand embankment. This is because sand is a frictional material and can only form an embankment by exerting a horizontal frictional force on the clay. The geotextile carries this load and so reduces the load on (and therefore stress in) the clay and hence reduces the pore pressure rise when the embankment is built. Also, for failure or large deflections to occur at the clay surface, a significant amount of stretching of the surface must take place. The reinforcement inhibits this action as well helping to keep settlement down.

5.2 It is interesting to note that there is heave next to the boundary for the unreinforced models. This would not be expected in the field and is due to an unforeseen failure mechanism due to the boundary, probably because of a frictional effect. It does not occur in the reinforced models because the reinforcement only permits low variations in settlement and so the heaving is reduced.

6.0 To conclude it is possible to say that the embankments **modelled** behaved in line with established theories. The faster loading led to higher pore pressures and greater settlement, and differential settlement was reduced by using a geotextile reinforcement.

Figure 2. Mid-clay pore pressure measurements

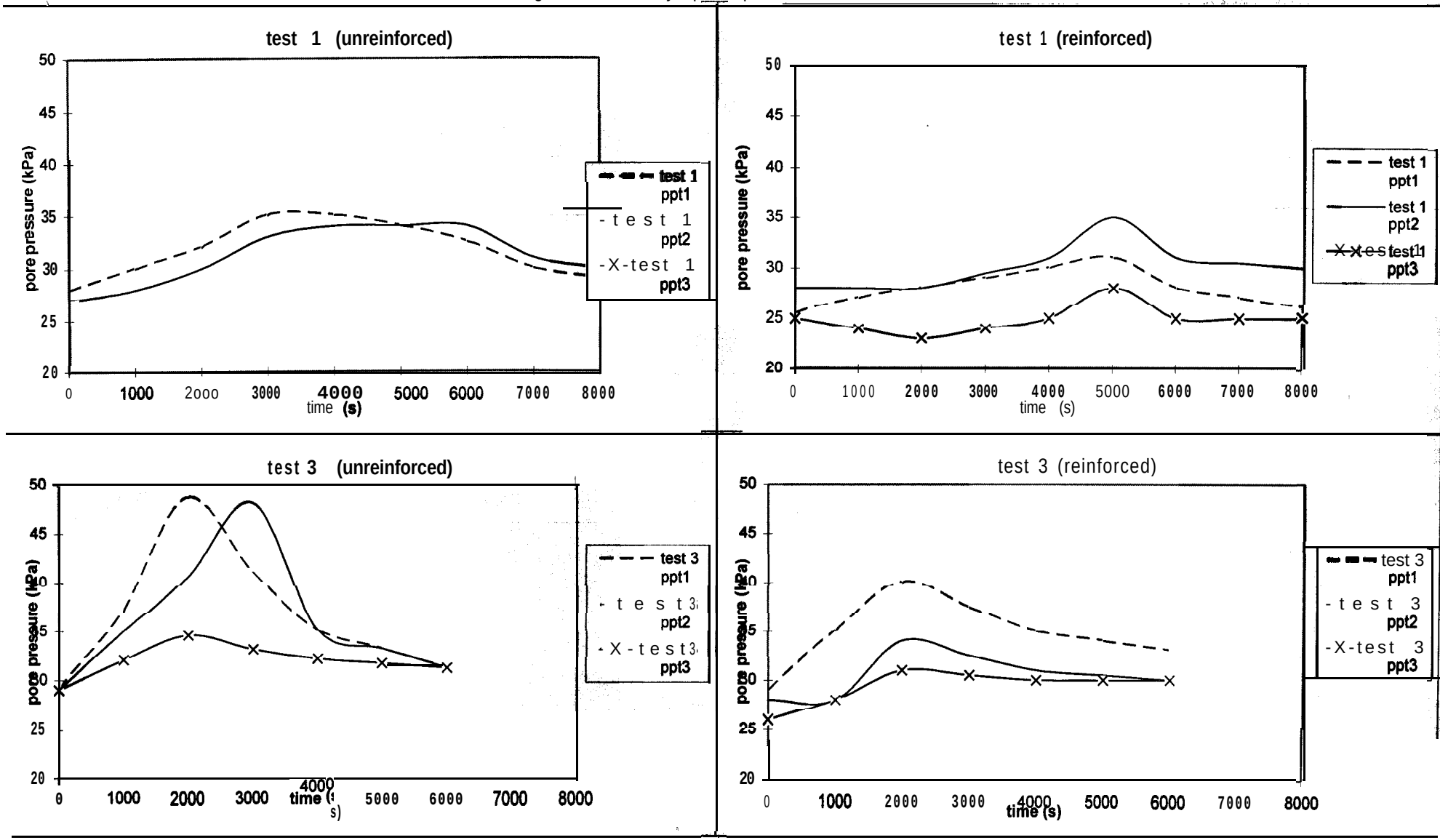

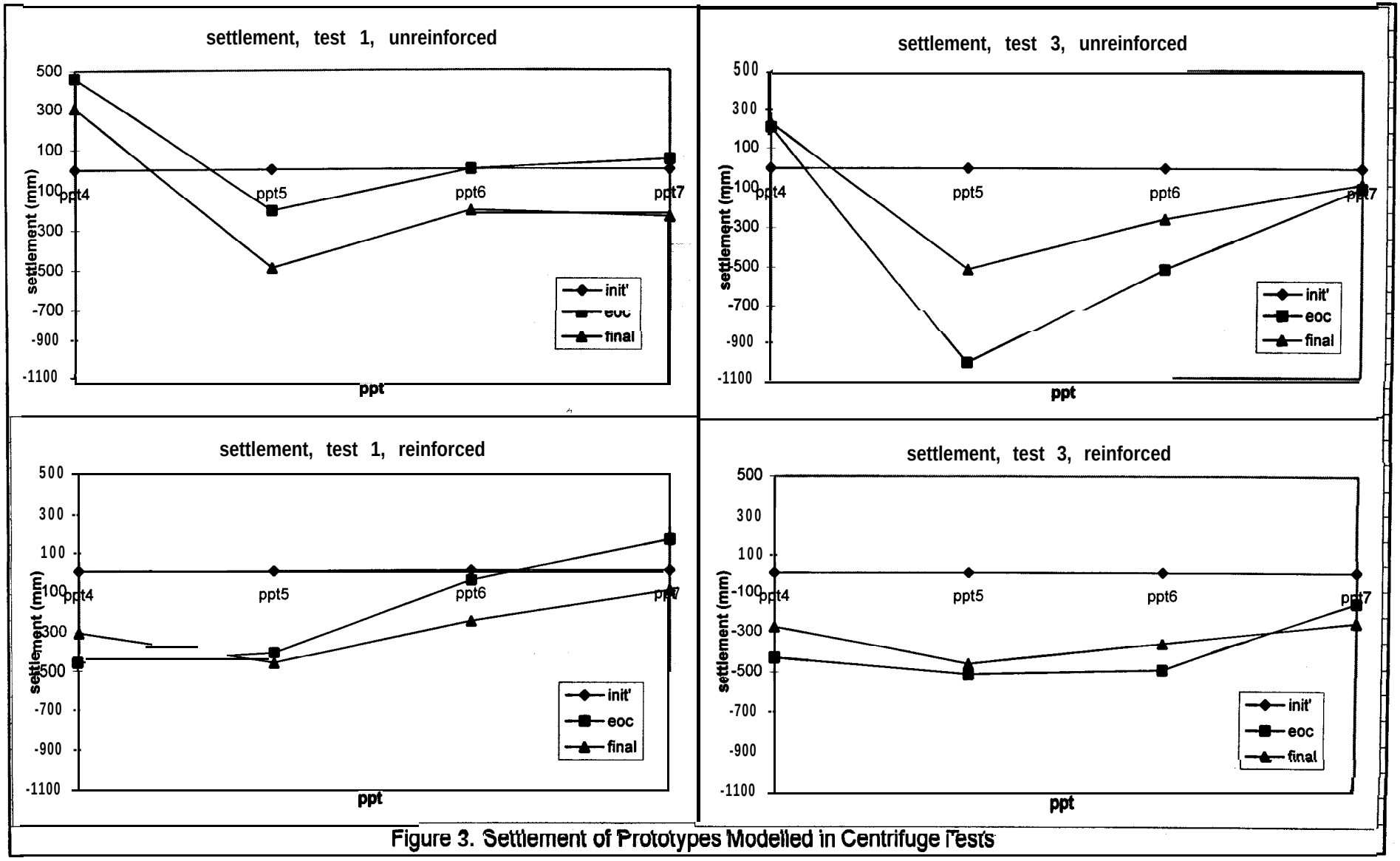

Figure 3. Settlement of Prototypes Modelled in Centrifuge Tests

PART IIB A3 GEOTECHNICAL MODELLING

COURSEWORK 2 : FINITE ELEMENT MODELLING REPORT

NICHOLAS SARTAIN, GIRTON

0.0 A finite element package called GeoFEAP was used to model soil structures previously tested in a drum centrifuge. The program was used to model the load/ deflection response of the structures and the stress paths that they were subjected to.

1.0 The program was run using the Cam Clay constitutive soil model. Before using the program, it was therefore necessary to calculate the appropriate Cam Clay parameters of the soil to be studied. This was done from test data supplied. The results of these calculations are:

λ = 0.130 (gradient of consolidation curve, fig 7.4)
κ = 0.028 (gradient of swellback curve, fig 7.4)
M = 0.87 (gradient of line joining yield points in fig 8.8)
e = 1.92 (@ 1kPa on isotropic consolidation line)

2.0 Initially, a clay rigid footing was incrementally loaded by a uniformly distributed load (UDL).The results of this loading are shown in figure 1. Four soil cases were loaded. Case 1 was slightly overconsolidated clay in drained conditions, case 2 was heavily overconsolidated clay in drained conditions. Cases 3 and 4 were for undrained conditions.

2.1 From the plots of load vs vertical displacement, it is clear that the drained soil is much less stiff than the undrained soil. However, the plot of load vs horizontal displacement shows the undrained samples deflecting most. This is because they are having to deflect at constant volume. The drained samples are deflecting more in the vertical direction because they can compress. Stiffness increases with overconsolidation ratio but the effect is small before failure. Both soils are responding elastically before failure. Failure is seen by disproportionately large increases in displacement with load and it can be seen that both undrained samples failed under the applied loading. This indicates that the undrained soil behaves more brittly as well as more stiffly than the drained soil. Overconsolidation ratio effects significantly at what load failure occurs at. This is because the location of the yield surface of a soil is defined partly by the maximum previous stress in the soil.

2.2 The plots of effective stress paths for the undrained soil are as expected for the Cam Clay model. The undrained samples show no change in effective stress as the load increases until failure occurs and then there is a large change. The drained tests show a steady increase in effective stress as the load is increased as the pore fluid seeps away quickly so takes no load. The difference between the plots for elements 81 and 86 are due to the differences in load applied as the test progressed. The deviatoric stress in element 86 is lower than in element 81 because the lateral earth pressure is higher relative to the vertical stress due in the soil because element 86 is near the edge of the footing.

3.0 The input file was now adjusted so as to model the embankments tested in the centrifuge tests. It was possible to model the construction of the embankments and to model them as either reinforced or not as in the centrifuge tests. Figure 2 shows the displacement along the top surface of the clay foundations the embankment is constructed. The deflections of the undrained models are shown only up to failure as they became excessive for plotting after failure.

3.1 The form of the plots in figure 2 are as expected with the soil rotating about the feet of the embankments. As before, the undrained soil initially is stiffer than the drained soil, but fails first in a brittle fashion. The reinforcement appears to have little influence on the drained soil's displacement. This is not surprising as the drained displacement is a long term function and the reinforcement increases the strength of the soil in the short term whilst excess pore pressures dissipate. The reinforced model in the undrained test would therefore have been expected to perform significantly better than the unreinforced model. In fact it performed worse. This indicates that either there was an error in the input file or that the soil yields close to the stresses created by stage 4 of the construction and that the program found the soil to have just yielded for the case with the reinforcement and to have just not yielded for the case without reinforcement.

3.2 All the embankments have failed in that the final displacements are all large in comparison with the size of the embankments. The undrained ones have failed in a brittle manner and the undrained ones have settled stably but significantly.

3.3 Figure 3 shows the horizontal displacement at the toe of the embankments. It tells much the same storey as for the rigid footing. The drained tests have larger displacements than the undrained ones until failure, again because of the requirement to keep constant volume.

3.4 Figure 4 shows the stress paths in p'-q and p-q space during construction for the locations of the pore pressure transducers used in the centrifuge tests. It can be seen that there is little difference between plots for comparable reinforced and unreinforced models before yield. After yield it is harder to say what is happening as failure occurs rapidly and so the plots begin to not mean much.

3.5 Pore pressure transducers (ppts) 1, 2 and 3 were in the main body of the foundation. The stress paths of the undrained tests remain much more stable than those near the surface of the foundation (ppts 4, 5, 6 and 7) because the displacement is much lower. This is a problem with the finite element method.

3.6 The effective stress plots show the correct trends. The undrained analyses show no change in effective stress as the embankments are constructed. This is because all the load from the embankment is being carried by the pore fluid. For the drained test, the stress in the soil increases by less as you move towards the toe of the embankment from the centre. This is as expected as the embankment is sloped to the toe. The gradient of the p'-q plot is the same for all the locations in the soil because this is a soil property for vertical loading.

3.7 The total stress plots are harder to understand. The gradients for the undrained soils are lower than for the drained ones. This is probably because the undrained soil is behaving more like a fluid in a beaker and so has large lateral soil forces. This keeps

the deviatoric stress down. The drained soil is more likely to deform and carry the load vertically, behaving more like a solid. This keeps the deviatoric stress relatively high. It can be seen again that the stresses in the soil reduce with distance from the centre of the embankment. Brittle soil failures are associated with great fluctuations in stress. The undrained total stress plots show this clearly. The drained soil doesn't fail as such, but its deflections are so large that it can be said to have failed. This is not shown clearly on the stress paths.

4.0 To conclude, it appears that the finite element program models as expected the stresses and deflections in clay before yield, but becomes less reliable once the soil has yielded. It is probably necessary to use a finer mesh and use correspondingly smaller increments of load to get a more accurate picture of the behaviour after yield.

Figure 1. Load vs displacement and stress paths for a rigid footing

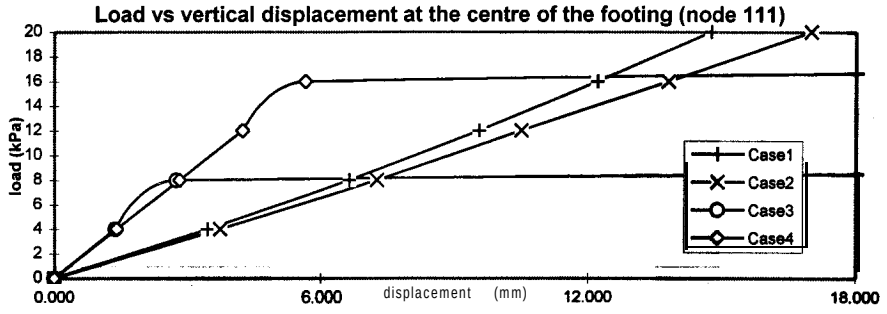

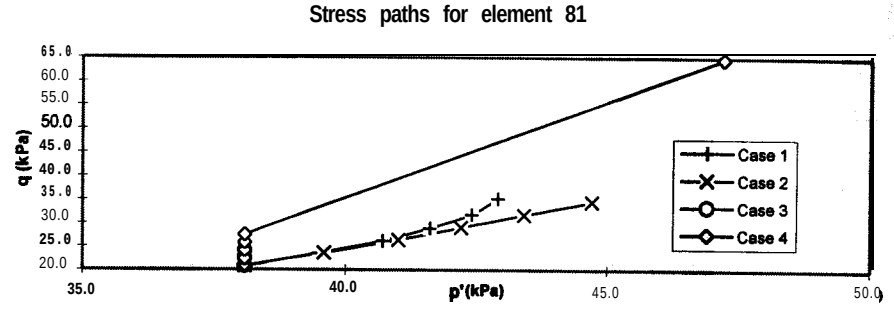

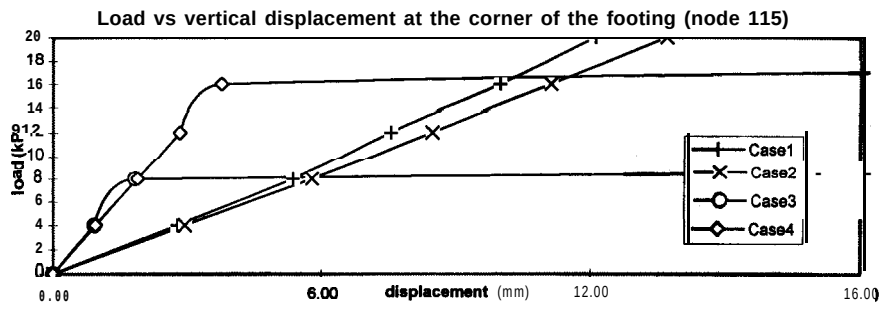

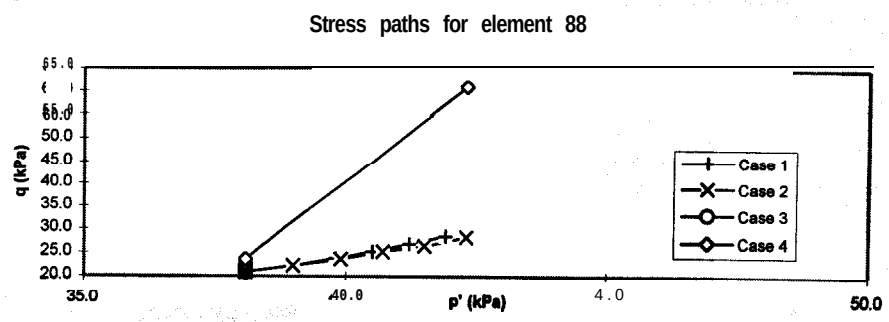

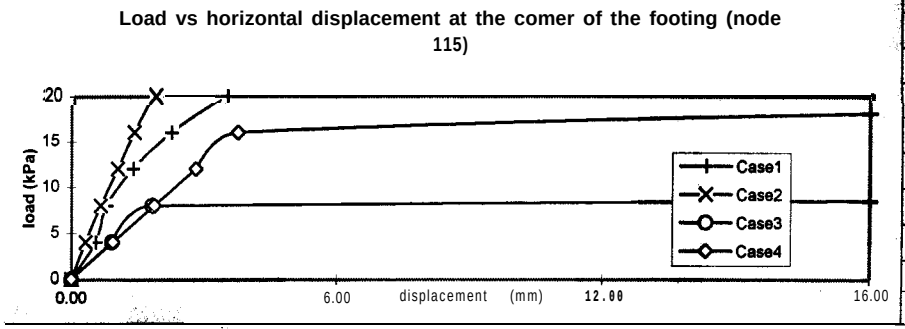

Figure 2. Load vs displacement along the top surface of the clay foundation for embankment construction

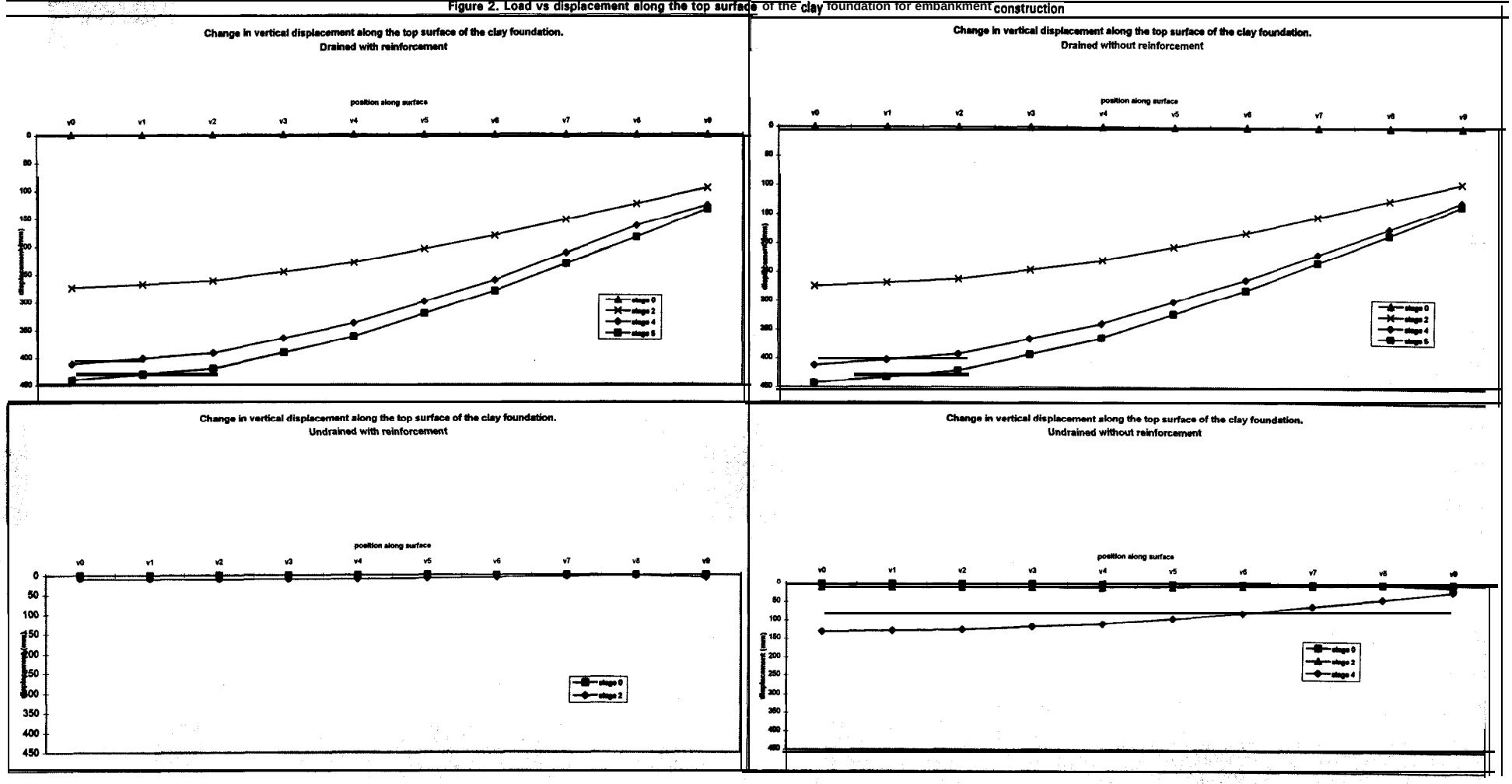

Figure 3. Horizontal displacement at the toe of the embankment

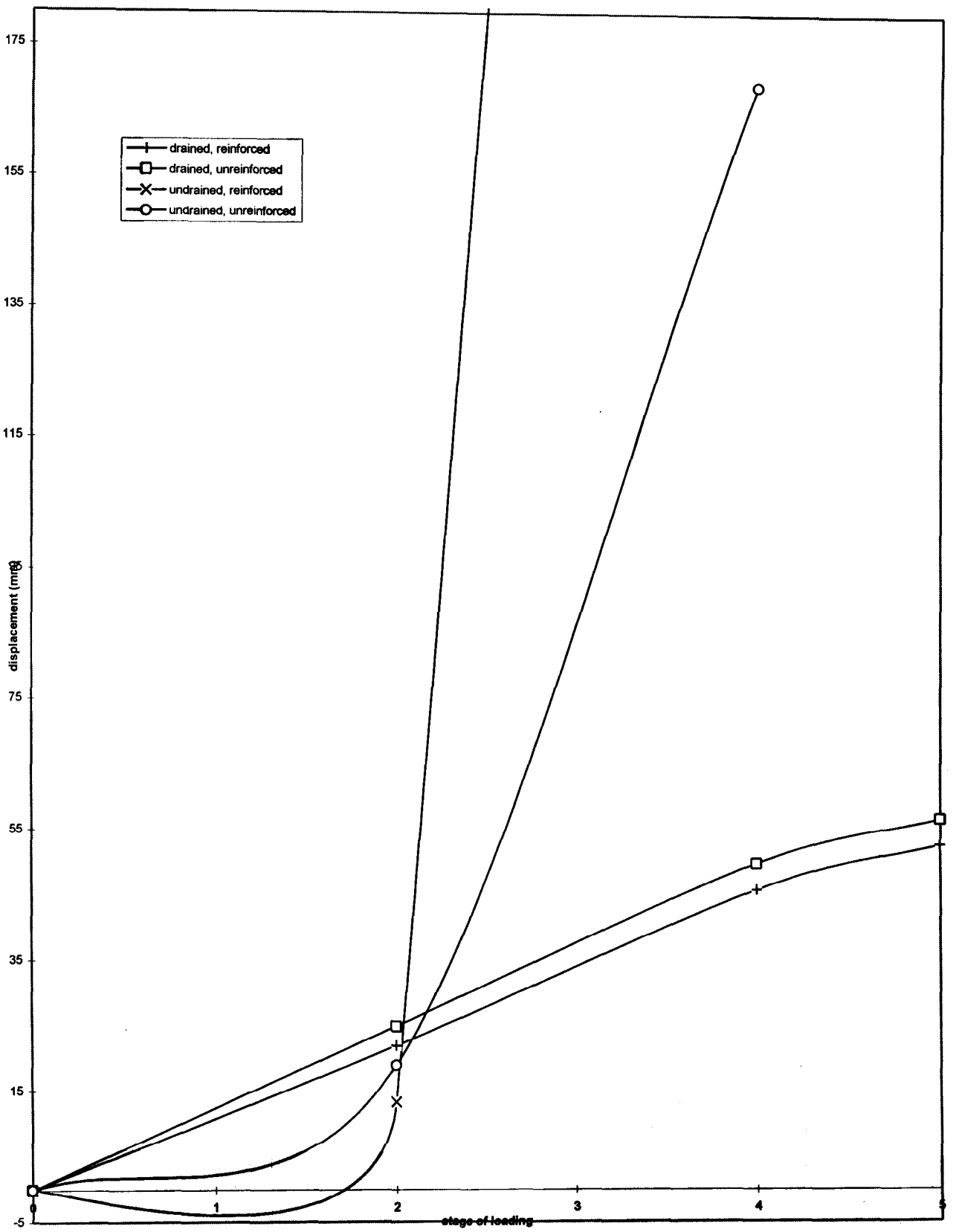

Figure 4. Stress paths at the locations of the pore pressure transducers

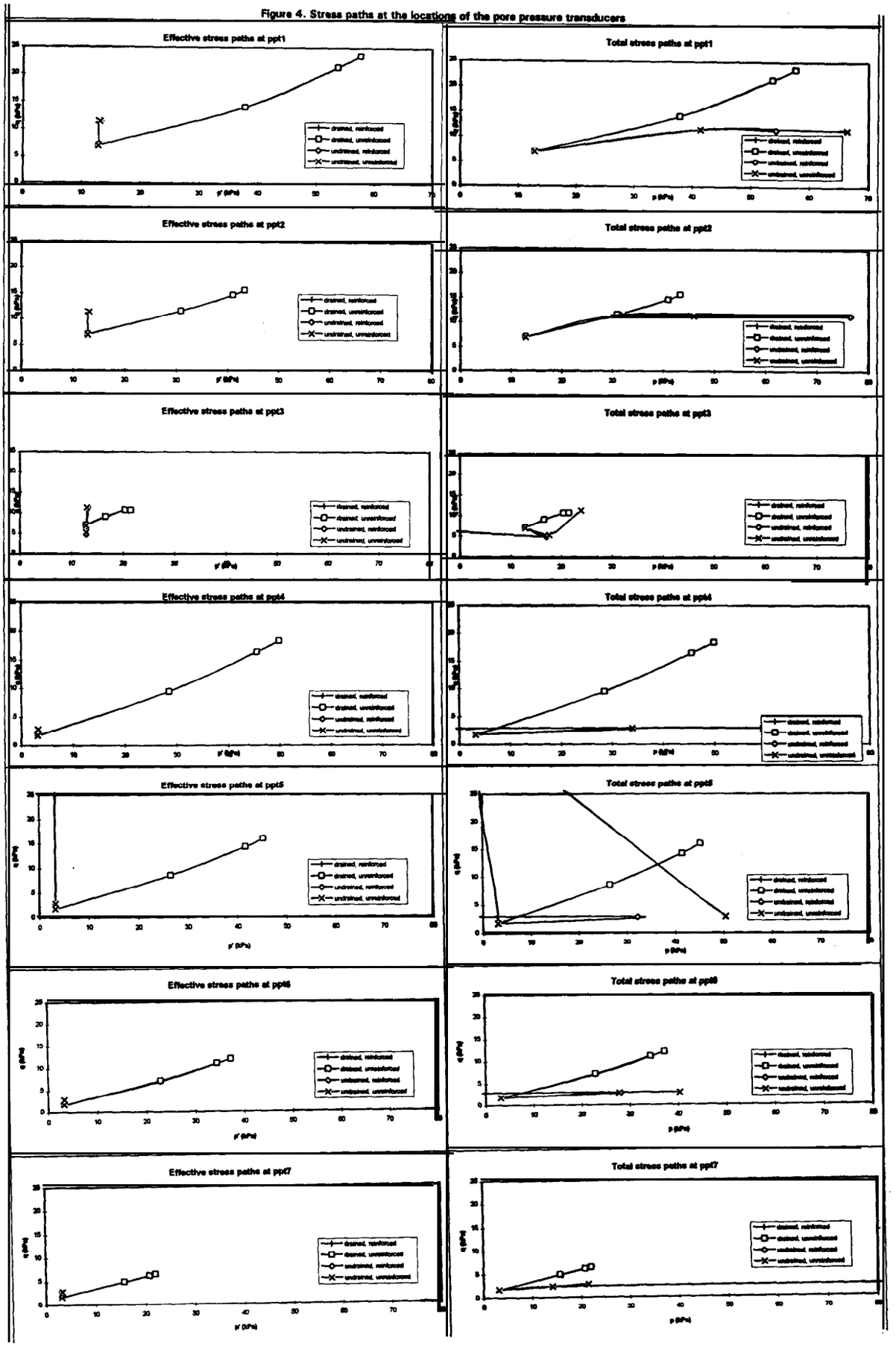

PART IIB A3 GEOTECHNICAL MODELLING

COURSEWORK 3 : FINAL REPORT

NICHOLAS SARTAIN, GIRTON

1.0 INTRODUCTION

This report compares and contrasts physical centrifuge modelling and numerical finite element modelling in geotechnical engineering. It completes work done with the centrifuge and on the computer which involved the analysis of the construction of a sand embankment on a clay foundation. In both cases the prototype modelled was the same, the same materials were used and the same boundary conditions were imposed. This report attempts to estimate whether or not these methods are valid as a means of predicting displacement, capacity and failure in geotechnical design.

2.0 CENTRIFUGE TEST

The clay foundation in the centrifuge test was instrumented with pore pressure transducers just below the surface and at around mid-depth. These were used to measure the excess pore pressures generated during construction of the embankment and to measure the vertical displacement after settlement had occurred and their excess pore pressures had dissipated.

Without performing an extensive flow net type analysis using parabolic isochrone theory and without considering the time taken for construction, the excess pore pressures can be calculated by estimating the weight of sand deposited above a given point in the foundation. The prototype height of the embankment at its crest is 4.5m and if we assume the unit weight of dry sand (γ') to be approximately 7 kN/m^3 , the excess pore pressure (Au) under the crest of the embankment is 7 x 4.5 = 31.5 kPa. This is the location of pore pressure transducer (ppt) 1. Similar calculations at the locations of ppts 2 and 3 give Au = 20.8 and 0.0 kPa respectively. The peak measured excess pore pressures at these locations were =19.0 kPa for ppts 1 and 2, and =5 kPa for ppt 3. These were for test 3, the faster of the two performed. I expect these values to be what a detailed analysis would find. The peak value for ppt 1 is reached just before the end of construction showing that the speed of construction was slow enough for excess pore pressures to begin to dissipate before construction was complete, and so the calculated value can never be achieved. The peak value for ppt 2 is reached just after the end of construction and is approximately equal to the calculated value. This is because pore water from the region near ppt 1 is dissipating towards ppt 2 faster than the pore water from ppt 2 can dissipate away as it has a larger driving pressure (greater overburden). This too is the reason for the peak in pore pressure at ppt 3. The pore water from underneath the embankment is being forced towards ppt 3 faster than it can escape to low pressure areas (drains). The figures from test 1 (a slower test) are generally much lower than for test 3. This further confirms that dissipation of pore pressures is occurring faster than they are being built up by construction, rendering simple analyses useless in predicting them.

Likewise, it is not trivial to predict the settlement of the embankment. The shear strength of the soil is reduced by excess pore pressures and so it may be assumed that as the pore pressures in the centrifuge tests were found to be close to those predicted, the ultimate

displacements would be too. Intermediate displacements cannot be reliably taken from ppt readings due to the unknown effects of transients during construction.

3.0 COMPARING FE AND CENTRIFUGE RESULTS

The finite element analysis was performed for undrained and drained cases. The drained case corresponds directly to the centrifuge model when all transient pore pressures have died away and equilibrium has been re-established. Hence, direct comparisons can be made between the FE analysis and the centrifuge test. The undrained case, however does not correspond to anything in the centrifuge tests because the speed of construction was so slow and the drains were so nearby that drainage occurred. Therefore there is nothing to compare the undrained analysis with and in real constructions totally undrained conditions will very rarely be found.

Figure 1 shows the displacements at the surface of the clay layer for the drained FE analyses and for the centrifuge tests when the excess pore pressures had dissipated. Some of the points have been found by iteration. It can be seen from the figure that the form of the displacement is the same for both the computer prediction and for the physical test. However, the magnitudes of the displacements are different. The reason for the differences in magnitude are probably due to inaccuracies in the inputting of clay parameters in the computer. It is not easy to know the exact stiffness (for example) of the soil used in the test as these values were calculated by averaging values taken from a number of laboratory tests. It can also be seen that the computer models the centre line boundary better than the centrifuge test because it can make it effectively frictionless.

In the centrifuge tests it was noted that the reinforcement tended to reduce the differential settlement of the embankment although it had little effect on the overall settlement. This difference was not found in the FE analyses. This is possibly because the settlement profile was smoother in the first place or possibly because a drained analysis can be thought of as one of a very long timescale, and so it could be argued that ultimately the reinforcement wouldn't have had much effect on the settlement in the centrifuge tests so long as they were left for long enough.

There can be no comparisons between the FE models and the centrifuge tests in terms of pore pressures. Again, this is because the FE analyses only considered fully drained or fully undrained conditions. By definition, fully drained conditions require there to be zero excess pore pressure and this must agree with the centrifuge test so long as it is left for long enough. As mentioned above, the centrifuge tests never measured anything approaching fully undrained conditions so attempts at comparison with the FE case are meaningless.

It is clear that FE calculations of drained and undrained analyses are not adequate for this problem and that some form of inbetween, time related analysis is required. This would clearly result in a much more complicated code with capacity for calculating transient Pore pressures.

4.0 MATERIAL PROPERTIES

From the parametric studies performed, the values of κ, λ or e did not significantly effect the behaviour of the embankment. The factors to which the embankment was sensitive to

were the overconsolidation ratio (OCR) of the clay foundation and M, the gradient of the critical state line in the q-p' plane.

The larger the OCR the bigger the failure envelope in the q-p' plane becomes and the stiffer the clay becomes. This obviously means that the clay can withstand greater pressures and will deflect less for a given pressure so the embankment would be less likely to fail on a clay with a high OCR than on one with a low OCR.

M is a measure of the ratio of q, the deviatoric stress against p', the vertical effective stress at the critical state. The critical state is when the soil deforms to large strain with no increase in applied stress. The deviatoric stress is a weighted ratio of lateral to vertical stresses in the clay and increases as the lateral stress increases. As the embankment is built, the vertical stress in the soil under the crest will increase and there will be a corresponding, but modest increase in lateral stress. However, under the slope of the face of the embankment, the vertical stress increases moderately, but the lateral stress will increase disproportionately to balance the lateral stresses induced under the crest. In other words, the lateral stress in some parts of the foundation will increase faster than the vertical stresses due to the non-uniform loading of the embankment. This in turn will lead to an increase in the ratio of q to p' and will lead this soil to a position closer to the critical state line and failure. Hence, if M is increased then there is less chance of any soil reaching its critical state under the embankment and so of the embankment failing. Because the behaviour of the embankment and clay studied was found to be very sensitive to the value of M, it can be assumed that it was on the borderline between failing and not in the original analyses and this might explain some of the seemingly anomalous outputs (such as the reinforced embankment failing before the unreinforced one in the undrained condition).

κ, λ and e are less significant in the behaviour of the embankment because their exact values within the limits given have less effect on whether or not the soil reaches its critical state.

5.0 ANALYTICAL MODEL

Analysis of the embankment by simple hand methods is not straightforward unless some fairly gross approximations are made. I have analysed the embankment using a Tresca model for collapse load in appendix 1. The collapse height of the embankment is predicted to be 10.8m using this method. The model blocks are of such width that the chosen failure mechanism just fits in the foundation. The height of these blocks were then calculated as the average height of the embankment over that width (this gives 1.6m and 4. lm as shown). It was the assumed that these stress blocks would keep their relative heights as the embankment grew or shrunk so the blocks were labelled height h and 2.56h. Values for c_u, OCR, γ'_{clay} and γ_{sand} were assumed. The collapse height is obviously far from the actual collapse height and is also large enough to make invalid the mechanism chosen as the width of the embankment would have increased so much. The reasons for this include the neglecting of the surface friction (a significant oversight), a Tresca analysis is a totally undrained analysis, and that the soil parameters used are only rough estimates.

6.0 THE RELEVANCE OF CENTRIFUGE AND FE MODELLING TO DESIGN

Analytical solutions to problems in soil mechanics can only generally be found for problems with relatively simple loading, geometry, topography and soil condition. This is

because of the number of parameters involved in soil mechanics and because of their complicated interaction. It is therefore necessary to use whatever tools available to try to improve the accuracy of modelling for design. Centrifuge and FE models are becoming more and more important as bases for design and will continue to do so. Both have their advantages and their limitations.

The benefits of centrifuge modelling are that it is possible to use material from site for the tests, that site geometry can be approximated well, that soil stresses are modelled correctly (and this will therefore give the exact response of the soil in the ground provided the material used hasn't been disturbed or allowed to swell or dry out during sampling) and that different site conditions can be investigated relatively easily (for example dry and wet conditions). The main drawbacks with centrifuge modelling are the time taken and therefore expense of modelling (especially if several models are required), and the difficulty of instrumentation. Sometimes producing accurate models and stress histories is also difficult, and it is not always possible to get all the information you require because of the difficulties of instrumentation. Also, as we found out in these experiments, the modelling of the boundary conditions for a given problem is not always satisfactory and can lead to significant errors in the analysis if you are not wary.

The benefits of FE analysis are that complex problems can be investigated, boundary conditions can be modelled accurately, parametric studies are straightforward and it is relatively quick once the initial parameters are entered into the computer. The problems with FE analyses are that they are sensitive to material parameters which have to be determined by separate analysis, that it is not possible to perform all types of analysis (for example, in the work we have done only fully drained and undrained cases were looked at when a time dependent analysis would have been more suitable) and that they are sensitive to human error. It is very easy to use FE models badly and get answers to problems which are very wrong if you don't understand what is likely to happen and if you don't understand the program very well. i.e. you can use the wrong size or shape of elements, use too many or too few, make errors in modelling the boundary conditions etc. The other main problem with many FE programs is that they use elastic methods. To get accurate predictions of real life soil behaviour, a plastic method of analysis with a suitable (for the particular soil you are studying) constitutive equation relating think stresses and strains is required.

I we have shown in the work we have done that both centrifuge testing and FE modelling can be very useful tools in the design of geotechnical structures, provided that adequate safeguards are present against reading too much into results that may be erroneous due to limitations with these methods. They have been shown to incur less errors than simple hand methods (which have too many approximations) and so have a very important role to play in geotechnical design.

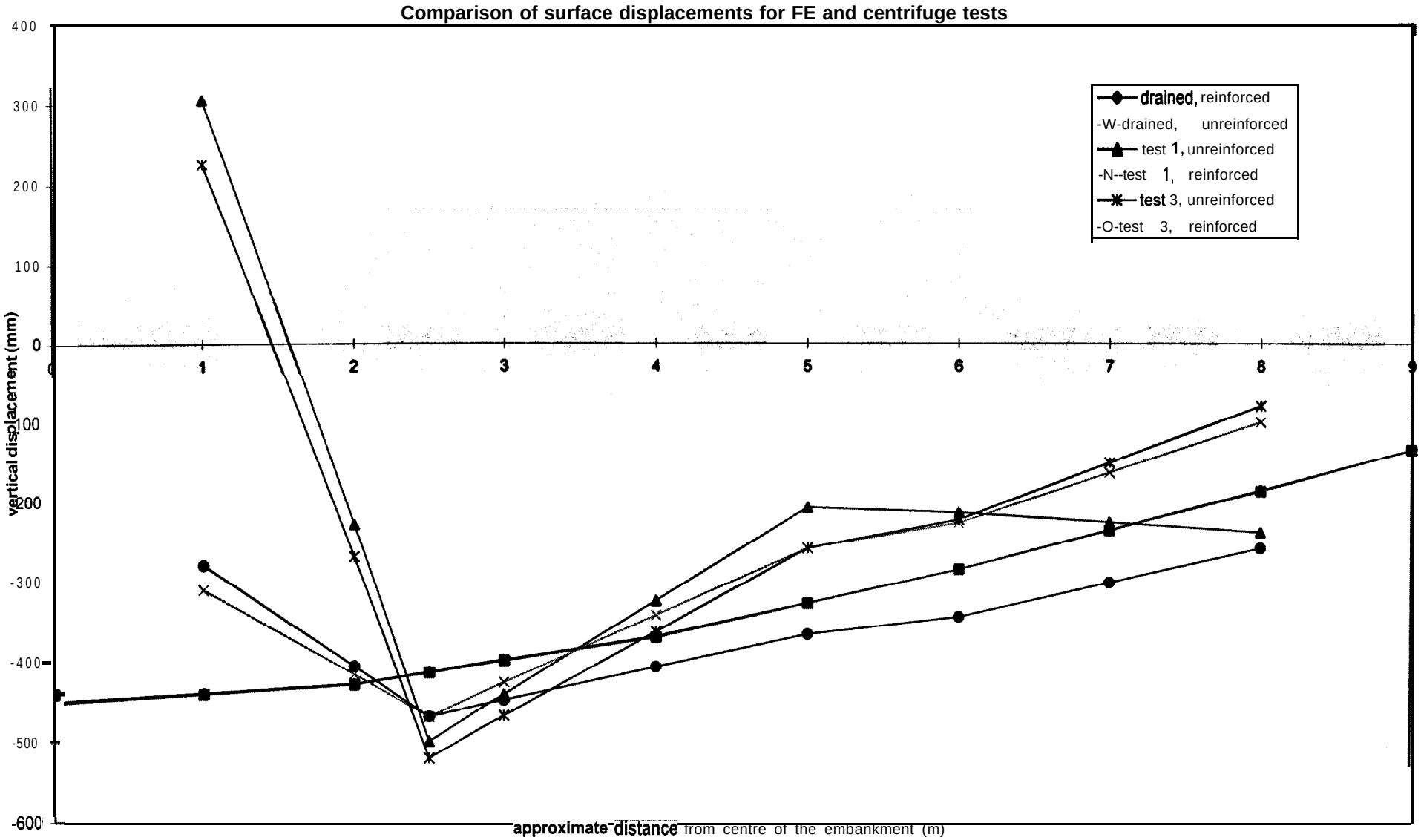
Comparison of surface displacements for FE and centrifuge tests
400
300
200
100
0
-100
-200
-300
-400
-500
-600
vertical displacement (mm)
0
1
2
3
4
5
6
7
8
9
drained, reinforced
-W-drained, unreinforced
test 1, unreinforced
-N--test 1, reinforced
test 3, unreinforced
-O-test 3, reinforced
approximate distance from centre of the embankment (m)

APPENDIX 1 - ANALYTICAL SOLUTION.

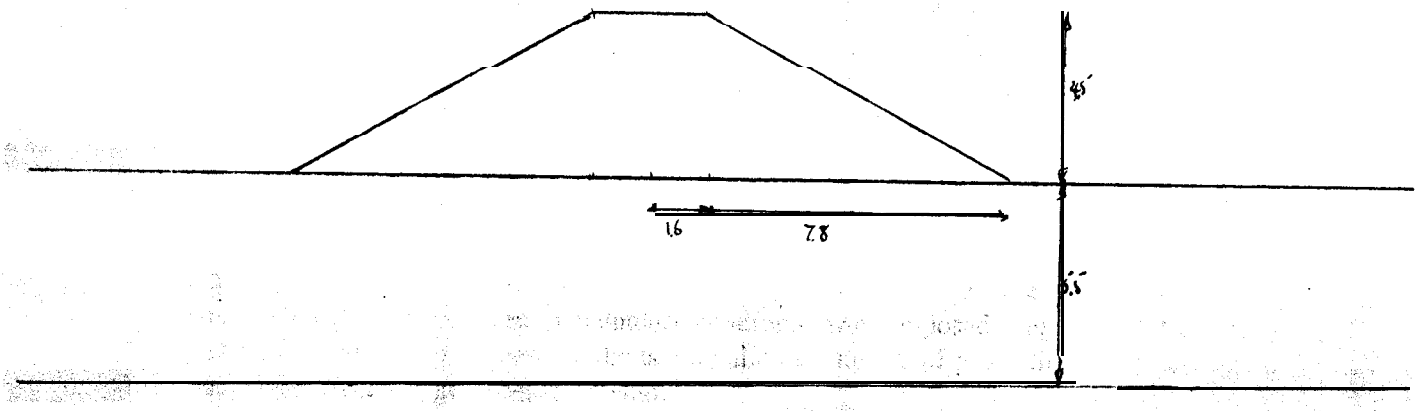

PROTOTYPE (DIMS IN m)

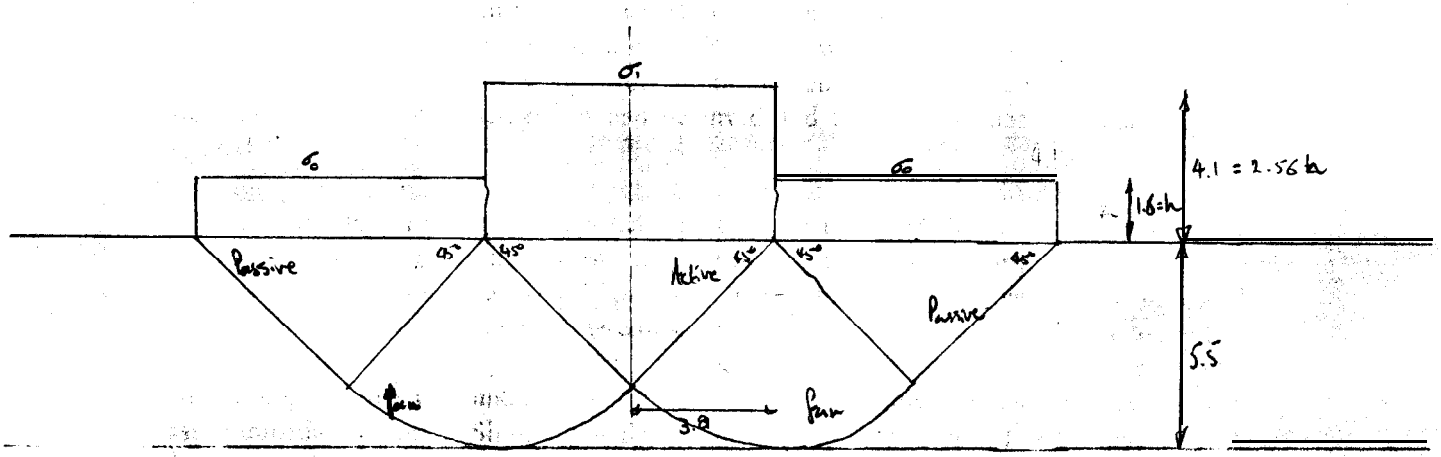

UNDRAINED MODEL

For clay, $C_u \simeq 0.2\sigma_v'(OCR)^{0.7}$

$OCR = 1.1$

$\sigma_v' = \gamma'_{clay} z$ (overburden not included as undrained analysis)

take $z = \frac{5.5}{2} = 2.75$

$\gamma'_{clay} \simeq 14$ kPa

$\Rightarrow C_u \simeq 0.2 \times 14 \times 2.75 \times (1.1)^{0.7}$

$\simeq 8.23$ kPa

TRESCA ANALYSIS:

$\sigma_1 - \sigma_0 = (2+\pi) C_u$

$(2.56h - h)\gamma_{sand} = 5.14 \times 8.23$ $\quad \gamma_{sand} \simeq 7$ kPa

$h = 3.86$ m @ failure.

This is equivalent to embankment height of 10.8 m.